

DESIGN OF WETTED WALL BIOAEROSOL CONCENTRATION CYCLONES

A Dissertation

by

YOUNGJIN SEO

Submitted to the Office of Graduate Studies of
Texas A&M University
in partial fulfillment of the requirements for the degree of

DOCTOR OF PHILOSOPHY

December 2007

Major Subject: Mechanical Engineering

DESIGN OF WETTED WALL BIOAEROSOL CONCENTRATION CYCLONES

A Dissertation

by

YOUNGJIN SEO

Submitted to the Office of Graduate Studies of
Texas A&M University
in partial fulfillment of the requirements for the degree of

DOCTOR OF PHILOSOPHY

Approved by:

Chair of Committee, Andrew R. McFarland

Committee Members, Yassin A. Hassan

Bryan W. Shaw

John S. Haglund

Sridhar Hari

Head of Department, Dennis L. O'Neal

December 2007

Major Subject: Mechanical Engineering

ABSTRACT

Design of Wetted Wall Bioaerosol Concentration Cyclones. (December 2007)

Youngjin Seo, B.S., Korea Aerospace University, South Korea;

M.S., Texas A&M University

Chair of Advisory Committee: Dr. Andrew McFarland

A wetted wall cyclone is a device that delivers hydrosol in a single stage from which real-time detection of airborne particles can be readily achieved. This dissertation presents the design, development, and characterization of a family of wetted wall bioaerosol cyclone concentrators that consume very low power and are capable of delivering very small liquid effluent flow rate of highly-concentrated hydrosol. The aerosol-to-aerosol penetration cutpoint for the cyclones is about $1\mu\text{m}$. The aerosol-to-hydrosol collection efficiency for the 1250 L/min cyclone is above 90% for particle sizes greater than $2\mu\text{m}$ at the 1 mL/min liquid effluent flow rate. The aerosol-to-hydrosol collection efficiency for the 100 L/min cyclone is above 85% for particle sizes larger than $2\mu\text{m}$ at the 0.1 mL/min liquid effluent flow rate when it is operated at air flow-rate of 100 L/min. The pressure drop across the 1250 L/min and 100 L/min cyclones are approximately 22 inches of water and about 6.4 inches of water, respectively.

A study, based on the empirically obtained aerosol-to-aerosol collection efficiency, was conducted to develop a performance modeling correlation that enables prediction of the aerosol performance as a function of the Reynolds number and Stokes number. Since the Reynolds number and Stokes number govern the particle motions in the cyclone, the aerosol performance could be expressed in terms of the Reynolds number

and Stokes number. By testing the three cyclones (100, 300, and 1250 L/min cyclones) with several different air flow rates, the aerosol-to-aerosol collection efficiencies for wide range of the Reynolds numbers ($3,500 < Re < 30,000$) were able to be obtained. Performance modeling correlations for wetted wall cyclones show that the aerosol-to-aerosol collection efficiency in the cyclone can be well predicted by the Reynolds number and Stokes number.

DEDICATION

To my family

ACKNOWLEDGEMENTS

I would like to express my appreciation and gratitude to Dr. Andrew R. McFarland, my advisor, for his encouragement, guidance, and instruction. In addition, his patience inspired me to work much harder. He supported my endeavors during my time at Texas A&M, and while working on my dissertation.

I would also like to thank Dr. Sridhar Hari and Dr. John Haglund for their consistent help and invaluable comments on my dissertation. I am also grateful to Dr. Yassin A. Hassan and Dr. Bryan Shaw for being my committee members and helpful suggestions.

I want to express many thanks to all the ATL personnel for their time and support, Mr. Manpreet Phull, Dr. Taewon Han, Dr. Satya Seshadri, Dr. Shishan Hu, Dr. Maria King, Mr. Charles Cox, Mr. Daniel LaCroix, Dr. Vishunu Karthik, Mr. Michael Baehl and Mr. Gary Bradley.

My study in the Aerosol Technology Lab was funded by REDCOM, U.S. Army, and their financial support for this work is gratefully acknowledged.

I would like to express many thanks to my lovely wife, Jiyoung Park for her support. Finally, I give thanks for the love of my parents. Once again, I'm thankful for all my family has given me. Without them, I would have never completed my dissertation and obtained my PhD.

TABLE OF CONTENTS

	Page
ABSTRACT.....	iii
DEDICATION.....	v
ACKNOWLEDGEMENTS.....	vi
TABLE OF CONTENTS.....	vii
LIST OF FIGURES	x
LIST OF TABLES.....	xv
 CHAPTER	
I INTRODUCTION.....	1
General Background	1
Previous Study	2
Objectives of the Present Study	3
Theoretical Background.....	5
II A FAMILY OF WETTED WALL CYCLONES	7
1250 L/min Wetted Wall Cyclone	7
100 L/min Wetted Wall Cyclone	9
Stokes Scaling Process.....	9
Principle of Collecting Particulate Matters through Wetted Wall Cyclones .	10
III EXPERIMENTAL METHODOLOGY.....	11
Experimental Apparatus and Methodology for Aerosol Characteristics Test ...	11
Test apparatus	11
PSL suspension	13
Aerosol-to-aerosol test and aerosol-to-hydrosol test.....	13
Analysis and calculation of results	15
Aerosol-to-aerosol collection efficiency.....	15
Aerosol-to-hydrosol collection efficiency	17
Uncertainty Analysis for Aerosol Test Results.....	17
Quality Assurance for Aerosol Tests	19
Experimental Apparatus and Methodology for Pressure Drop Test.....	20

CHAPTER	Page
Experimental Apparatus and Methodology for Debris Test.....	20
Experimental Apparatus and Methodology for Low Temperature Test.....	21
Test apparatus	21
Preliminary heating system for the 1250 L/min cyclone.....	21
Preliminary heating system for the 100 L/min cyclone.....	22
Temperature measurement.....	23
 IV RESULTS AND DISCUSSION.....	 24
1250 L/min Cyclone	24
Aerosol-to-aerosol collection efficiency.....	24
Wetting pattern on the impacting wall – effect of an atomizer.....	24
Aerosol-to-hydrosol collection efficiency	25
Pressure differential across the cyclone.....	26
Debris test	27
Fine Arizona dust (mass median aerodynamic diameter: 10 μm)	27
ASHRAE test dust	28
Second-cut cotton linters.....	28
Low temperature test.....	29
Preliminary heating system - temperature profile with purely air flow..	29
Preliminary heating system - temperature profile with liquid-in.....	30
Final heating system	31
Conclusion for the 1250 L/min cyclone.....	31
100 L/MIN Cyclone.....	32
Aerosol-to-aerosol collection efficiency.....	32
Aerosol-to-hydrosol collection efficiency	33
Pressure differential across the cyclone.....	33
Sensitivity studies	34
Effect of wetting agent (Tween-20).....	34
Effect of liquid effluent flow rate	34
Time constant.....	35
Rate of liquid evaporation.....	37
Effect of ethylene glycol (EG) on the evaporation rate	37
Effect of cooling the cyclone using ice water on the evaporation rate ...	38
Effect of EG in a cooled cyclone on the evaporation rate	38
Effect of EG in a cooled cyclone on the particle collection	39
Low temperature test.....	40
Preliminary heating system - temperature profile with purely -22°C	40
air	40
Preliminary heating system - temperature profile with -22°C air and	40
also with liquid-in	40
Final heating system for -22°C air	41
Preliminary heating system – temperature profile with -32°C air and	41
also with liquid-in	41

CHAPTER	Page
Conclusion for the 100 L/min cyclone.....	42
V PERFORMANCE MODELING OF A FAMILY OF WETTED WALL CYCLONES	44
Motivation.....	44
Aerosol-to-Aerosol Collection Efficiency	45
Aerosol Performance of Three Cyclones at Similar Reynolds Numbers	46
Regression Process.....	47
High Reynolds number region	48
Low Reynolds number region.....	49
Relationship Between the Stk_{50} Number and Reynolds Number in the Cyclones.....	49
Conclusion	50
VI SUMMARY AND FUTURE WORK	51
REFERENCES..	53
APPENDIX.....	56
VITA.....	146

LIST OF FIGURES

	Page
Figure 1.1. Typical near-real-time liquid-based detection system.....	56
Figure 1.2. Wetted wall cyclone	57
Figure 1.3. Section view of the Black and Shaw cyclone.....	58
Figure 1.4. Interface between the skimmer and the body of the Black and Shaw cyclone	59
Figure 2.1. Interface between a redesigned liquid skimmer and the body of the 1250 L/min cyclone	60
Figure 2.2. 1250 L/min cyclone. a) components, b) assembly	61
Figure 2.3. 100 L/min cyclone version 2.0	62
Figure 2.4. Comparison of inlet geometry for three cyclones	63
Figure 3.1. Schematic of setup for aerosol experiment	64
Figure 3.2. Schematic of pressure drop test.....	66
Figure 3.3. Schematic of debris test.....	67
Figure 3.4. Cold temperature experimental setup	68
Figure 3.5. Preliminary heating system for the 1250 L/min cyclone and thermo-couple locations	70
Figure 3.6. Preliminary heating system for the 100 L/min cyclone and thermo-couple locations	71
Figure 3.7. Thin film RTD location for the skimmer	72
Figure 4.1. Aerosol-to-aerosol collection efficiency as a function of particle size	73

Figure 4.2. Aerosol-to-hydrosol collection efficiency as a function of particle size for the 1250 L/min cyclone and Black and Shaw cyclone. Liquid effluent flow rate: 1 mL/min	74
Figure 4.3. Concentration factor as a function of particle size. Liquid effluent flow rate: 1 mL/min.	75
Figure 4.4. Pressure differential across cyclones as a function of air flow rate	76
Figure 4.5. Pressure coefficient for the 1250 L/min cyclone as a function of Reynolds number	77
Figure 4.6. 1250 L/min cyclone inner wall, 6 minutes after adding 2000 mg of Arizona dust	78
Figure 4.7. 1250 L/min cyclone inner wall, 8 minutes after adding 600 mg of ASHRAE test dust	79
Figure 4.8. 1250 L/min cyclone inner wall, 6 minutes after adding 170 mg of the second-cut cotton linters	80
Figure 4.9. Temperature profiles with the preliminary heating system. Incoming air temperature: -40°C. Heaters and blowers were turned on simultaneously...	81
Figure 4.10. Temperature profiles with the preliminary heating system. Incoming air temperature: -26°C. Heaters and blowers were turned on simultaneously.	82
Figure 4.11. Temperature profiles with the preliminary heating system. Incoming air temperature: -20°C. Heaters and blowers were turned on simultaneously.	83
Figure 4.12. Open area location in the heater #2	84

Figure 4.13. Liquid freezing inside the 1250 L/min cyclone. Incoming air temperature: -26°C.....	85
Figure 4.14. Liquid freezing on the vortex finder. Incoming air temperature: -26°C	86
Figure 4.15. Final heating system for the 1250 L/min cyclone	87
Figure 4.16. Temperature profiles with the final heating system. Incoming air temperature: -30°C. Heaters and blowers were turned on simultaneously.	92
Figure 4.17. Aerosol-to-aerosol collection efficiency as a function of particle size	93
Figure 4.18. Aerosol-to-hydrosol collection efficiency as a function of particle size for the 100 L/min cyclone. Liquid effluent flow rate: 0.1 mL/min	94
Figure 4.19. Concentration factor as a function of particle size for the 100 L/min cyclone. Liquid effluent flow rate: 0.1 mL/min.....	95
Figure 4.20. Pressure differential across the 100 L/min cyclone as a function of air flow rate	96
Figure 4.21. Aerosol-to-hydrosol efficiency for the 100 L/min cyclone as a function of fraction volume of Tween-20. Tested particle: 3 μ m PSL. Liquid effluent flow rate: 0.1 mL/min.....	97
Figure 4.22. Aerosol-to-hydrosol collection efficiency & concentration factor for the 100 L/min cyclone as a function of the liquid effluent flow rate. Tested particle: 3 μ m PSL.	98
Figure 4.23. Instantaneous hydrosol collection efficiency with “wet start” for the 100 L/min cyclone as a function of time. Tested particle: 3 μ m PSL	99

Figure 4.24. Instantaneous hydrosol collection efficiency with “dry start” for the 100 L/min cyclone as a function of time. Tested particle: 3 μ m PSL	100
Figure 4.25. Evaporation rates with pure water and 30% EG at two different testing conditions	101
Figure 4.26. Evaporation rate with pure water in a cooled cyclone	102
Figure 4.27. Evaporation rate with 30% EG in a cooled cyclone	103
Figure 4.28. Temperature profiles when 4.2 W/in ² and 2.96 W/in ² were applied for heater #2 and #3, respectively. No liquid injection. Heating system and thermo-couple locations are shown in Figure 3.6	104
Figure 4.29. Final heating system for the 100 L/min cyclone	105
Figure 4.30. 100 L/min cyclone with the final heating system	107
Figure 5.1. Aerosol-to-aerosol collection efficiency for the 100 L/min cyclone as a function of the Stokes number	108
Figure 5.2. Aerosol-to-aerosol collection efficiency for the 1250 L/min cyclone as a function of the Stokes number	109
Figure 5.3. Aerosol-to-aerosol collection efficiency for the 300 L/min cyclone as a function of the Stokes number	110
Figure 5.4. Normalized differential A-A collection efficiency for the 1250 L/min cyclone at 1250 L/min as a function of the Stokes number	111
Figure 5.5. Comparison of the aerosol-to-aerosol collection efficiency of the 100 and 300 L/min cyclones operating at different flow rates, corresponding to the Reynolds number of 3600	112

Figure 5.6. Comparison of the aerosol-to-aerosol collection efficiency of the 300 and 1250 L/min cyclones operating at different flow rates, but close to the Reynolds number value of 7800	113
Figure 5.7. Comparison of the aerosol-to-aerosol collection efficiency of the 300 and 1250 L/min cyclones operating at different flow rates, but close to the Reynolds number of 12700	114
Figure 5.8. Measured and predicted aerosol-to-aerosol collection efficiency as a function of the Stokes number for high Reynolds number region.....	115
Figure 5.9. Measured and predicted aerosol-to-aerosol collection efficiency as a function of the Stokes number for low Reynolds number region.....	127
Figure 5.10. Stk_{50} values as a function of the Reynolds number	134

LIST OF TABLES

	Page
Table 2.1. Comparison of the Black and Shaw cyclone with the 1250 L/min cyclone ..	135
Table 2.2. Representative dimensions for three cyclones.....	136
Table 3.1. Uncertainty values in the Stokes number	136
Table 3.2. Optical filters and tracer dye used in fluorometric analysis	137
Table 3.3. Power input to each heater element of the preliminary heating system for the 1250 L/min cyclone	137
Table 3.4. Heater specifications of the preliminary heating system for the 100 L/min cyclone	138
Table 4.1. Comparison of heat flux between two heating systems for the 1250 L/min cyclone	138
Table 4.2. Series of procedures and time sequence followed in the time constant tests	139
Table 4.3. Effect of EG concentration on the A-H collection efficiency. Liquid effluent flow rate: 0.1 mL/min.....	139
Table 4.4. Effect of EG concentration on the A-H collection efficiency. Liquid effluent flow rate: 0.16 ~ 0.19 mL/min.....	140
Table 4.5. Effect of liquid effluent flow rate in the A-H collection efficiency	140
Table 4.6. Effect of 30% EG in a cooled cyclone.....	141
Table 4.7. Initial heat flux value for -22°C.....	141
Table 4.8. Optimized heat flux value for the cartridge heater	142
Table 4.9. Optimized heat flux value for the cartridge and skimmer heater	142
Table 4.10. Optimized heat flux for the preliminary heating system for -22°C	143

	Page
Table 4.11. Initial heat flux value for -32°C	143
Table 4.12. Optimized heat flux for the preliminary heating system for -32°C	144
Table 5.1. Cyclone flow rate and corresponding Reynolds number based on the slot width	144
Table 5.2. Coefficients of two sigmoid functions for two groups	145

CHAPTER I

INTRODUCTION

General Background

In the last decade, there have been disturbing reports of bio-terror events directed against the general public. Interpol indicates that the world is largely unaware and unprepared for bio-terror events. Some of the possible scenarios being contemplated include purported bio-terror attacks on public facilities such as conference halls and shopping malls. In the event of such attacks targeted against the public at large, it is imperative that the emergency response (ER) activities are initiated in a timely manner to prevent the various adverse effects. A highly efficient real-time detection system for such agents is thus a very critical aspect that determines the ER planning.

A real-time detection system is comprised of an inlet, pre-separator, concentrator, aerosol-to-hydrosol transfer stage, and analyzer, out of which the concentrator plays a very important role (Figure 1.1). While the inlet aspirates the air sample containing the agent to be detected, the pre-separator eliminates debris and other unwanted contaminants from the sample. The “cleaned” air-sample is then directed to a concentrator whose purpose is to provide a representative hydrosol sample to the analyzer and may involve two stages. In the first stage, a device substantially concentrates bio-agents present in the large volume of sampled air. In the second stage, the concentrated sample is converted from the aerosol to the hydrosol state to enable provision of a liquid sample to the

This dissertation follows the style and format of *Aerosol Science and Technology*.

analyzer. A wetted wall bioaerosol sampling cyclone is a versatile concentration device that combines the two functions of concentrating particles in the aspired air stream and transferring the concentrated particles to the liquid phase to facilitate subsequent analysis. As shown in Figure 1.2, liquid is input in such a way as to form a film onto which the aerosol particles are impacted. The shear force created by the airflow carries the liquid to a skimmer where the hydrosol and air flows are separated, and the hydrosol is extracted from the system.

Previous Study

Studies on the wetted wall cyclone were started in the late 1960's. Errington et al. (1969) built a cyclone separator that operated at a high volumetric flow rate and concentrated the particulate into a small liquid effluent flow rate (on the order of a few mL/min). White (1975) developed an axial flow cyclone for concentrating bioaerosol particles from a flow rate of 950 L/min of aerosol to a continuous liquid flow rate between 1 and 2 mL/min. The latter cyclone was further developed by Black and Shaw (2002) who opted for an air flow rate of 900 L/min and a liquid effluent flow rate of 1 mL/min. Figure 1.3 shows a sectional view of the Black and Shaw cyclone.

Experimental and numerical investigations were undertaken at the Aerosol Technology Laboratory (ATL), Texas A&M University on the Black and Shaw cyclone and the understanding obtained from the results of the investigations paved the way for the development of a new generation of cyclones with improved performance specifications. Performance investigation of the Black and Shaw cyclone was undertaken by Moncla (2004). He identified that the cyclone exhibited entrainment of liquid from

the internal wall into the exhaust air flow stream, which is called, “liquid bypass”. In addition, he observed a ring of recirculating liquid that spins near the skimmer tip during cyclone operation (Figure 1.4).

Moncla verified that the cut-point (particle size corresponding to 50% collection efficiency) of the aerosol-to-aerosol (A-A) penetration efficiency curve was near 1.0 μm . While the time response of the cyclone was found to be 3 minutes, liquid bypass increased the time response to 8 minutes. The decay response under conditions of no liquid bypass was 1.1 minutes. Pressure drop across the cyclone was measured to be around 26 inches of water (4,982 Pa).

In the Black and Shaw cyclone, a single hole was used for the liquid injection. Phull (2005) investigated alternate methodologies for liquid injection and showed that the aerosol-to-hydrosol (A-H) collection efficiency with the air-blast atomizer was higher than that with any other methodologies. That is because the air-blast atomizer wets the impacting wall evenly so that all particles that strike the wall are able to be collected. Therefore, he concluded that the air-blast atomization would be the most effective way.

Objective of the Present Study

Since the liquid recirculation and liquid bypass issues were seriously degrading the cyclone performance, initial research efforts were devoted toward exploring ways to eliminate these issues. These efforts, however, later evolved into the design and development of a new generation of cyclones with enhanced performance characteristics from the viewpoint of both aerosol testing and low temperature testing. The following

series of objectives were laid out to be the benchmarks for the new generation of a high volume flow rate cyclone:

- Elimination of the liquid recirculation and liquid bypass issues.
- Operation of the cyclone at 1250 L/min with a liquid output flow rate of 1 mL/min.
- Low pressure differential across the cyclone – it should not be significantly more than the Black and Shaw cyclone.
- Design of a heating system to allow operation at temperatures as low as -24°C - The power budget for heating was approximately 350 W.

In addition, a second cyclone that could be operated at a reduced air flow rate of 100 L/min was also proposed to be developed. Performance specifications of this cyclone were listed below:

- Low energy consumption (pressure drop) - pressure differential across the cyclone should be less than 10 inches of water.
- High concentration factor by using a liquid effluent flow rate of 0.1 mL/min (about 3 drops/min).
- High aerosol-to-hydrosol collection efficiency for particles in the size range of 1 – 10 μm AD - performance characteristics such as the aerosol-to-aerosol collection efficiency and the aerosol-to-hydrosol collection efficiency should be at least comparable with that for the 1250 L/min cyclone.
- Maintaining functionality when air at sub-freezing temperatures was sampled (as low as -33°C)

Finally, the ultimate goal of the research work was to create a performance modeling correlation that enables prediction of the aerosol performance of the new generation of cyclones as a function of the Reynolds number and Stokes number.

Theoretical Background

Particle motion in dilute and disperse two-phase flow, as that of the cyclone, is governed by the Reynolds and Stokes numbers. Therefore, classification characteristics of cyclones are expressed as function of the Reynolds number and Stokes number. The primary parameter that governs the aerosol-to-aerosol collection efficiency is the Stokes number defined by

$$Stk = \frac{\tau U}{D_j / 2} = \frac{\rho_p d_p^2 U_{slot} C_c}{9\mu W} \quad (1.1)$$

where,

τ = relaxation time of the particle

W = slot width at the intersection of the inlet section to the cyclone body

U_{slot} = mean air velocity at the slot

ρ_p = particle density

D_p = particle diameter

C_c = slip correction factor

μ = dynamic viscosity of air.

The slip correction factor is defined by

$$C_c = 1 + 2.52 \left(\frac{\lambda}{d_p} \right) \quad (1.2)$$

where,

λ = mean free path of air at atmospheric pressure and room temperature (=0.066 μm).

The second parameter that affects the aerosol performance is the Reynolds number (Eqn. 1.3). While different authors have used different definitions (Moore et al. 1990, Zhu et al. 1999), in this study, the Reynolds number is calculated based on the slot width which is the critical parameter that governs the aerosol performance.

$$\text{Re} = \frac{\rho_{air} U_{slot} W}{\mu} \quad (1.3)$$

where,

ρ_{air} = air density.

CHAPTER II

A FAMILY OF WETTED WALL CYCLONES

1250 L/min Wetted Wall Cyclone

Experiments conducted by Moncla (2004) on the Black and Shaw cyclone indicated that one side angle of divergent section in the Black and Shaw cyclone was large enough to generate flow separation and recirculation that caused the liquid recirculation ring that spun near the skimmer tip. The fact was also verified by numerical studies (Hu and McFarland, 2007). The ring increased the response time which is the time taken by hydrosol to flow through the cyclone body and exit through the liquid sample extraction port. In addition, the ring of liquid could be a reason for the liquid bypass. In order to prevent the ring and bypass issues, the divergent section in the cyclone body was removed and the skimmer was redesigned. One of the most important parts of the design was the interface between the cyclone body and the skimmer (Figure 2.1). The liquid flow gap and the skimmer nose gap were optimized to prevent liquid bypass. In addition, the purpose of skimmer nose was to induce liquid into the nose gap. With these modifications, the issues were successfully eliminated.

When upgrading the Black and Shaw cyclone, the main body diameter was enlarged from 1.125" to 1.5". In addition, the slot length and inlet diameter were enlarged. Thus, pressure differential across the 1250 L/min cyclone was lowered so that nominal flow rate could be increased. Table 2.1 shows the differences between the Black and Shaw cyclone and the 1250 L/min cyclone.

The desired cutpoint, 1 μm , was already achieved from the Black and Shaw cyclone. The Stoke numbers and Reynolds numbers at the slot for the Black and Shaw cyclone at 900 L/min and the 1250 L/min cyclone at 1250 L/min were identical. The equality of the Reynolds numbers ensures that the gas flows are similar, and equality of the Stokes numbers ensures that the particle motions in the flow fields are also similar (Hinds, 1999). Therefore, similar aerosol performance could be expected between the Black and Shaw cyclone and 1250 L/min cyclone.

Phull (2005) verified that an air-blast atomization as a liquid injection method would be the most effective way for wetting the impacting wall evenly. Therefore, an air-blast atomizer has been used to provide liquid spray into cyclones.

The 1250 L/min cyclone was cast of stainless steel 316. The cast piece went through a secondary machining process to achieve desired dimensions and bolt patterns. Then inner surface of the cyclone was polished mechanically to prevent particle deposition due to the surface roughness. The surface smoothness was less than 16 micro-inches RMS (Root Mean Square) after polishing. The mechanical polishing was conducted by utilizing coarse grit flap wheels as a first step. All cast roughness was removed while using extreme caution not to remove an excessive amount of base metal. The coarse grit finish was followed by successively finer grit finishes until the desired finish was achieved. Polishing was the final process of fabricating the 1250 L/min cyclone and Figure 2.2 shows the cyclone along with its components.

100 L/min Wetted Wall Cyclone

One of the important performance specifications of the current state-of-the-art concentration devices is an improved concentration capability while operating at a low flow rate (low power consumption), compared to the contemporary devices. To this end, development of a cyclone operating at a lower flow rate (100 L/min) that could satisfy the above objectives was also pursued at ATL, guided by the understanding obtained on the 1250 L/min cyclone. The design methodology for the 100 L/min cyclone is described in the ‘Stokes Scaling Process’ section. Design, development, and Characterization of the 100 L/min wetted wall bioaerosol cyclone that would have a very high concentration factor ($\approx 1,000,000$) and deliver hydrosol in quantities as low as three drops per minute (0.1 mL/min) were fulfilled.

Figure 2.3 shows the cyclone version 2.0 that was operated at an air flow rate of 100 L/min. The fabrication methodology was the same as that for the 1250 L/min cyclone.

Stokes Scaling Process

Critical geometrical dimensions of the 100 L/min cyclone were intuitively determined by downscaling the geometrical details of the 1250 L/min cyclone according to the Stokes number. In the process of Stokes scaling D_j and U were the only parameters that needed to be considered. The scaling equation is as follows,

$$\frac{D_1}{D_2} = \frac{U_1}{U_2} = \left(\frac{Q_1}{Q_2} \right)^{\frac{1}{3}} \quad (2.1)$$

where,

Q = air flow rate.

Figure 2.4 shows the cyclone inlet and body configurations for the three cyclones and Table 2.2 summarizes the characteristic geometrical details.

Principle of Collecting Particulate Matters through Wetted Wall Cyclones

As shown in Figures 2.2 and 2.3, inlet air flow containing the aerosol introduced through the flange at the top is accelerated through its passage through a convergence section and impacts on the wall (impacting wall) of the cyclone body right beneath the inlet section. There is a vortex finder that helps to create a vortex flow inside the cyclone, subsequent to the impaction process. The rotating vortex flow is then extracted through the skimmer exit by a blower. An atomizer located approximately midway in the inlet section of the cyclone provides the liquid spray to uniformly wet the impacting wall. The atomizer utilizes two needles for uniform dispersion; one for liquid and the other for air. It is important that the angle between the two needles is well adjusted to ensure that the whole impacting wall will be covered with the liquid spray. Aerosol matter prevalent in the extracted air stream gets size-classified; deposits on the cyclone wall recovered by the sprayed liquid are carried downstream and extracted through the sample extraction port. The skimmer is essential for separating liquid from the inner wall of the cyclone from the air flow.

CHAPTER III

EXPERIMENTAL METHODOLOGY

Experimental Apparatus and Methodology for Aerosol Characteristic Test

Test apparatus

Figure 3.1 displays a bench-scale test setup used to evaluate the particle collection characteristics of the wetted wall cyclones. Eight sizes of polystyrene latex beads (PSL) (Duke Scientific, Palo Alto, CA & Bangs Lab, Fishers, IN), i.e., 0.4, 0.49, 1, 1.5, 2, 3, 5, and 10 μm were used to characterize the aerosol performance. Tests were conducted by alternately exposing the cyclones and a reference filter.

A Collison nebulizer (Models CN60, BGI, Inc. Waltham, MA) was used to generate Polystyrene Latex (PSL) particles below 3 μm size. The Collison nebulizer creates liquid droplets, of which about 1% contains polystyrene beads. The Collison nebulizer works by using compressed air that is used to extract the liquid into a sonic velocity air jet, wherein it is sheared into droplets. This liquid/air jet is impacted against the inside wall of the jar to remove the larger fraction of the droplets. The air pressure to the nebulizer was set at 138 kPa (20 psig). Upon evaporation of the liquid phase the aerosol consists of small residual nuclei from the droplets without PSL particles, and the PSL particles from the populated droplets.

The Collison nebulizer was not able to atomize particles larger than 3 μm , hence, a single-jet atomizer using compressed dry air was used to atomize particles larger particles such as 5 μm and 10 μm . The atomizer was placed vertically on one end of the

experimental setup. A PSL solution was made (30 drops of PSL in 100 mL of distilled water) and pumped into the atomizer at a flow rate of 2 mL/min using a peristaltic pump (Fisher Variable-Flow Peristaltic Pumps, Fisher Scientific, Inc. Austin, TX). Compressed dry air at 138 kPa (20 psig) was forced through the air needle of the atomizer, which created a spray from the liquid coming out of the liquid needle.

Prior to exposure of the cyclone or reference filter, the generated aerosol traveled through an Air Blender™ to enhance the mixing of the aerosol stream and then through a set of flow straighteners to diminish large scale turbulent eddies generated by the blender. A Laminar Flow Element (CME, Davenport, IA) was used to monitor high volumetric flow rates (> 300 L/min) at downstream of either the cyclones or reference filter (203 mm \times 254 mm (8 inch \times 10 inch) glass fiber filter (Type A/E, Pall, East Hills, NY)). A Laminar Flow Element (LFE) embraces a system of minute parallel capillary passages. In each of these passages, a laminar flow is established which produced a nearly linear relationship between the differential pressure and the flow rate. Then, this effective differential pressure over the LFE is captured via a differential pressure transducer. A digital flow-meter (Model No. 4045E, TSI Inc., Shoreview, MN) was used to monitor low volumetric flow rates (< 300 L/min) through the cyclone or reference filter (47 mm diameter glass fiber filter (Type A/E, Pall, East Hills, NY)). Liquid, at a predetermined inflow rate, was provided to the cyclone by a CAVRO pump (Model XP 3000, Cavro Scientific Instruments Inc., San Jose, CA). As determined by Phull (2005), a 0.1% v/v of the Tween-20 was used as a collection fluid when testing both the Black and Shaw cyclone and the 1250 L/min cyclone. The hydrosol sample was recovered from the 1250 L/min cyclone by a peristaltic pump (Fisher Variable-Flow Peristaltic Pumps, Fisher

Scientific, Inc. Austin, TX). A micro-diaphragm liquid pump (Model PML 5239-NF31, KNF Neuberger, Trenton, NJ) was used to extract the hydrosol from the 100 L/min cyclone. Another micro-diaphragm pump served as a compressed air source for the air-blast atomizer. A blower (Model 119104, Ametek, Inc. Paoli, PA) provided the air flow through the system.

PSL suspension

A PSL suspension, the Master Suspension, was prepared by diluting commercially-available concentrated fluorescently-tagged polystyrene latex. Sixty mL of concentrated PSL was added to five hundred forty mL of distilled water to prepare the Master Suspension for each size. To have consistent concentrations of PSL output from the nebulizer, it was refilled with the PSL Master Suspension before each test. Each run took ten minutes, which time was appropriate for collecting sufficient PSL such that the fluorescence of the reference sample was significantly greater (~ at least 20X) than the background fluorescence. At the end of a test, the leftover suspension was placed in a “Recycled PSL Suspension” container and could be used as the Master Suspension for other sets of tests.

Aerosol-to-aerosol test and aerosol-to-hydrosol test

A glass fiber filter (Type A/E, Pall, East Hills, NY) was used as the reference filter to collect the PSL particles. Blowers were turned on and then the Collision nebulizer or a single-jet atomizer was turned on to generate the PSL particles. After running for ten minutes, the nebulizer or the atomizer was turned off. However, blowers

were run for another thirty seconds to collect all of the PSL particles at the filter upstream. Then the filter was transferred into a container. To dissolve the PSL from the filter, a predetermined amount of ethyl acetate was added into the container and a threaded lid for the container had to be on during soaking. Then the container was left for approximately one hour to ensure proper mixing.

When testing cyclones to obtain the aerosol-to-aerosol collection efficiency, Vaseline was applied on the inner wall of the cyclone body to prevent particle bounce. An exhaust filter was placed at the cyclone downstream to collect penetrated particles that exit the cyclone. First, blowers were turned on and the PSL particles were introduced. The nebulizer or the atomizer was turned off in 10 minutes. The blowers were run for another thirty seconds to collect the PSL particles at the cyclone upstream. Then the exhaust filter was put into a container. A predetermined amount of ethyl acetate was supplied into the container to dissolve the PSL from the filter. The container with a threaded lid was left for about one hour before analysis.

For the aerosol-to-hydrosol collection efficiency, the entire system such as blowers and all pumps were simultaneously actuated. When the liquid effluent flow rate reached a steady state, the Collision nebulizer or a single-jet atomizer was turned on. The system was operated for ten minutes, at which time the Collision nebulizer or the atomizer was turned off. The blower and pumps were operated for addition two minutes to recover hydrosol particles remaining in the cyclone and liquid flow lines. The blower and pumps were turned off. The hydrosol sample, which was collected in the receiver tube, was transferred to a glass container. The liquid was evaporated with a heat gun (Type 3458, STEINEL, Bloomington, MN) and then a predetermined amount of ethyl acetate was

added to the container to dissolve the dried PSL. This solution was set aside for about an hour to allow the dissolution process to reach completion. At the end of each set of tests (replicate samples for same test conditions), the cyclone was rinsed with ethyl acetate and then with distilled water.

Analysis and calculation of results

Aerosol-to-aerosol collection efficiency

The Aerosol-to-aerosol collection efficiency, η_{AA} , was based on the flurometric readings of the cyclone after-filter and the reference filter. In particular:

$$\eta_{AA} = 1 - \frac{C_{m,air,exhaust}}{C_{m,air,reference}} \quad (3.1)$$

where,

$C_{m,air,exhaust}$ = aerosol concentration based on fluorometric reading from the cyclone after-filter

$C_{m,air,reference}$ = aerosol concentration based on fluorometric readings from the reference sample.

The aerosol concentration of fluorescent dye in the sampled air, as calculated from analysis of the fluorescence of a solution was:

$$C_{m,air} = \frac{F V}{t Q} \quad (3.2)$$

where,

$C_{m,air}$ = relative mass concentration of the fluorescent tracer in the sampled air

F = numerical reading of the fluorometer

V = solution volume

t = time for a test

Q = air flow rate.

A fluorometer (Model FM109515, Quantech, Barnstead International, Dubuque, IA) was used to quantify the fluorescence of the reference and cyclone effluent samples. The fluorometer is a device that exploits some of the principles of fluorescence in order to identify and quantify fluorescent molecules (dyes). Fluorescent dyes absorb light at one energy level (or wavelength) and emit light at a lower energy level (or longer wavelength). The wavelength range for which fluorescent molecules absorb light is relatively small (usually less than 50 nanometers). What this means is that light outside a specific wavelength range will not cause the molecule to fluoresce. The fluorometer exploits this fact to identify one fluorescent molecule within a sample that may contain many several fluorescent molecules. Procedures in detail are as following,

1. A strong light source which produces light within a specific light range (Quartz Halogen lamp) is focused down to a tight beam.
2. The tight beam of light is sent through a filter which removes most of the light outside of the target wavelength range for a particular fluorescent molecule.
3. The filtered light beam passes through the liquid target sample striking some of the fluorescent molecules in the sample.
4. Light emitted from the fluorescent molecules that is traveling orthogonal to the excitation light beam pass through a secondary filter that removes most of the light outside of the target wavelength range.

5. The filtered light then strikes a photomultiplier tube (PMT) which allows the instrument to give a relative measurement of the intensity of the emitted light.

Aerosol-to-hydrosol collection efficiency

The aerosol-to-hydrosol collection efficiency, η_{AH} , was determined from:

$$\eta_{AH} = \frac{C_{m,air,hydrosol}}{C_{m,air,reference}} \quad (3.3)$$

where,

$C_{m,air,hydrosol}$ = aerosol concentration based on fluorometric readings of the hydrosol sample.

Uncertainty Analysis for Aerosol Test Results

The uncertainty associated with the collection efficiency and the Stokes number was analyzed using the Kline-McClintock equation (1953). The relative uncertainties in parameters were obtained by the manuals from manufacturers or reasonable assumptions. The uncertainty in the collection efficiency was $\pm 5.21\%$ according to the Eqn (3.4).

$$W_{\eta} = \left[(e_{RFL_{cyc,lin}})^2 + (e_{RFL_{ref,lin}})^2 + (e_{RFL_{cyc,p}})^2 + (e_{RFL_{ref,p}})^2 + (e_{V,cyc})^2 + (e_{V,ref})^2 + (e_{t,cyc})^2 + (e_{t,ref})^2 + (e_{Q,cyc})^2 + (e_{Q,ref})^2 + (e_{gen})^2 \right]^{\frac{1}{2}} \quad (3.4)$$

where,

W_{η} = relative uncertainty in the efficiency

$e_{RFL,cyc,lin}$ = relative uncertainty in fluorometric reading for cyclone due to non-linearity error $\sim \pm 0.1$ %

$e_{RFL,ref,lin}$ = relative uncertainty in fluorometric reading for reference due to non-linearity error $\sim \pm 0.1$ %

$e_{RFL,cyc,p}$ = relative uncertainty in fluorometric reading for cyclone due to reading error (precision error) $\sim \pm 0.19$ %

$e_{RFL,ref,p}$ = relative uncertainty in fluorometric reading for reference due to reading error (precision error) $\sim \pm 0.19$ %

$e_{V,cyc}$ = relative uncertainty in ethyl acetate volume for cyclone $\sim \pm 0.1$ %

$e_{V,ref}$ = relative uncertainty in ethyl acetate volume for reference $\sim \pm 0.1$ %

$e_{t,cyc}$ = relative uncertainty in timing measurement for cyclone $\sim \pm 1$ sec

$e_{t,ref}$ = relative uncertainty in timing measurement for reference $\sim \pm 1$ sec

$e_{Q,cyc}$ = relative uncertainty in flow rate measurement for cyclone $\sim \pm 2$ %

$e_{Q,ref}$ = relative uncertainty in flow rate measurement for reference $\sim \pm 2$ %

e_{gen} = variance in aerosol generator $\sim \pm 2.29$ %

$e_{particle}$ = relative uncertainty in particle sizing $\sim \pm 3$ to 20 %

According to the Eqn. (3.5), the relative uncertainty associated with the Stokes number was approximately ± 9 % and also displayed in Table 3.1.

$$W_{Stk} = [(e_{\mu})^2 + 4(e_w)^2 + (e_L)^2 + (e_{p_p})^2 + (e_Q)^2 + \left(\frac{2.52\lambda + 2d_p}{2.52\lambda + d_p} \right)^2 (e_{d_p})^2]^{\frac{1}{2}} \quad (3.5)$$

where,

W_{Stk} = relative uncertainty in the Stokes number

e_{μ} = relative uncertainty in viscosity of air $\sim \pm 0.74$ %

e_w = relative uncertainty in slot width measurement $\sim \pm 3$ %

e_L = relative uncertainty in slot length measurement $\sim \pm 3$ %

e_{ρ_p} = relative uncertainty in particle density $\sim \pm 0.1$ %

e_Q = relative uncertainty in flow rate measurement $\sim \pm 2$ %

e_{d_p} = relative uncertainty in particle size $\sim \pm 3$ %

λ = mean free path of air at atmospheric pressure and room temperature ($= 0.066$ μm).

Quality Assurance for Aerosol Tests

A leakage test was always conducted on the cyclone and the reference filter assembly in advance of tests with aerosol particles. Each connection was sealed with o-rings, gaskets, or vacuum grease to ensure leakage free.

As described in the ‘PSL suspension’ section, a batch of the ‘master suspension’ was prepared. The Collison nebulizer was refilled with the master suspension prior to each test to ensure consistent concentration of PSL. To ensure adequate mixing, the batch was continuously stirred with a magnetic stirrer and also was shaken hard for 10 seconds prior to the refill. At the end of a set of experiments, the nebulizer was rinsed with ethyl acetate, isopropyl, and water to remove any residual PSL particles that could affect subsequent test results. In addition, the cyclone was also rinsed with ethyl acetate, isopropyl, and water.

During the fluorometric analysis, it was verified that the concentration of samples was within the linear range. In addition, the fluorescence concentration of samples was significantly greater than the background fluorescence. The fluorometric reading was normally at least 20 times more than the background.

Experimental Apparatus and Methodology for Pressure Drop Test

Pressure differential across the cyclone is a measure of the power expended by the device for the concentration process. Figure 3.2 shows the schematic of the experimental setup. A laminar flow element (CME, Davenport, IA), measuring air flow rate was located at the 1250 L/min cyclone upstream. A digital flow-meter (Model No. 4045E, TSI Inc., Shoreview, MN) was used at the 100 L/min cyclone upstream when testing the 100 L/min cyclone. There were two vacuum pressure taps upstream and downstream of the cyclone so that a relationship between air flow rate and pressure differential across the cyclone could be obtained.

Experimental Apparatus and Methodology for Debris Test

Debris has been considered a possible cause of liquid bypass; hence, tests were carried out to determine the debris loading failure level of the 1250 L/min cyclone fluidic system (failure by liquid bypass in the skimmer or plugging of the hydrosol transport lines or plugging of the hydrosol aspiration pump). Three materials such as fine Arizona dust, ASHRAE test dust, and second-cut cotton lintens were used for this test. Figure 3.3 shows the schematic of experimental setup. Grounded four-inch aluminum pipe (3' long) was installed on top of the 1250 L/min cyclone to aide in the aerosolization of debris. It

is to be noted that the test materials were released into the pipe using a glass nebulizer (Product number: 14606, TED PELLA, Inc. Redding, CA).

Experimental Apparatus and Methodology for Low Temperature Test

Test apparatus

Figure 3.4 shows the low temperature cyclone testing rig by using an ultra low temperature freezer (Model number: C85-12, So-Low Environmental Equipment Co., Cincinnati, OH). It was a closed-loop system that incorporated a freezer to provide cold air to the cyclone. The freezer was filled with 185 Kg of thermal ballast. When the freezing system was turned on, it allowed both the thermal ballast and freezer itself to come down to the desired temperature. When air started to run through the closed flow system, the thermal ballast was able to absorb the heat, hence, maintaining a constant air temperature coming out of the freezer. The air was moved by two blowers (Model number: 119104, Ametek, Inc. Kent, OH) in series. A serial blower arrangement was necessary to overcome the pressure drops in the insulated lines, freezer, and cyclone. The flow rate through the cyclone was determined by measuring the pressure drop across the cyclone with a pressure gauge (Model number: 2020, 2030, and 2060, Dwyer Instrument, Inc. Michigan city, IN).

Preliminary heating system for the 1250 L/min cyclone

A preliminary heating system on the 1250 L/min cyclone that provided constant heat flux to the cyclone body was fabricated. Figure 3.5 displays the cyclone with its heaters and thermocouple locations. The system consisted of customized thermofoil

heaters (Chromalox, Houston, TX) and a customized cartridge heater (WATLOW, Houston, TX). Table 3.3 shows the power input to each of the heater elements. The flexible heater was mainly etched foils between two silicone rubbers and then vulcanized. The outer surface of the cyclone was also polished to enhance heat conduction from flexible heaters to the cyclone body by reducing thermal contact resistance. Adhesive tape with good thermal conductivity (Model number: F9469PS, 3M, St. Paul, MN) was used to attach the heaters to the cyclone wall. During testing, the cyclone was placed in a block of Polyurethane foam to thermally isolate the cyclone from the surroundings.

Preliminary heating system for the 100 L/min cyclone

Figures 3.6 and Table 3.4 show a preliminary heating system for the 100 L/min cyclone and its heater specifications, respectively. Commercially available rectangular shape heaters (Table 3.4) were used to apply heat fluxes to the cyclone. While fixed voltage of 120 V was provided into the heaters on the heating system for the 1250 L/min cyclone, input voltage into the heaters for the 100 L/min cyclone was able to be varied using dimmer switches.

Based on previous experience with the 1250 L/min cyclone, the entire cyclone body was wrapped with heaters. A methodology for attaching heaters on the cyclone was the same as one used for the 1250 L/min cyclone. In addition, the cyclone was insulated during tests. Figure 3.6 shows the thermo-couple locations in the 100 L/min cyclone.

Temperature measurement

Temperature of the air entering and exiting the cyclone was measured with T-type thermocouples (Part number: TFE-T-24-SLE, Omega, Inc. Stamford, CT), and the temperature in the cyclone wall was measured with T-type thermocouples (Part number: TT-T-30-SLE, Omega, Inc. Stamford, CT) mounted in the cyclone wall. To embed tiny thermocouples in the wall, holes in 0.030" diameter were drilled and the remaining wall thickness after drilling was only 0.020". Thermo-couples were installed using an epoxy (Model number: Omegabond 101, Omega, Inc. Stamford, CT). The thermal conductivity of the epoxy was 1.04 W/mK and its electrical conductivity was $10^{-15} \Omega^{-1}\text{-cm}^{-1}$. A temperature meter with USB Data Acquisition Modules for Thermocouples Process Signals (Model: OMB-DAQ-56, Omega, Inc. Stamford, CT) was utilized to record the temperatures from the thermocouples. One of the most critical parts for the test was the tip of the skimmer that stayed inside the cyclone. A thin film Resistance Temperature Detector (RTD) was pasted near the tip of the skimmer (Figure 3.7) and the tip temperature was monitored using a single channel RTD meter (Model number: Dpi32, Omega, Inc. Stamford, CT). In addition, a borescope (Model number: PS12, Gradient Lens Corporation, Rochester, NY) was used to observe the inside of the cyclone so that conditions leading to the formation of ice and its location could be visualized.

CHAPTER IV

RESULTS AND DISCUSSION

1250 L/min Cyclone

Aerosol-to-aerosol collection efficiency

The Black and Shaw cyclone and the 1250 L/min cyclone were compared in this section. The 1250 L/min cyclone was operated at an air flow rate of 1250 L/min while the Black and Shaw cyclone was operated at an air flow rate of 900 L/min. Figure 4.1 presents the aerosol-to-aerosol collection efficiency curves for the Black and Shaw cyclone and 1250 L/min cyclone. It can be seen from Figure 4.1 that the aerosol-to-aerosol penetration cut-point for the 1250 L/min cyclone was near 1 μm , very close to that of the Black and Shaw cyclone. The Stk_{50} for both cyclones was around 0.05.

Wetting pattern on the impacting wall – effect of an atomizer

A visualization test was conducted to verify the wetting pattern of liquid spray on the impacting wall using several different angles (45° , 53° , and 60°) between the two needles in the atomizer block. A 1250 L/min cyclone, fabricated out of clear acrylic was used for this test. It was observed that the region of the impacting wall just beneath the spray needle that would be approximately 10 % of the slot length was not wet when the 45° atomizer was used. The region of the impacting wall opposite the atomizer was not wet when using the 60° atomizer. It seemed that an optimum angle would be between

45° and 60°. When the 53° atomizer was tested, the whole impacting wall was evenly wet.

The cyclone with three different atomizers was tested with the 3 µm red PSL. When the 45° and 60° atomizers were used, the red PSL was recovered from the impacting wall using cotton swabs at the end of each test. However, when the 53° atomizer was tested, there was no PSL deposition on the impaction wall, which supports the visualization test result. Therefore, the 53° atomizer has been used when testing the 1250 L/min cyclone.

Aerosol-to-hydrosol collection efficiency

Figure 4.2 presents the aerosol-to-hydrosol collection efficiency as a function of particle size. It is to be noted that the liquid effluent flow rate for both the Black and Shaw cyclone and the 1250 L/min cyclone was 1 mL/min. There was a significant difference in the collection characteristics between the two cyclones for the particle sizes bigger than 2 µm. The aerosol-to-hydrosol collection efficiencies with 0.5 and 1 µm PSL were around 10% and 40%, respectively, for both cyclones. The efficiencies with 2 and 3 µm were around 85% and 93%, respectively for the 1250 L/min cyclone. The efficiencies remained above 90% for particle sizes larger than 3µm. However, with the Black and Shaw cyclone the efficiencies with 2 and 3 µm were around 80% and drops to around 50% with 5µm and 10µm PSL particles. With the Black and Shaw cyclone the wetting pattern on the impaction wall was not as perfect as that with the 1250 L/min cyclone. In addition, liquid bypass was observed every four out of five runs from the Black and Shaw cyclone, which lowered the aerosol-to-hydrosol collection efficiency

represented by large Y-error bars. Higher aerosol-to-hydrosol collection efficiency with the 1250 L/min cyclone indicates the enhancement in performance of the 1250 L/min cyclone. In addition, a relatively small Y-error bar represents that the 1250 L/min cyclone performed well consistently. This was clearly a significant improvement over the predecessor version for which the collection efficiency decreased with increasing particle size beyond 3 μm .

The aerosol-to-hydrosol collection efficiency was converted to the form of concentration factor (Eqn. 4.1) in Figure 4.3. It clearly shows that with the 1250 L/min cyclone, the factor was above 1,000,000 and was almost twice the factor of the Black and Shaw cyclone for particles sizes beyond 5 μm . It is to be noted that the liquid effluent flow rate was 1 mL/min.

$$\text{C.F.} = \frac{\text{Concentration}_{\text{effluent_liquid}}}{\text{Concentration}_{\text{aerosol_inflow_system}}} \quad (4.1)$$

Pressure differential across the cyclone

Experimental results presented in Figure 4.4 show that the pressure differential across the 1250 L/min cyclone at 1250 L/min was about 22 inches of water. In addition, the differential across the Black and Shaw cyclone at 900 L/min was around 26 inches of water. In the 1250 L/min cyclone, more than 30% air could be drawn for the lower pressure differential as that in the Black and Shaw cyclone. The pressure coefficient (K) (Eqn. 4.2) for experimental conditions at which the cyclones were tested was calculated. Figure 4.5 shows a plot for K as a function of the Reynolds number with log-log scales. The K value was approximately 2.7. In addition, the empirical value was compared with that for numerical prediction of the 1250 L/min cyclone (Hu and McFarland, 2007).

$$K = \frac{\Delta P}{\frac{1}{2} \rho_{\text{air}} U_{\text{slot}}^2} \quad (4.2)$$

where,

ΔP = pressure drop across the cyclone.

Debris test

Fine Arizona dust (mass median aerodynamic diameter: 10 μm)

Three different amounts of the dust were injected into the transport pipe and it took about 10 to 15 seconds to release 100 mg. It is to be noted that a peristaltic pump (Fisher Variable-Flow Peristaltic Pumps, Fisher Scientific, Inc. Austin, TX) was used to extract liquid.

- 1) 100 mg: The test was repeated several times and liquid bypass was not observed. After each test, the cyclone was disassembled and the inner surface was observed. The surface was relatively clean.
- 2) 300 mg: The test was repeated twice. Mud was continuously extracted from the cyclone. There was no bypass.
- 3) 400 mg: The test was also repeated twice. The cyclone functioned properly without liquid bypass.

Figure 4.6 shows the inner surface of the cyclone, 6 minutes after releasing 2000 mg of the dust for about four minutes. The liquid removed most dust and the cyclone was functioning for 10 minutes without the bypass. Even when 2000 mg of fine Arizona dust was released into the cyclone for two minutes, mud was continuously extracted and the cyclone performed successfully for the following five minutes.

ASHRAE test dust

This dust consists of 5% cotton-linters, 23% carbon black, and 72% fine test dust (nominal 0-80 μm size). It took about 10 to 15 seconds to inject the dust to release 100 mg.

- 1) 100 mg: The test was repeated 8 times and bypass was observed all the time.
- 2) 40 mg: Liquid bypass was observed.
- 3) 20 mg: There was no bypass and the cyclone performed successfully for the following five minutes.

As shown in Figure 4.7, cotton-linters/carbon not washed by the liquid were still seen on the inner wall and the skimmer, 8 minutes after adding 600 mg of the dust for two minutes.

Second-cut cotton linters

There was liquid bypass when only 20 mg of the linters was injected for a minute. Figure 4.8 shows the inner surface of the cyclone, 6 minutes after adding only 170 mg of the linters for about two minutes. Most linters were still in the cyclone.

Low temperature test

Preliminary heating system - temperature profile with purely air flow

The preliminary heating system (Figure 3.5) with the fixed power input (Table 3.3) was tested with three different incoming air temperatures (-40°C, -26°C, and -20°C). Wall temperatures were monitored using five thermocouples and a thin film RTD. Prior to conducting tests with liquid-in, tests with only air flow were conducted. According to the Eqn. (4.3), liquid flow had almost no effect on wall temperature change, but the air flow would be the dominating factor on wall temperature change.

$$\dot{m} C_p \Delta T_{(air)} \gg \dot{m} C_p \Delta T_{(water)} \quad (4.3)$$

where,

\dot{m} = mass flow rate (0.028333 Kg/s for air at -23°C and 0.000016667 Kg/s for water at -23°C)

C_p = specific heat (1009 J/KgK for air at -23°C and 4200 J/KgK at 23°C)

1) Air temperature: -40°C

Figure 4.9 shows the temperature profiles from thermo-couples when the heating system and blowers were turned on simultaneously. Dark blue line represents the incoming air temperature. Temperature at the 'C' location reached 0°C within 1 minute after turning on blowers. Temperatures of the rest of the locations fell below 0°C within 3 to 9 minutes. From the temperature profiles, it was concluded that a liquid freezing problem would arise in the cyclone if the incoming air temperature was -40°C.

2) Air temperature: -26°C

When the cyclone was tested with -26°C incoming air, temperatures in the wall except the 'A' location remained above 0°C (Figure 4.10). Therefore, the freezing problem would not be expected if the air temperature was around -26°C .

3) Incoming air temperature: -20°C

Wall temperatures remained well above 0°C when the cyclone was tested at -20°C (Figure 4.11). It was also expected that the cyclone would perform successfully at -20°C .

Preliminary heating system - temperature profile with liquid-in

After verifying the wall temperature profiles with purely air flow, tests with liquid-in were conducted. The same preliminary heating system and fixed power input were used. As expected, ice formed on the inner wall of the 1250 L/min cyclone and the skimmer tip at -40°C . An interesting observation was captured using the borescope when the incoming air temperature was around -26°C . There was a significant amount of ice on the narrow ($\sim 0.45''$) band between heater #2 and #3 and also on the open area ($0.7'' \times 1.2''$) (Figure 4.12) for a RTD near the bottom of the impacting wall. Figure 4.13 shows this ice build up. From this observation, it was concluded that heat could not spread toward the sides when the incoming air temperature was extremely cold (-20°C or below). Therefore, it was suggested that the cyclone must be completely wrapped with heaters to prevent this problem. Figure 4.14 shows ice on the vortex finder when power for the vortex finder cartridge heater was turned off, which confirmed the necessity of the vortex finder cartridge heater.

Final heating system

From the empirical observation and a numerical study (Hu, S. 2007) regarding low temperature tests, a final heating system was designed (Figure 4.15). There were several differences between the preliminary heating system and final heating system. The size of the open window for the final system was 0.4"×0.4", while the size for the preliminary system was 0.7"×1.2". The narrow band between two heaters no longer existed with the final system. Variable heat flux was applied through the final system - a higher heat flux was applied where the average flow velocity was relatively faster (higher heat transfer coefficient) such as the slot area. Table 4.1 compares the applied heat flux between the two heating systems. Total power input for the final heating system was approximately 315W. Figure 4.16 shows the temperature profiles from the RTDs (Figure 4.15-a) when the cyclone with the final heating system was tested with purely air flow (incoming air ~ -30°). In conclusion, the 1250 L/min cyclone with the final heating system was able to work with -24°C air without any freezing problems.

Conclusion for the 1250 L/min cyclone

Efforts were taken to upgrade the Black and Shaw cyclone. As a result, a 1250 L/min wetted wall cyclone was developed. The aerosol-to-aerosol penetration cutpoint of the 1250 L/min cyclone was 0.95 μm ($\text{Stk}_{50} = 0.05$). The aerosol-to-hydrosol collection efficiency was > 90% for particle sizes greater than, or equal to, about 3 μm . In addition, the concentration factor was above 1,000,000. Pressure drop across the 1250 L/min cyclone was approximately 22 inches of water at a nominal flow rate of 1250 L/min.

According to the debris test, fine Arizona dust up to 1000 mg/min did not cause liquid bypass. However, small amount (20 mg/min) of the linters that could not be extracted plugged the liquid flow gap and the skimmer nose gap, which caused the bypass.

Cold temperature tests were conducted to prevent liquid from freezing in the cyclone. According to experimental and numerical studies, a final heating system that consumed 315 W (power budget: 350 W) was developed. The 1250 L/min cyclone equipped with the final heating system could operate at -24°C.

100 L/min Cyclone

Aerosol-to-aerosol collection efficiency

Experimental evaluation of a preliminary version of the 100 L/min cyclone (version 1.0) indicated that the aerosol-to-aerosol penetration cutpoint was 1.45 μm . Stokes scaling methodology was adopted to design the subsequent version (version 2.0) in which the slot width was reduced by 30% to obtain the desired cutpoint value (1 μm) according to the Eqn. (4.4).

$$Stk_{50,1} = \frac{d_{p50,1}^2 C_C \rho_P U_1}{9\eta D_{j,1}} = Stk_{50,2} = \frac{d_{p50,2}^2 C_C \rho_P U_2}{9\eta D_{j,2}}$$

$$\frac{d_{p50,1}^2 U_1}{D_{j,1}} = \frac{d_{p50,2}^2 U_2}{D_{j,2}} \Rightarrow \frac{d_{p50,1}^2 Q_1}{W_{j,1}^2} = \frac{d_{p50,2}^2 Q_1}{W_{j,2}^2}$$

$$\frac{d_{p50,1}}{W_{j,1}} = \frac{d_{p50,2}}{W_{j,2}} \quad (4.4)$$

Figure 4.17 presents the aerosol-to-aerosol collection efficiency curves for the 100 L/min cyclone version 1.0 and 2.0. It can be seen from the Figure that the cutpoint of the cyclone version 2.0 was 1.05 μm , very close to the desired value of 1 μm . Further studies with the 100 L/min cyclone were performed using version 2.0.

Aerosol-to-hydrosol collection efficiency

It is to be noted that the 53° atomizer was used for the 100 L/min cyclone because the impaction wall was evenly wet with the atomizer. Figure 4.18 presents the aerosol-to-hydrosol collection efficiency for the 100 L/min cyclone. It can be seen that the efficiency was above 85%, for particle sizes larger than 2 μm . It is to be noted that the liquid effluent flow rate was 0.1 mL/min and 0.025% v/v of Tween-20 was used as a collection fluid. The above result, converted to the form of the concentration factor, presented in Figure 4.19, clearly shows that the factor was of the order of 900,000 for particles sizes beyond 2 μm .

Pressure differential across the cyclone

Experimental results presented in Figure 4.20 show that the pressure differential across the 100 L/min cyclone followed a quadratic increase with increasing flow rate and was about 6.4" for an air flow rate of 100 L/min. The K value from the cyclone was close to 2.5 (Figure 4.5).

Sensitivity studies

A series of sensitivity studies were performed to examine the effect of certain select parameters on the performance characteristics of the cyclone. Furthermore, studies were performed to assess the time response of the device to an input signal.

Effect of wetting agent (Tween-20)

Wetting agent is a substance that reduces the surface tension of the liquid and aids the liquid to spread out more easily and evenly across the cyclone walls. In other words, use of a wetting agent improves the aerosol-to-hydrosol collection efficiency. Tween-20 was used as a wetting agent in this study. Effect of the wetting agent on the aerosol-to-hydrosol collection efficiency of the cyclone was examined for a particle size of 3 μm and liquid effluent flow rate of approximately 0.1 mL/min. Figure 4.21 shows the aerosol-to-hydrosol collection efficiency as a function of volume fraction of Tween-20. It can be seen that the concentration of the wetting agent needed to be at least 0.025%v/v, to maximize the aerosol-to-hydrosol collection efficiency. Further increase in the concentration did not affect the collection.

Effect of liquid effluent flow rate

Effect of the liquid (0.025% v/v of Tween-20) effluent flow rate on the performance was examined. This is one of the most important parameters that influence the extent to which the aerosol deposited on the cyclone walls can be recovered. While a low liquid effluent flow rate may not be sufficient to recover the entire deposited aerosol, a high value may decrease the concentration factor, in spite of being able to recover more

aerosols. Hence, the primary objective of this study was to determine the optimum value of the liquid flow rate that needed to be used.

Figure 4.22 presents the results of the aerosol-to-hydrosol collection efficiency as well as the concentration factor, obtained during the testing of several different liquid effluent flow rates. It can be seen that while there was a slight increase in the collection efficiency initially with an increase in the liquid rate, the curve nearly flattened out at further increase. However, increasing liquid flow rate was seen to drastically decrease the concentration factor. A four-fold increase in the liquid flow rate reduced the concentration factor by a factor of 4. In this respect, it seems that the optimum value would be governed by the sensitivity requirements of the analysis mechanism that would be downstream of this stage.

Time constant

Time constant is defined as the time required for the response to an input stimulus to rise from zero to 63.2% of its final steady value. The test was essential to estimate the minimum time it takes for the cyclone to collect and extract the hydrosol. There were two kinds of experiments for the time constant test. One was a “wet start” experiment and the other was a “dry start” experiment. For the “wet start” experiment, prior to collecting the hydrosol samples, the whole system was turned on and brought into steady-state condition. Hence, results of this study would be categorized as the “wet start” time constant response. PSL of 3 μm size was used for this test. The test consisted of three cyclone runs and nine reference runs. Table 4.2 provides the series of procedures and time sequence followed in the conduct of the tests.

For the initial response of the system, fraction of the full-scale (F) for each sample was first found according to

$$F = \frac{\eta_{AH}}{\bar{\eta}_{AH}} \quad (4.5)$$

where,

$\bar{\eta}_{AH}$ = average aerosol-to-hydrosol collection efficiency over all of the samples near the full-scale collection capability of the cyclone.

For each test of a cyclone, the first five samples following the start of the PSL flow were used to evaluate the initial response. These values were then averaged together and a curve whose equation is given in (4.6) was fit.

$$F = 1 - \frac{1}{1 + At^B} \quad (4.6)$$

where the constants A and B are found by optimizing the curve fit. The time at which 63% of the full-scale collection efficiency was realized (t) could then be calculated using Equation (4.6) and the values of A and B . The time constant for the decay of the cyclone, once the aerosol input was removed, was found using the Eqn (4.7)

$$F = \frac{1}{1 + At^B} \quad (4.7)$$

and the same techniques for the initial response were followed.

The instantaneous hydrosol collection efficiencies obtained as a function of time with “wet start” are presented in Figure 4.23. According to the full-scale collection efficiency, the time constant response of the cyclone was shown to be 1.16 minutes and the decay response of the cyclone was 1.78 minutes.

Figure 4.24 shows the instantaneous hydrosol collection efficiency as a function of time with “dry start”. According to the full-scale collection efficiency, the time constant response of the cyclone was shown to be 1.8 minutes and the decay response of the cyclone was 1.53 minutes.

As verified by Phull (2005), time constant responses of the 1250 L/min cyclone with “wet start” and “dry start” were 1.25 minutes and 1.2 minutes, respectively.

Rate of liquid evaporation

For long term operation, it is necessary to achieve low liquid evaporation in the 100 L/min cyclone. The 100 L/min cyclone consumes approximately 0.25 mL/min at room temperature, which amounts to about 11 L in 30 days. This creates significant need for water in field tests, where the availability may be sometimes low. In addition, when the cyclone is operated in hot and dry condition, rate of liquid evaporation would be higher. Thus, efforts were invested to find ways to reduce the rate of liquid evaporation in the cyclone. The first method uses a mixture of water and ethylene glycol (EG) as a collection fluid. In the second method, the cyclone body is enclosed in an ice bath to chill the liquid film in the cyclone. Combination of these two methods would work towards reducing the vapor pressure of the liquid film, resulting in reduced evaporation rate.

Effect of ethylene glycol (EG) on the evaporation rate

According to Raoult’s law, if the water is mixed with other materials, e.g. EG, the mole fraction of the water in the mixture would decrease. Consequently, the saturation

vapor pressure of the water would decrease. For example, when the volume fraction of EG in a solution is 0.3, the mole fraction of water would be approximately 0.877 compared to pure water. As shown in Figure 4.25, the evaporation rate decreased by about 20-30% when a solution containing 30% EG was used as a collection fluid.

Effect of cooling the cyclone using ice water on the evaporation rate

The saturation vapor pressure of water increases quadratically with increasing temperature. In other words, the average energy of the particle present would increase when temperature is increased. This implies that more of them are likely to have enough energy to escape from the surface of the liquid, which will result in an increase of saturation vapor pressure and the evaporation rate. Thus, the evaporation rate of the liquid inside the cyclone could be reduced if the liquid film could be cooled. The liquid rivulets in the cyclone are very thin and heat capacity of the liquid rivulets is much less than that of the cyclone wall. Therefore, it is reasonable to assume that the temperature of the liquid rivulets would be the same as that of the cyclone wall. The cyclone wall was chilled by submerging the whole cyclone in ice water ($\sim 1^{\circ}\text{C}$). As shown in Figure 4.26, the evaporation rate for pure water in a cooled cyclone was around 15 % lower.

Effect of EG in a cooled cyclone on the evaporation rate

The evaporation rate was decreased by about 40% when 30% EG solution was used in the experiment and the cyclone was cooled (Figure 4.27).

Effect of EG in a cooled cyclone on the particle collection

At room conditions, three different EG concentrations (30%, 40%, and 50%) were tested with 3 μm PSL. As shown in Table 4.3, the aerosol-to-hydrosol collection efficiency was around 63% when the liquid effluent flow rate was 0.1 mL/min. However, the collection efficiency was around 94% when the liquid effluent flow rate was around 0.19 mL/min (Table 4.4). In addition, effect of liquid (30% EG) effluent flow rate on collection efficiency was verified and the results are shown in Table 4.5. It would be recommended that the effluent flow rate be around 0.16 mL/min to yield collection efficiency above 90%.

When the liquid (0.025% v/v Tween-20) in-flow rate in the 100 L/min cyclone was 250 $\mu\text{L}/\text{min}$, the liquid effluent flow rate was around 100 $\mu\text{L}/\text{min}$ at room condition and the aerosol-to-hydrosol collection efficiency for 3 μm PSL particle was around 83.4%. When 30% EG was used in a cooled cyclone, the liquid effluent flow rate was about 135 $\mu\text{L}/\text{min}$ when the in-flow rate was 150 $\mu\text{L}/\text{min}$. The aerosol-to-hydrosol collection efficiency at the testing condition was about 77% for 3 μm PSL particles. The particle collection efficiency remains at a similar level, but the total liquid in-flow rate decreased from 250 to 150 $\mu\text{L}/\text{min}$, which resulted in a total liquid consumption of about 40% (Table 4.6).

Low temperature test

Preliminary heating system - temperature profile with purely -22°C air

Several different heat fluxes in the heaters #2 and #3 (Figure 3.6) were tested to verify how much heat flux would be required to maintain the inner wall temperatures ('A' and 'B' locations) around 10 °C when incoming air temperature was -22°C. Figure 4.28 shows that temperature at the two locations remained around 10°C when the heat fluxes of 4.2 W/in² and 2.96 W/in² were applied to the heater #2 and #3, respectively.

Preliminary heating system - temperature profile with -22°C air and also with liquid-in

Efforts were taken to verify the minimum power/heat-flux input to prevent liquid from freezing at -22°C. During this test, the inner wall temperatures were monitored using thermo-couples and the cyclone inside was continuously observed using the borescope. The flux value for each heater was decreased gradually from the values in Table 4.7. The reason why the flux of 5 W/in² in Table 4.7 was chosen as the initial value was because it was learned from Figure 4.28 that the value would be high enough to prevent liquid from freezing at -22°C. First the vortex finder cartridge heater was examined. When the flux value for the cartridge heater was decreased down to 2.55 W/in², ice was not observed for 15 minutes on the vortex finder. With the voltage control methodology using a dimmer switch, the value of 2.55 was the smallest; hence, the value of 2.55 W/in² would be an optimized flux value for the cartridge heater (Table 4.8).

For a skimmer heater, the liquid was able to be collected for 15 minutes without any freezing issues when the flux value for the skimmer heater was 4.7 W/in². When testing the flux values, lower than 4.7 for the heater, ice started to build on the skimmer

during operation. Table 4.9 shows the applied flux for the heating system after optimizing the skimmer heater.

The same methodology was applied for the rest of the heaters when determining the minimum heat fluxes. Table 4.10 shows the optimized heat flux value for the preliminary heating system for the 100 L/min cyclone to prevent liquid from freezing at -22 °C.

Final heating system for -22°C air

According to the experimentally obtained results in Table 4.10 and design experience of the final heating system for the 1250 L/min cyclone, a final custom-made heating system was proposed in Figure 4.29. Figure 4.30 displays the 100 L/min cyclone with the final heating system. Total power input for the heating system would be 27 W to prevent liquid from freezing when the incoming air temperature was -22 °C.

Preliminary heating system - temperature profile with -32°C air and also with liquid-in

Experiments were conducted to verify the minimum heat fluxes at each location (Figure 3.6) when incoming air temperature was -32 °C. Table 4.11 shows the heat flux values for the preliminary heating system as initial values. The values in Table 4.11 were twice of the optimized values at -22 °C (Table 4.10). Then the fluxes were decreased to verify the minimum heat flux values. It is to be noted that the cyclone performed normally without any ice formation for 15 minutes at -32°C when the values in Table 4.11 were applied into the system. Then the flux values were reduced gradually to determine the minimum ones. The flux values for each heater were optimized in the

same approach as previously mentioned in case of -22°C air. Table 4.12 shows the optimized flux values at -32 °C incoming air temperature. The cyclone performed successfully for 15 minutes at -32 °C when the values in Table 4.12 were applied. Total power consumption was approximately 50 W.

Conclusion for the 100 L/min cyclone

A new wetted wall cyclone with an operational flow rate of 100 L/min and an aerosol-to-aerosol penetration cutpoint of 1 µm was developed. Pressure differential across the cyclone was estimated to be about 6.4 inch of water (1.6 KPa) at the flow rate of 100 L/min. The aerosol-to-hydrosol collection efficiency was around 85% with three drops of hydrosol every minute (0.1 mL/min), for particle sizes larger than 2 µm. This resulted in a high value of the concentration factor (of the order of 900,000) with the above liquid effluent flow rate.

While the aerosol-to-hydrosol collection efficiency could be increased up to 94% by increasing the liquid effluent flow rate to 0.4 mL/min, it would also result in a reduction in the concentration factor. Results of sensitivity studies performed to examine the effect of wetting agent (Tween-20) showed that the aerosol-to-hydrosol collection efficiency was not affected as long as the concentration of the agent was above 0.025%. Results of time-response studies showed that the cyclone time constant response was approximately 1.16 minutes and 1.8 minutes for “wet start” and “dry start”, respectively.

It was found that the evaporation rate can be decreased by 40% when 30% EG solution in a cooled cyclone was used in the experiment. In addition, the ethylene glycol

(EG) as a collection fluid would not degrade the aerosol-to-hydrosol collection efficiency as long as the liquid effluent flow rate was around 0.15 mL/min.

From cold temperature tests, it was verified that approximately 30 W and 50 W were required to prevent liquid from freezing at -22°C and -32°C for the 100 L/min cyclone, respectively.

CHAPTER V

PERFORMANCE MODELING OF A FAMILY OF WETTED WALL CYCLONES

Motivation

Moore and McFarland (1990) had previously evaluated the performance of family of Stairmand type mini-cyclones. Results of their study demonstrated that the aerosol performance characteristics were a function of the Reynolds number over a fairly wide range of the Reynolds numbers (Re). Zhu and Lee (1999) studied a family of cyclones, smaller than Moore and McFarland cyclones. They also verified that the Stk_{50} number was affected by the Reynolds number.

It is important to recall here that both the nature of flow and the geometrical features in the current generation of bioaerosol sampling cyclones are different. For example, unlike the traditional Stairmand type cyclone evaluated by Moore and McFarland (1990) and Zhu and Lee (1999), current family of the wetted wall cyclones (100, 300, and 1250 L/min cyclones) has a converging inlet section. Further, flow impacting on the cyclone wall swirls and exits the cyclone on the far-end (Seo et al., 2006, Hu and McFarland, 2007). In addition, the Reynolds number values (calculated based on the entrance slot width and average velocity) of the wetted wall cyclones spanned a shorter range (3,500 to 30,000).

The above features prompted us to undertake a closer inspection of the experimental results obtained from a family of three cyclones operating over a wide

range of physical flow rate values, with the primary objective of determining if there would exist a common basis for the performance of the cyclones. This chapter presents the outcome of the above investigation; theoretical models were evolved to predict the collection efficiency characteristics as a function of the Reynolds and Stokes numbers and the variation of the cut-point Stokes number (Stk_{50}) with the Reynolds number.

Aerosol-to-Aerosol Collection Efficiency

Performance characteristics were obtained at several flow rates for each cyclone: the 100 L/min cyclone at air flow rates of 80, 100, 120, 160, and 200 L/min, the 1250 L/min cyclones at air flow rates of 400, 640, 750, 1000, 1250, and 1500 L/min, and the 300 L/min at air flow rates of 120, 150, 170, 185, 200, 240, 300, and 400 L/min, respectively. Table 5.1 consolidates the whole range of experiments performed on the different cyclones at various flow rates in terms of the Reynolds numbers.

Figures 5.1 and 5.2 show the aerosol-to-aerosol collection efficiency characteristics of the 100 L/min cyclone and 1250 L/min cyclone, respectively. Figure 5.3 shows the characteristics of the 300 L/min cyclone. It can be seen from the figures that the efficiency curves converged at the higher efficiency end ($>90\%$) and for the Stokes numbers mostly beyond a value of 0.2. However, the tail region of all the efficiency curves clearly exhibited a preferential shift toward lower Stokes number values for increasing values of the physical flow rate (Reynolds numbers), suggesting that there would exist a dependence of the cut-point (Stk_{50}) value on the Reynolds number.

The aerosol-to-aerosol collection efficiency curve for the 1250 L/min cyclone at 1250 L/min was re-plotted in the form of the lognormal distribution in Figure 5.4.

The slope of the aerosol-to-aerosol collection efficiency curves was determined by the parameter (Eqn. 5.1),

$$\sigma_g = \sqrt{\frac{D_{84}}{D_{16}}} \quad (5.1)$$

where,

D_{84} = particle size that corresponds to the A-A collection efficiency of 84%

D_{16} = particle size that corresponds to the A-A collection efficiency of 16%.

The slope for all nineteen curves in the wetted wall cyclones was 1.54 ± 0.05 , from which it was learned that the efficiency curve was independent of the Reynolds number. The slope of the Stairmand-type sampling cyclones (Moore and McFarland, 1990) was seen to be 1.49 ± 0.04 .

Aerosol Performance of Three Cyclones at Similar Reynolds Numbers

A collation of experimental data indicates that the performance characteristics of the different devices exhibited a trend governed by dynamic similarity. Collection efficiency curves obtained on the different cyclones at similar Reynolds numbers are presented in Figures 5.5 through 5.7, for Reynolds numbers in the range of 3500 and 13000. While Figure 5.5 presents a comparison of the performance curves of 100 and 300 L/min cyclones operating at different flow rates corresponding to a Reynolds number of 3600, Figures 5.6 and 5.7 present a comparison of the performance curves of the 300 and 1250 L/min operating at different flow rates but closed to a Reynolds number value of 7800 and 12700, respectively.

It can be seen from the presented data that the classification characteristics were very close for similar Reynolds number values. This result clearly indicates that

irrespective of the flow rates, performance characteristics of the different cyclones were identical when standardized to the Reynolds number basis. Further, when the above result was considered in unison with the previous results, it emerges that the cut point Stokes number for the current family of cyclones could be expressed as a function of the Reynolds number, irrespective of the physical flow rate and the geometrical details of the cyclone.

Regression Process

Efforts were invested to correlate the experimental data obtained on the different cyclones over the whole range of physical flow rates using special curve-fitting software (Sigma Plot). Different variations of the standard sigmoidal and logistic functions were examined on the nineteen sets of experimental data to determine the best correlation. Results of the above effort indicated that two different correlations had to be developed; one for the high Reynolds number region ($Re > 6400$) and the other one for the low Reynolds number region ($Re < 6400$). The general form of the function for the low Re region was

$$\text{Sigmoid, 3 parameter, } y = \frac{a}{1 + e^{-\left(\frac{x-b}{c}\right)}} \quad (5.2),$$

whereas that for the high Re region was

$$\text{Logistic, 3 parameter, } y = \frac{a}{1 + \left(\frac{x}{b}\right)^c} \quad (5.3)$$

In the above equations, y is the aerosol-to-aerosol collection efficiency and x is the Stokes number. Parameters a , b , and c are either constants or functions of the Reynolds number and obtained by a regression analysis of the combined experimental data.

High Reynolds number region

Using all six sets of data from the 1250 L/min cyclone, four sets of data (at 200 L/min, 240 L/min, 300 L/min, and 400 L/min) from the 300 L/min cyclone, and two sets of data (at 160 L/min and 200 L/min) from the 100 L/min cyclone, the original equation was as follows,

$$\eta_{A-A} = \frac{96.85 - 0.0002 \times \text{Re}_{\text{SlotWidth}}}{1 + \left(\frac{\text{Stk}}{0.1143 - 2 \times 10^{-6} \times \text{Re}_{\text{SlotWidth}}} \right)^{(-1.894 + 8 \times 10^{-6} \times \text{Re}_{\text{SlotWidth}})}} \quad (5.4)$$

After tuning the original equation, a final form of the correlation was shown in Eqn. (5.5).

$$\eta_{A-A} = \frac{100}{1 + \left(\frac{0.114 - 2 \times 10^{-6} \times \text{Re}_{\text{SlotWidth}}}{\text{Stk}} \right)^{2.07}} \quad (5.5)$$

Figure 5.8 presents a comparison of the predictions obtained from the above correlation to experimental data spread over Reynolds number values that range from 6400 to 30000 that showed good agreement; R-Square values for all twelve data points were seen to be greater than 0.99, indicating an excellent fit to experimental data.

Low Reynolds number region

Three sets of data (80 L/min, 100 L/min, and 120 L/min) from the 100 L/min cyclone and four sets of data (120 L/min, 150 L/min, 170 L/min, and 185 L/min) from the 300 L/min cyclone were used for obtaining the correlation for this region. An original form of the equation was

$$\eta_{A-A} = \frac{98.267 - 0.0004 \times \text{Re}_{\text{SlotWidth}}}{1 + e^{-\left(\frac{\text{Stk} - 0.2011 + 1 \times 10^{-5} \times \text{Re}_{\text{SlotWidth}}}{0.0566 - 2 \times 10^{-6} \times \text{Re}_{\text{SlotWidth}}}\right)}} \quad (5.6)$$

After several tuning, the original equation was changed to the final form (Eqn. 5.7).

$$\eta_{A-A} = \frac{100}{1 + e^{-\left(\frac{\text{Stk} - 0.2 + 1.2 \times 10^{-5} \times \text{Re}_{\text{SlotWidth}}}{0.057}\right)}} \quad (5.7)$$

Representative comparisons of the correlation predictions to experimental data for the low Reynolds number region are shown in Figure 5.9, and indicated a fairly good comparison. It was seen that the R-Square value for data points in this region were 0.96 and higher, except for one data point for which it was around 0.953. Table 5.2 presents a summary of the above results in which the parameters a, b, and c were displayed for each group. It can be seen that while parameters a and c were constants, parameter b was a function of the Reynolds number.

Relationship between the Stk_{50} Number and Reynolds Number in the Cyclones

Cutpoint Stokes number (Stk_{50}) value deduced from the curve-fitting procedure for each of the nineteen data sets are expressed as a function of the Reynolds number in

Figure 5.10. It can be seen that the relationship between Reynolds number and the Stk_{50} was inversely proportional. There was an initial drastic reduction in the cutpoint value at the lower Reynolds numbers that evolved into a more gradual reduction for higher Reynolds numbers.

Conclusion

Experimental data for the aerosol-to-aerosol collection efficiency obtained on three wetted wall cyclones operating at physical flow rates ranging from 80 L/min to 1500 L/min were used to obtain theoretical correlations that expressed the performance of the wetted wall cyclones. Nineteen Stokes curves generated over a wide range of the Reynolds number from 3500 to 30000 were used in this effort.

Analysis of the data sets undertaken using the special curve-fitting software (Sigma Plot) revealed that the performance of the entire data set could be collapsed into two groups, based on the Reynolds number. Non-dimensional empirical correlations to predict the classification characteristics of each group of data were also evolved. A comparison of the correlation predictions to the experimental data for the high Reynolds number ($6400 < Re < 30000$) group shows that the R-Square values were more than 0.99, while that for the low Reynolds number region ($3500 < Re < 6400$) indicates that the R-Square values were higher than 0.95. Overall difference between experimental data and correlation predictions were smaller than the experimental uncertainty for the aerosol-to-aerosol collection efficiency, which was 5.21%.

CHAPTER VI

SUMMARY AND FUTURE WORK

A family of wetted wall bioaerosol sampling cyclones (1250 L/min and 100 L/min cyclone) that operate at a range of flow rates have been successfully developed based on the understanding obtained from combined experimental and numerical investigations performed on a preliminary version (Black and Shaw). Two major problems (liquid bypass and ring of recirculation), observed from the Black and Shaw cyclone were successfully eliminated during the development. The aerosol-to-aerosol penetration cutpoint from both the cyclones was approximately 1 μm . The aerosol-to-hydrosol collection efficiencies for the 1250 L/min cyclone and 100 L/min cyclone were > 90% and > 85%, respectively for particle sizes larger than 3 μm , with the concentration factors being >1,000,000 and approximately 900,000, respectively. In addition, the new family of cyclones are also operated at lower pressure drop values (a measure of the ideal power consumption) while being able to operate at higher values of flow rates. There was only 22 inches of water differential across the 1250 L/min cyclone at a nominal flow rate of 1250 L/min. The pressure differential across the 100 L/min cyclone was 6.4 inches of water, which was less than the initial objective (10 inches of water).

The heating system for the 1250 L/min cyclone that consumes only 317 W (power budget: 350 W) was successfully designed and developed. This system enables the 1250 L/min cyclone to operate with temperature of the incoming air as low as -24°C . For the 100 L/min cyclone, final heating system that consumed only 30 W to prevent liquid from

freezing at -22°C was designed. In addition, it was verified that 50 W would be required to prevent liquid from freezing at -32°C for the 100 L/min cyclone.

Efforts were taken to evolve empirical correlations that could predict the aerosol performance in the cyclone as a function of the Reynolds number and Stokes number. As a result, two correlations were developed; one for high Reynolds number (> 6400), and the other for low Reynolds number (< 6400). There was very good agreement between the measured data and the predicted data according to the correlations. R-Square values for most comparisons of the measured and predicted data were seen to be greater than 0.99. When developing a different size cyclone, the aerosol performance in the cyclone should be predicted using this performance modeling correlation.

REFERENCES

- Black, R.S. and Shaw, M.J. (2002). *Scientific Conference on Obscuration and Aerosol Research*. U.S. Army Research, Development and Engineering Command/Edgewood Chemical Biological Center, Edgewood, MD.
- Errington, F.P. and Powell, E.O. (1969). A Cyclone Separator for Aerosol Sampling in the Field. *J. Hyg.* 67:387-399.
- Hinds, W.C. (1999). *Aerosol Technology, Properties, Behavior, and Measurement of Airborne Particles*. 2nd Edition. John Wiley & Sons, New York.
- Hu, S. and McFarland, A.R. (2007). Numerical Performance Simulation of a Wetted Wall Bioaerosol Sampling Cyclone. *Aerosol Sci. Technol.* 41(2):160-168.
- Hu, S. (2007). Application of Computational Fluid Dynamics to Aerosol Sampling and Concentration. Ph.D. Dissertation, Department of Mechanical Engineering, Texas A&M University, College Station, TX.
- Kline, S.J., and McClintock, F.A. (1953). Describing Uncertainties in Single Sample Experiments. *Mechanical Engineering*. 75(1): 38.
- Moncla, B. (2004). A Study of Bioaerosol Sampling Cyclones. M.S. Thesis, Department of Mechanical Engineering, Texas A&M University, College Station, TX.
- Moore, M.E., and McFarland, A.R. (1990). Design of Stairmand-Typr Sampling Cyclones, *Am. Ind. Hyg. Assoc. J.* 51(3):151-159.
- Phull, M. (2005). An Improved Wetted Wall Bioaerosol Sampling Cyclone. M.S. Thesis, Department of Mechanical Engineering, Texas A&M University, College Station, TX.

- Seo, Y., Hu, S., Haglund, J.S., and McFarland, A.R. (2006). Experimental Study for Bioaerosol Collector Cyclone. *7th International Aerosol Conference*, St. Paul, MN.
- White, L.A., Hadley, D.J., Davids, D.E., and Naylor, R. (1975). Improved Large-volume Sampler for the Collection of Bacterial Cells from Aerosol. *Appl. Microbiology*. 29:335-339.
- Zhu, Y. and Lee, K.W. (1999). Experimental Study on Small Cyclones Operating at High Flowrates. *J. Aerosol Sci.* 30:1301-1315.

Other Sources Consulted

- Blachman, M.W. and Lippman, M.(1974). Performance Characteristics of the Multicyclone Aerosol Sampler. *Am. Ind. Hyg. Assoc. J.* 35:311-326
- Buchanan, L.M., Harstad, J.B., Phillips, J.C., Lafferty, E., Dahlgren, C.M., and Decker, H.M. (1972). Simple Liquid Scrubber for Large-Volume Air Sampling. *Appl. Microbiology*. 23:1140-1144.
- Fox, R.W., McDonald, A.T. and Prichard, P.J. (2004). *Introduction to Fluid Mechanics*. 6th Edition. J. Wiley & Sons, Inc., New York.
- Gnielinski, V. (1976). New Equations for Heat and Mass Transfer in Turbulent Pipe and Channel Flow, *Int. Chemical Engr.* 16:359-368.
- Haglund, J. (2003). Two Linear Slot Nozzle Virtual Impactors for Concentration of Bioaerosols. Ph.D. Dissertation, Department of Mechanical Engineering, Texas A&M University, College Station, TX.

- Hari, S., Hassan, Y.A., and McFarland, A.R. (2005). Computational Fluid Dynamics Simulation of a Rectangular Slot Real Impactor's Performance. *Nuclear Engineering and Design*. 235:1015-1028.
- Lefebvre, A.H. (1989). *Atomization and Sprays*. Hemisphere Publishing Corporation, NY.
- May, K.R. (1973). The Collison Nebulizer. Description, Performance & Application. *J. Aerosol Sci.* 4:235-243.
- Moore, M.E. and McFarland, A.R. (1993). Performance Modeling of Single-Inlet Aerosol Sampling Cyclones. *Environ. Sci. Technol.* 27:1842-1848.
- Ortiz, C. and McFarland, A. (1985). A 10- μm Two-Stage Inlet for Sampling Indoor Aerosols. *J. Air Pollution Control Association*, 35:1057-1060.
- Phan, H. (2002). Aerosol-to-Hydrosol Transfer Stages for Use in Bioaerosol Sampling. M.S. Thesis, Texas A&M University, College Station, TX.

APPENDIX

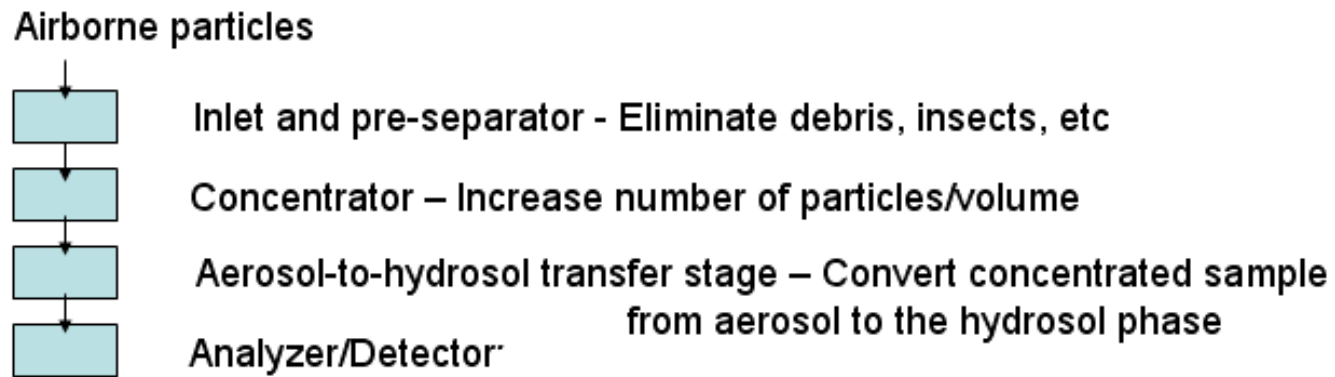


Figure 1.1. Typical near-real-time liquid-based detection system.

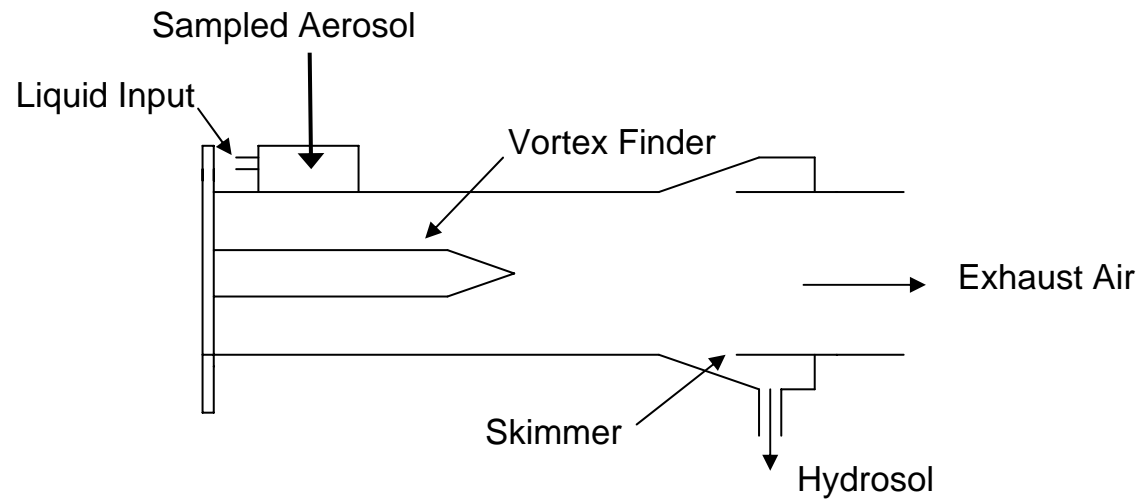


Figure 1.2. Wetted wall cyclone.

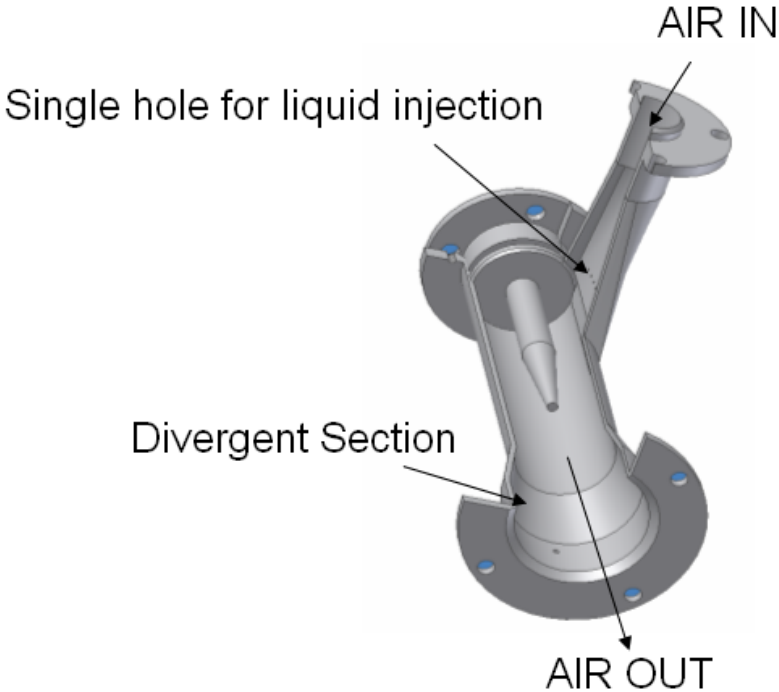


Figure 1.3. Section view of the Black and Shaw cyclone.

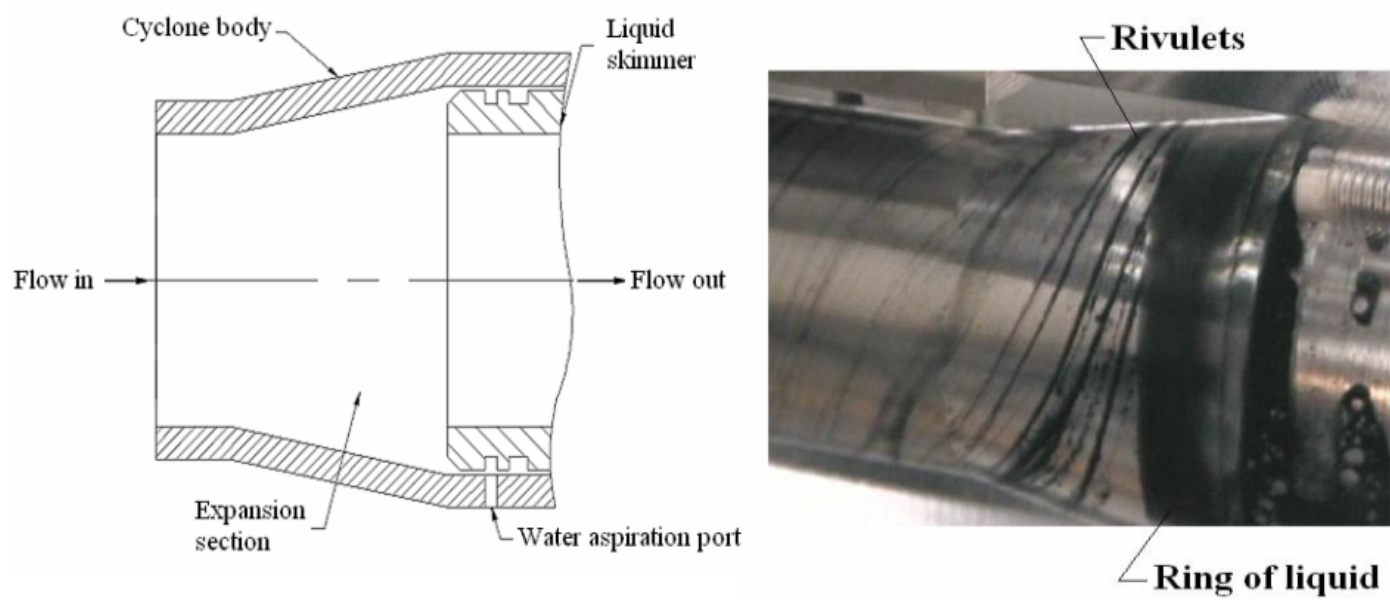


Figure 1.4. Interface between the skimmer and the body of the Black and Shaw cyclone.

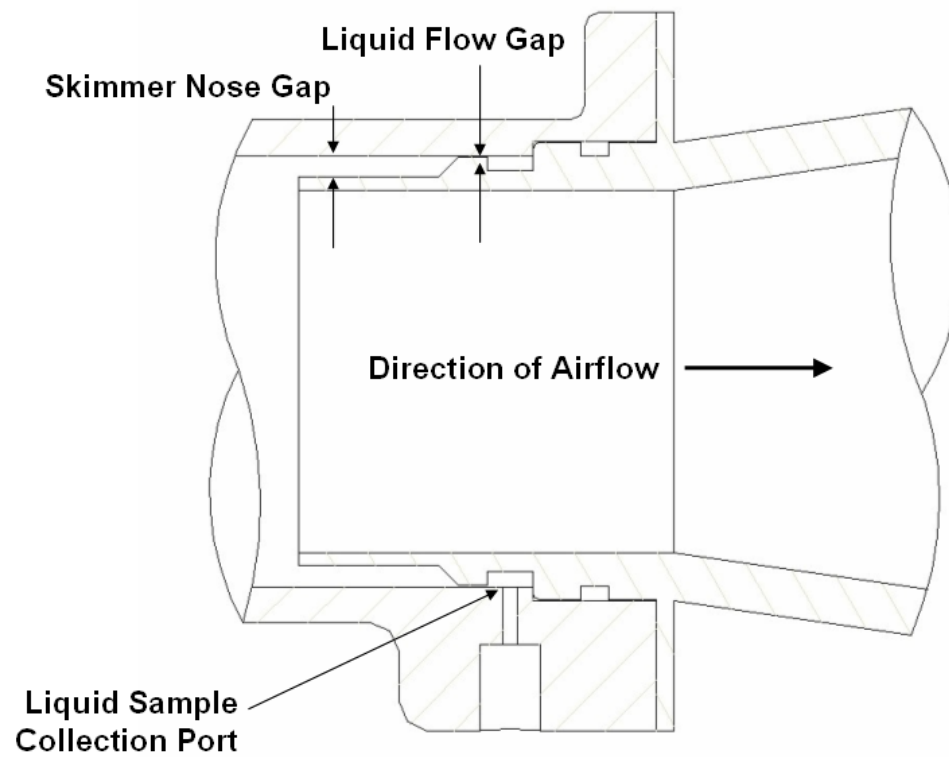


Figure 2.1. Interface between a redesigned liquid skimmer and the body of the 1250 L/min cyclone.

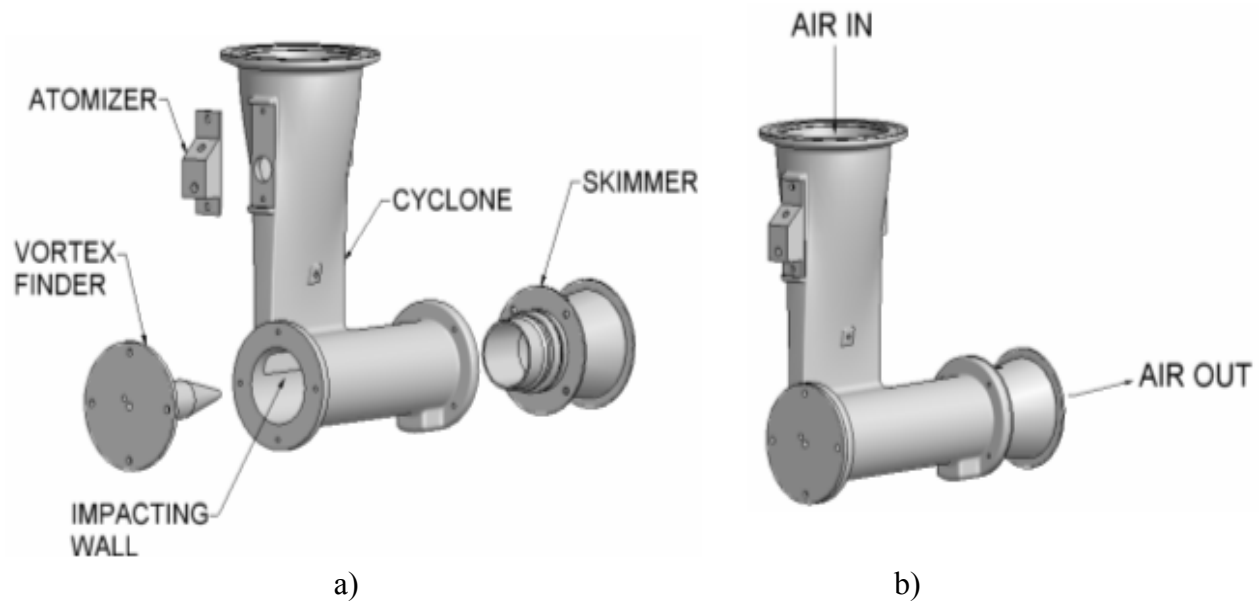


Figure 2.2. 1250 L/min cyclone. a) components, b) assembly.

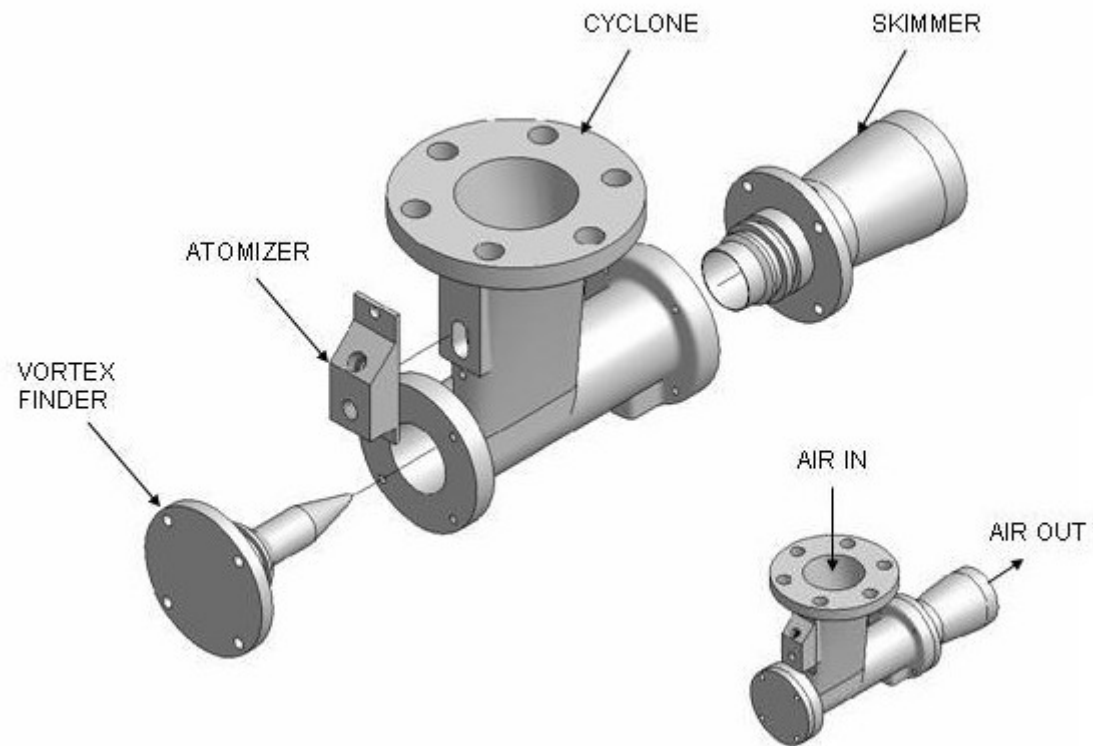


Figure 2.3. 100 L/min cyclone version 2.0.

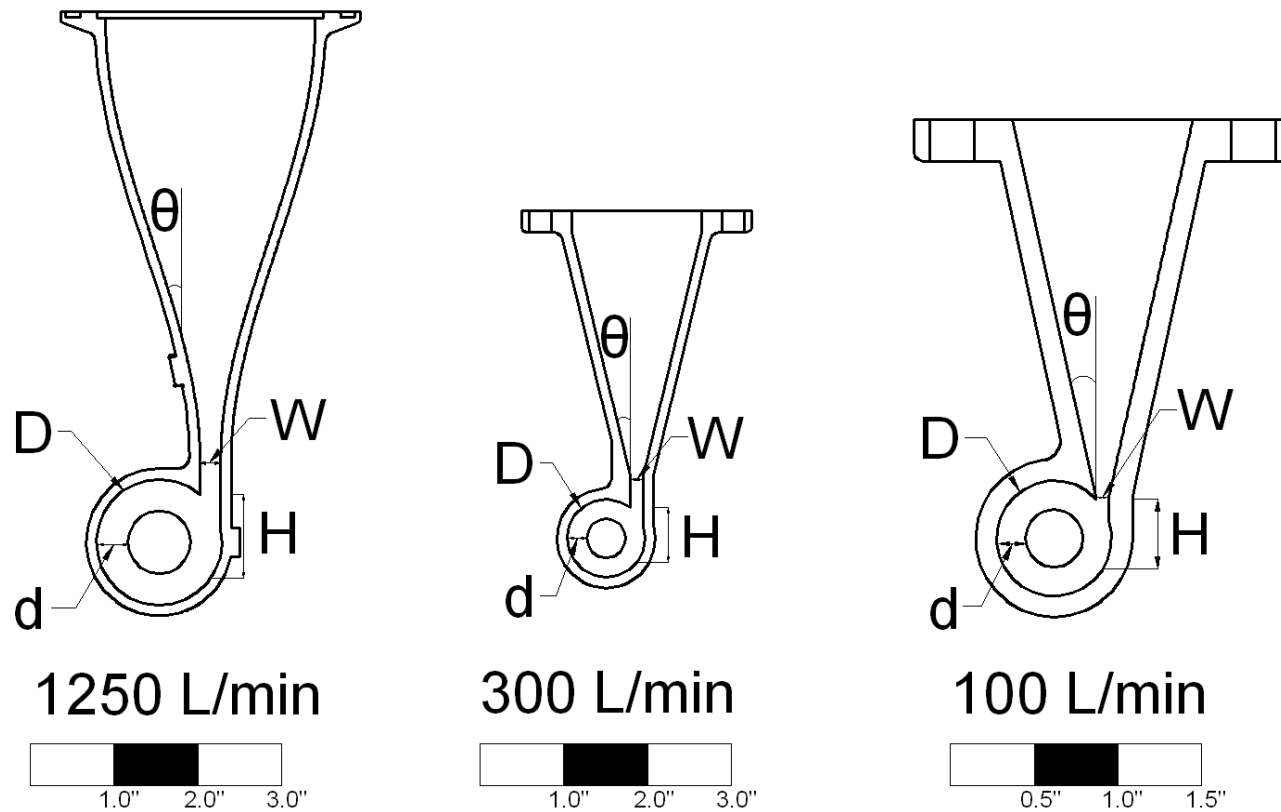
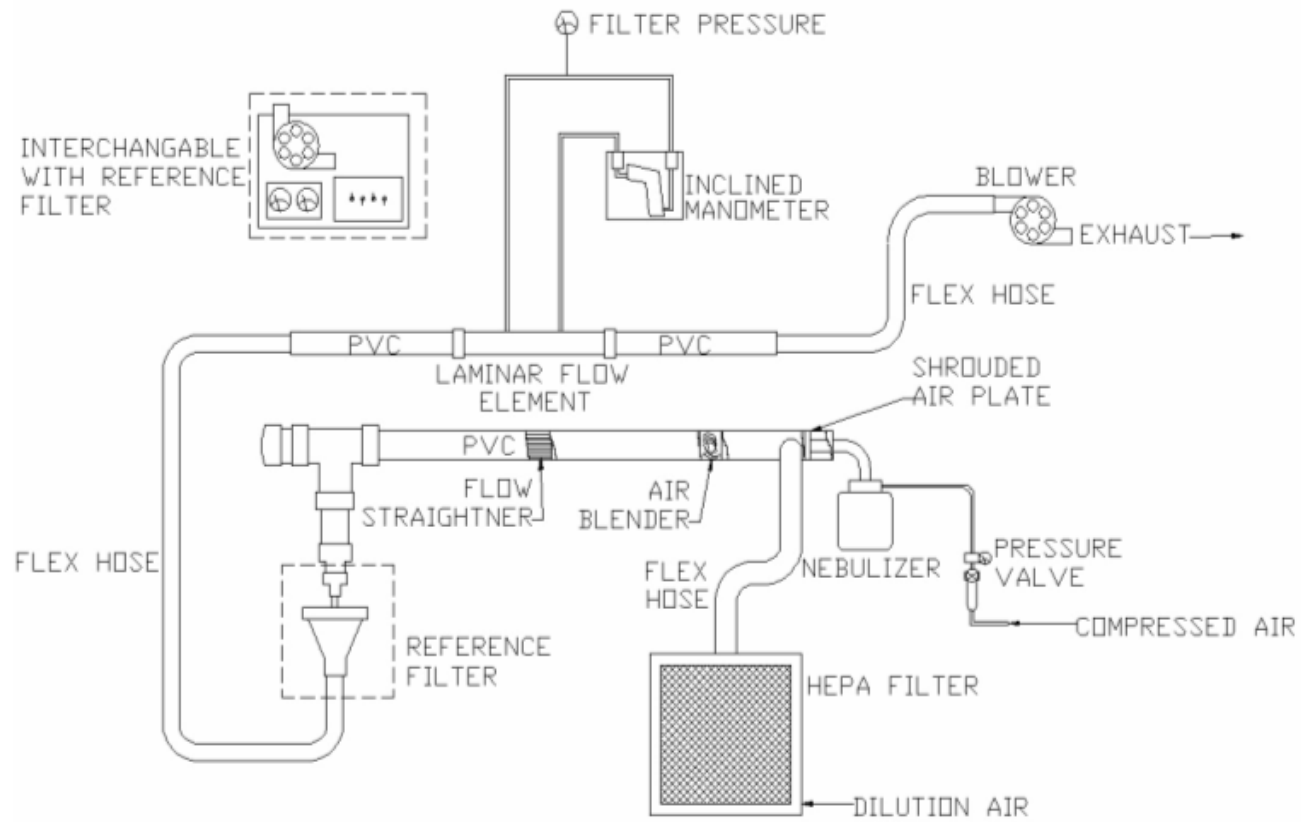
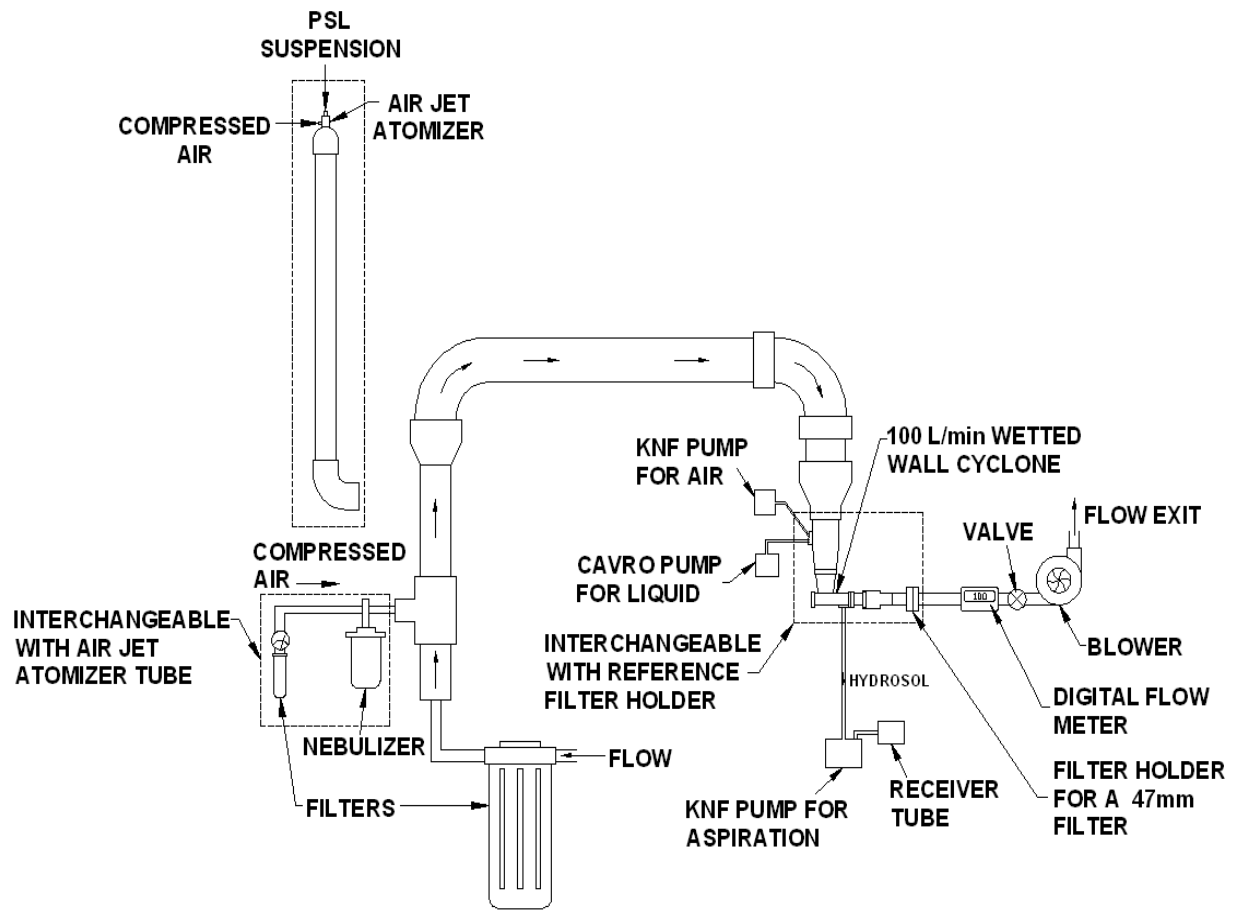


Figure 2.4. Comparison of inlet geometry for three cyclones.



a) High volumetric flow rate (> 300 L/min)

Figure 3.1. Schematic of setup for aerosol experiment.



b) Low volumetric flow rate ($< 300 \text{ L/min}$)

Figure 3.1 continued.

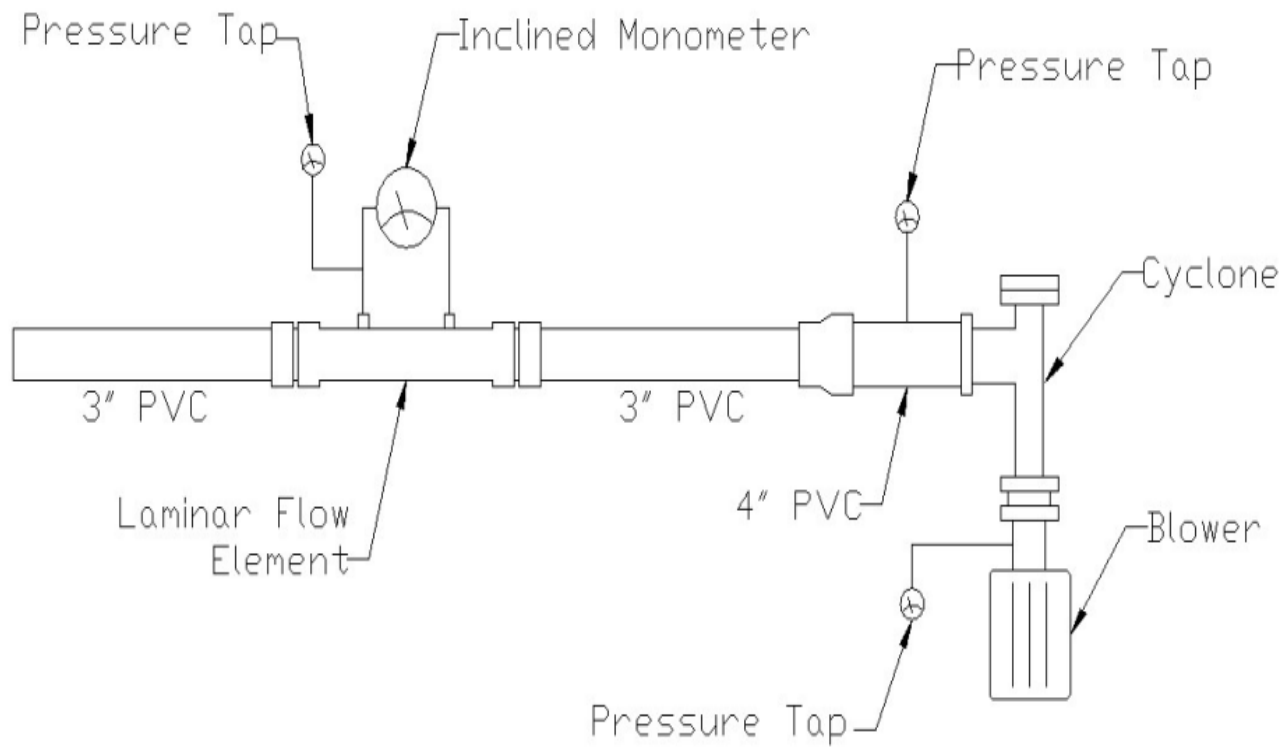


Figure 3.2. Schematic of pressure drop test.

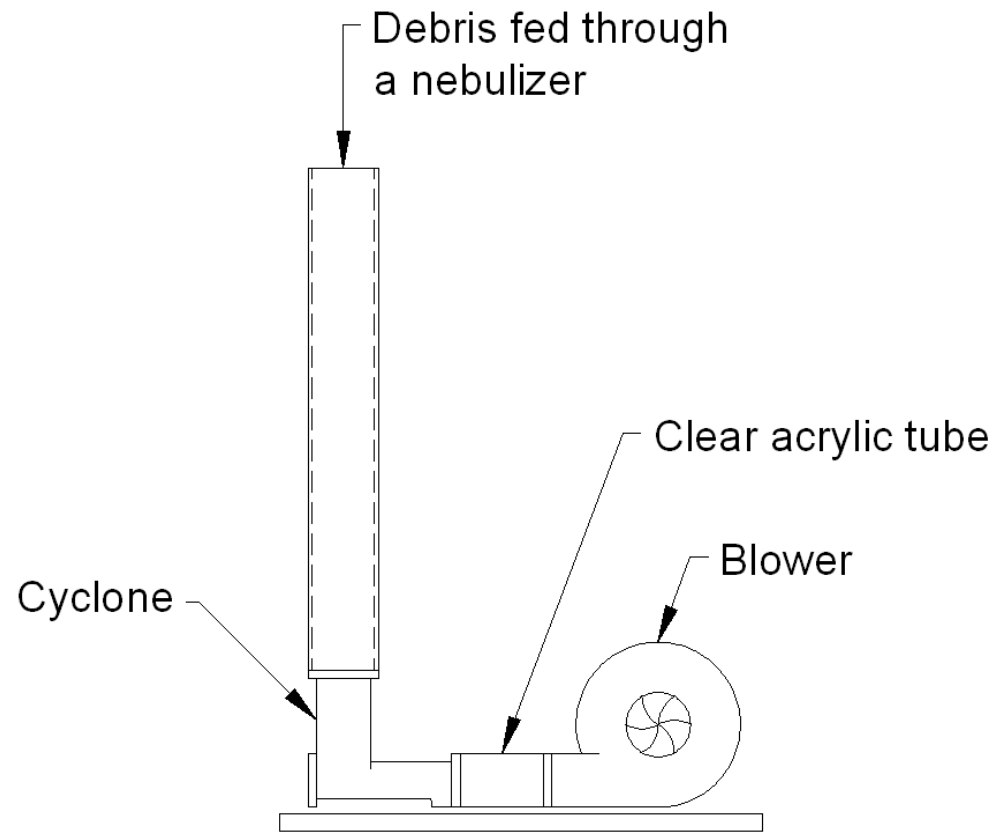
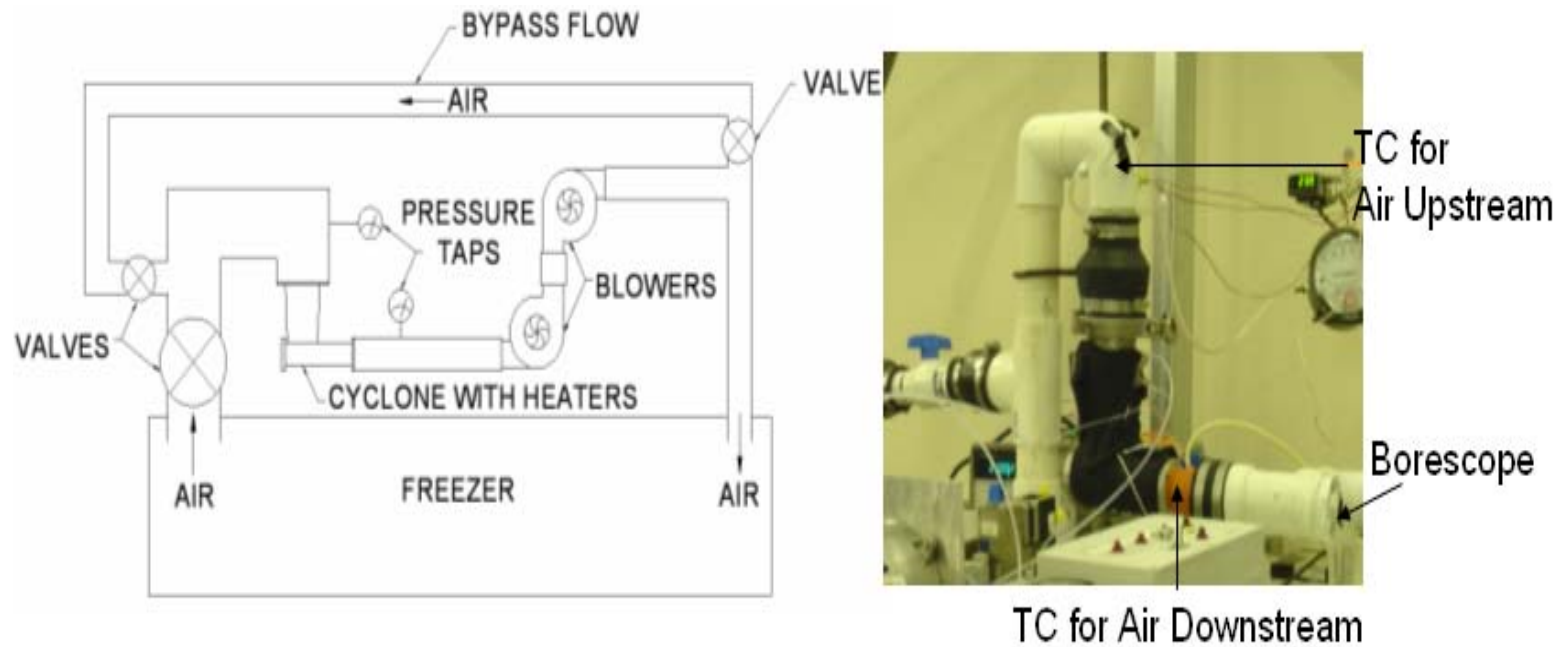
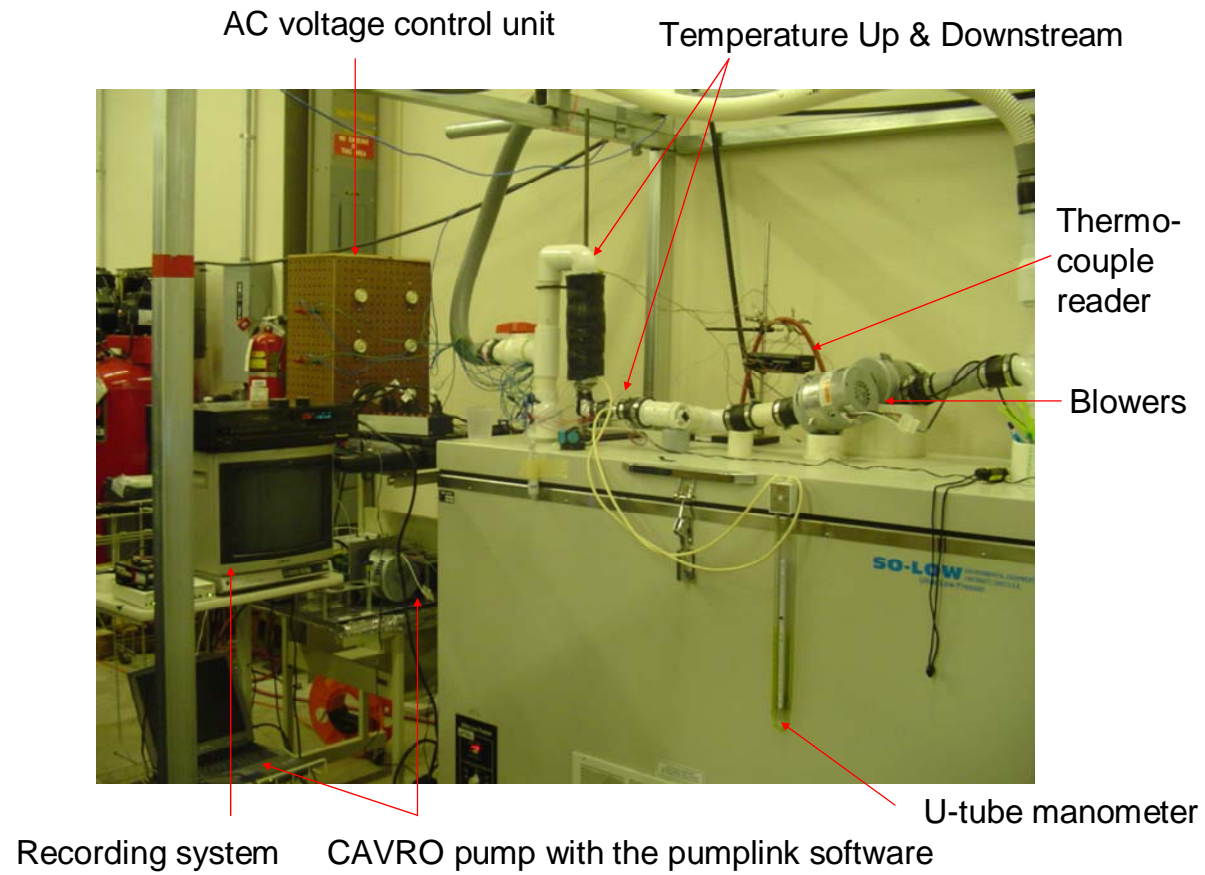


Figure 3.3. Schematic of debris test.



a) Setup for the 1250 L/min cyclone

Figure 3.4. Cold temperature experimental setup.



b) Setup for the 100 L/min cyclone

Figure 3.4 continued.

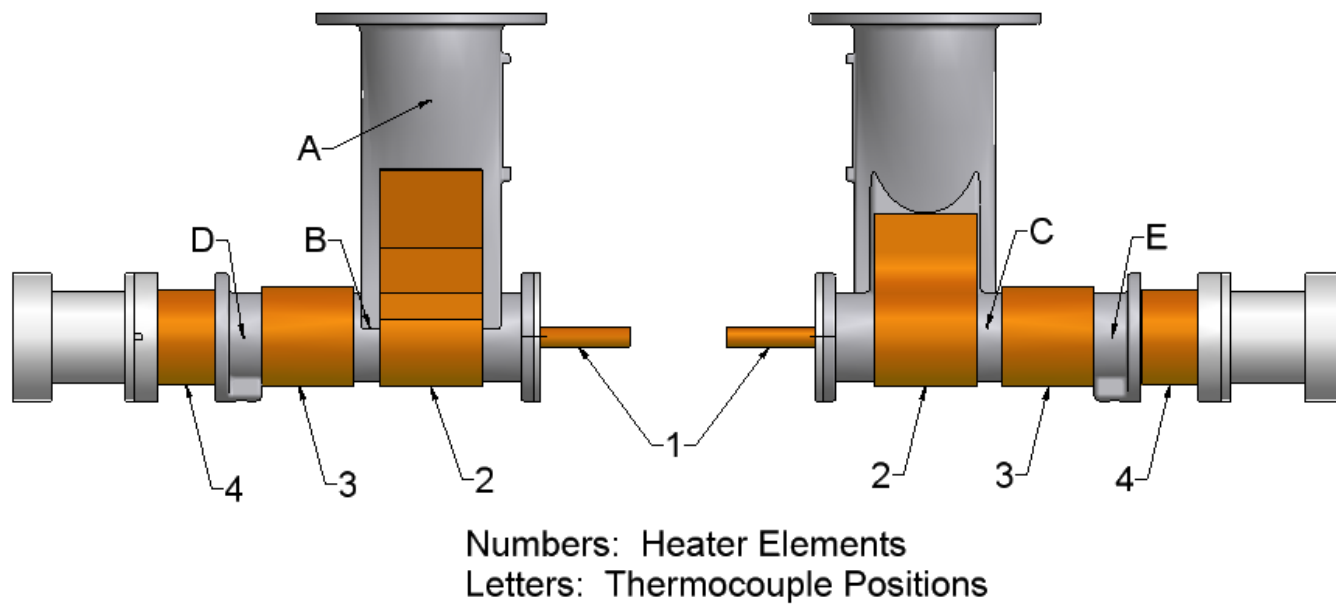


Figure 3.5. Preliminary heating system for the 1250 L/min cyclone and thermo-couple locations.

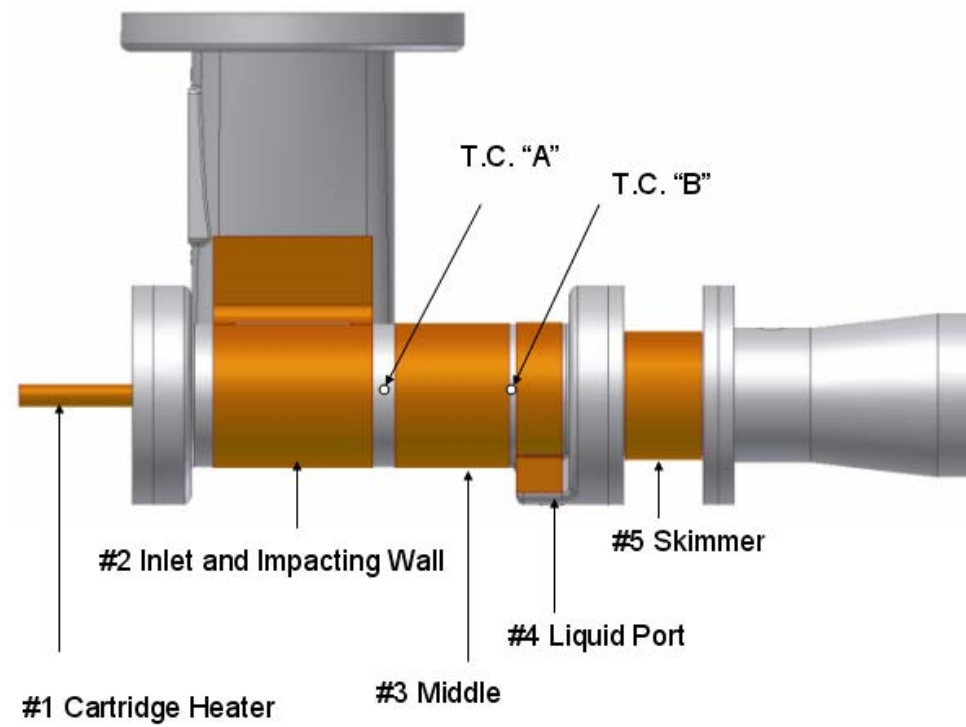


Figure 3.6. Preliminary heating system for the 100 L/min cyclone and thermo-couple locations.

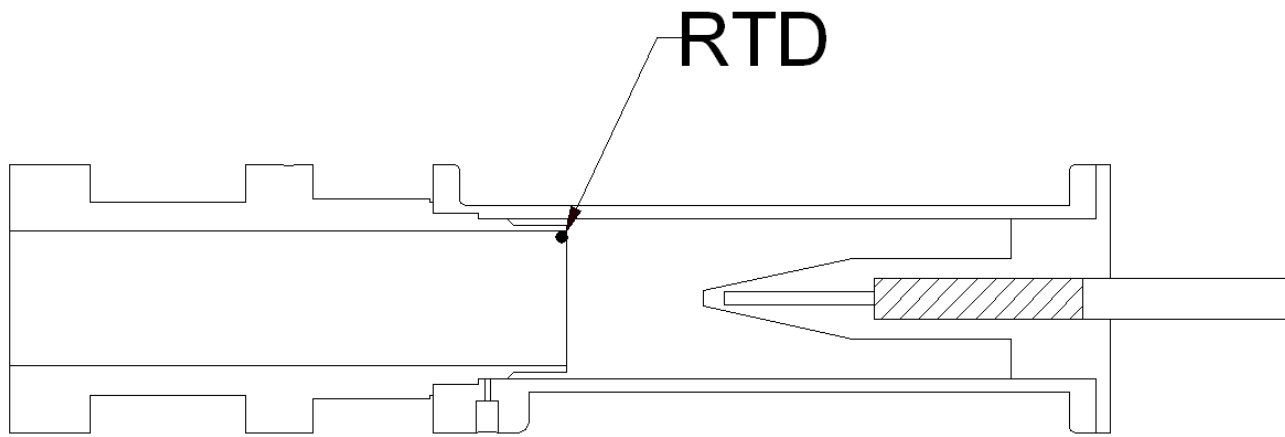


Figure 3.7. Thin film RTD location for the skimmer.

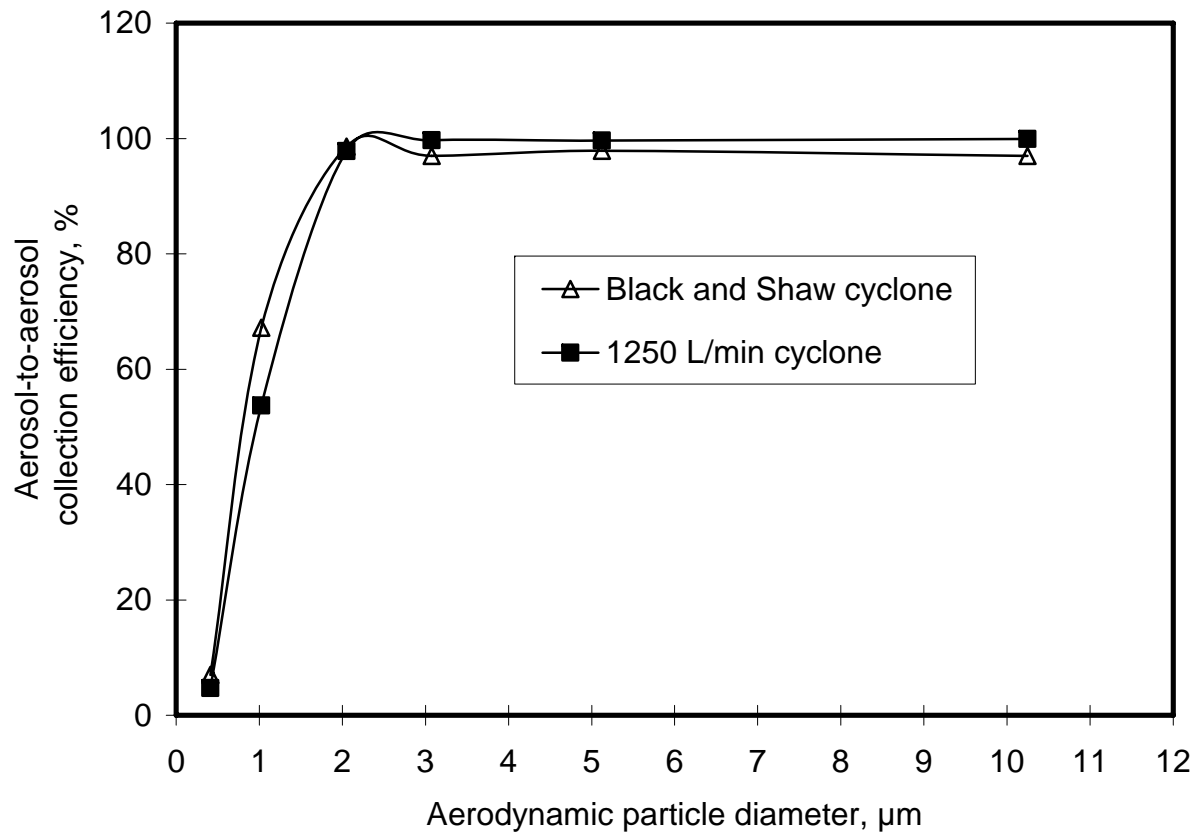


Figure 4.1. Aerosol-to-aerosol collection efficiency as a function of particle size.

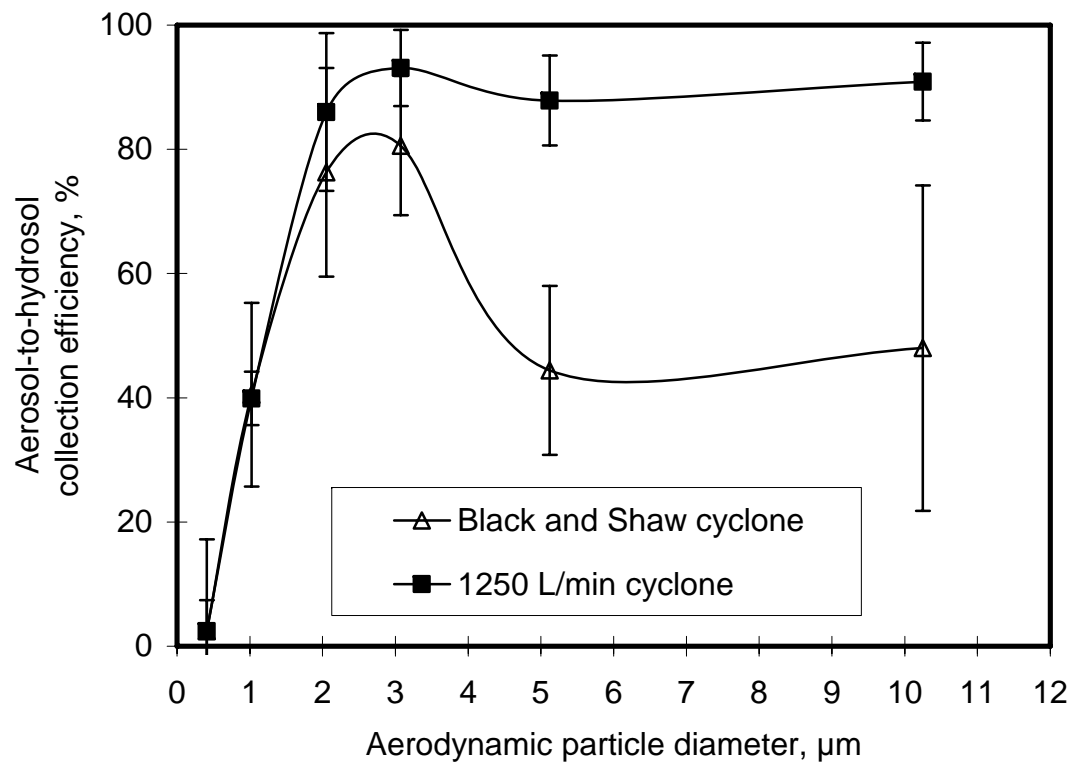


Figure 4.2. Aerosol-to-hydrosol collection efficiency as a function of particle size for the 1250 L/min cyclone and Black and Shaw cyclone. Liquid effluent flow rate: 1 mL/min.

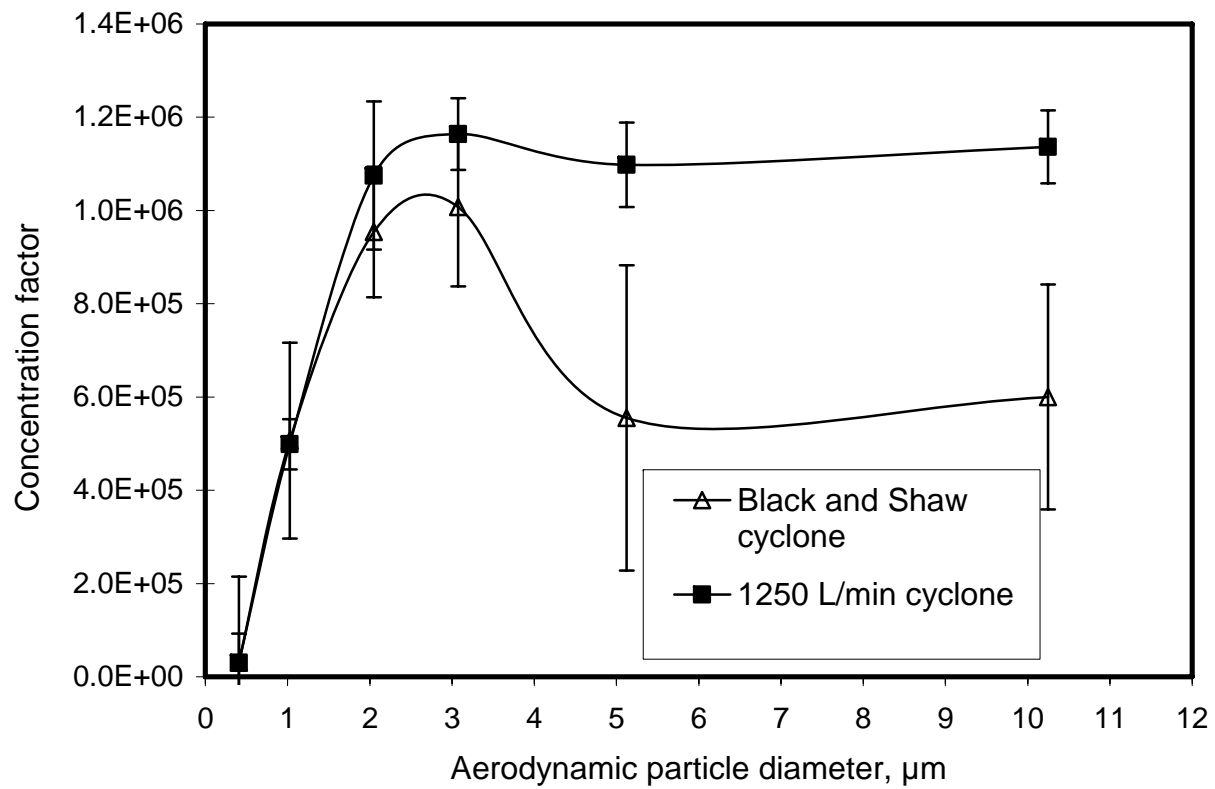


Figure 4.3. Concentration factor as a function of particle size. Liquid effluent flow rate: 1 mL/min.

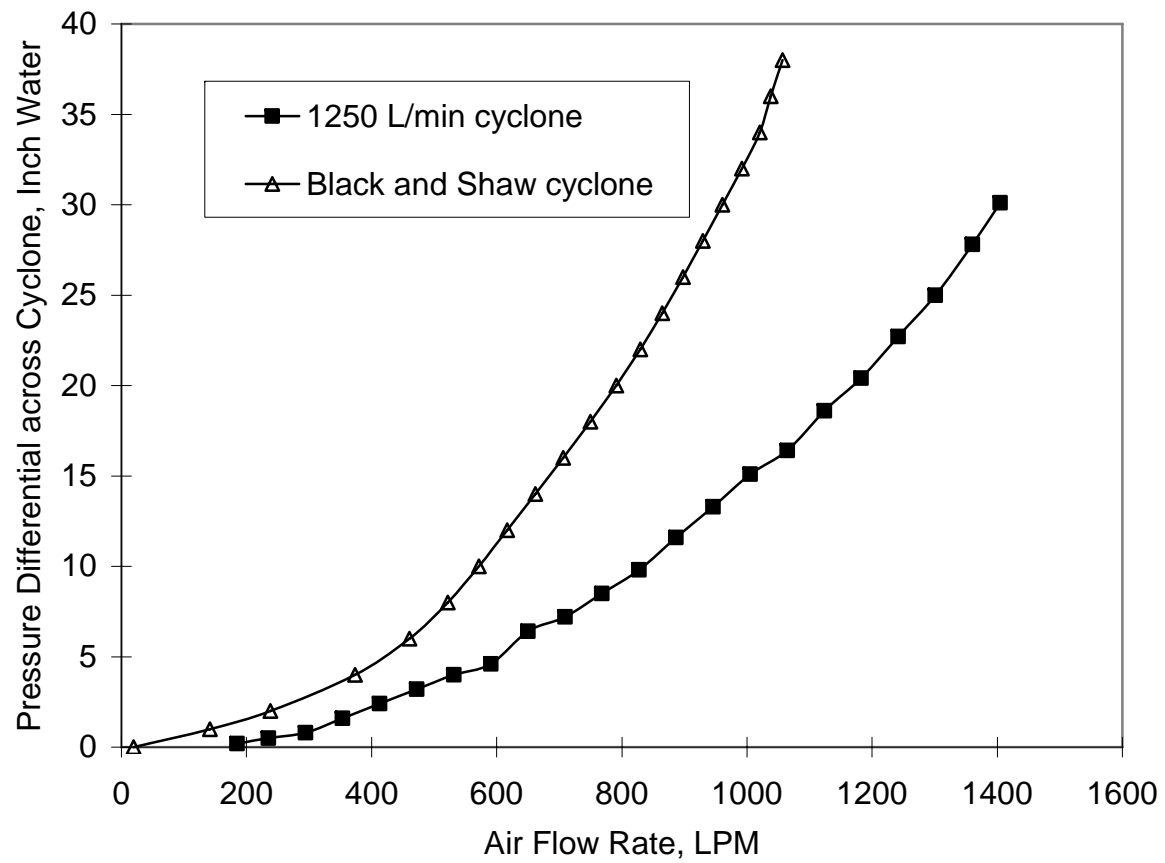


Figure 4.4. Pressure differential across cyclones as a function of air flow rate.

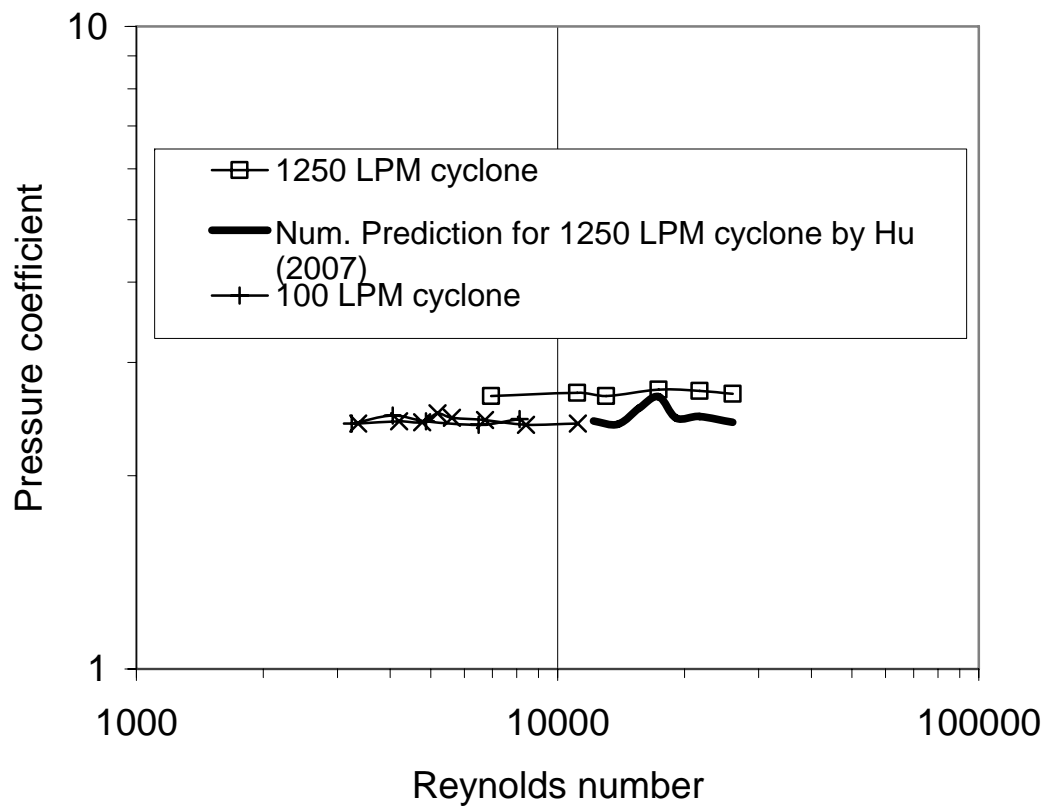


Figure 4.5. Pressure coefficient for the 1250 L/min cyclone as a function of Reynolds number.



Figure 4.6. 1250 L/min cyclone inner wall, 6 minutes after adding 2000 mg of Arizona dust.



Figure 4.7. 1250 L/min cyclone inner wall, 8 minutes after adding 600 mg of ASHRAE test dust.



Figure 4.8. 1250 L/min cyclone inner wall, 6 minutes after adding 170 mg of the second-cut cotton linters.

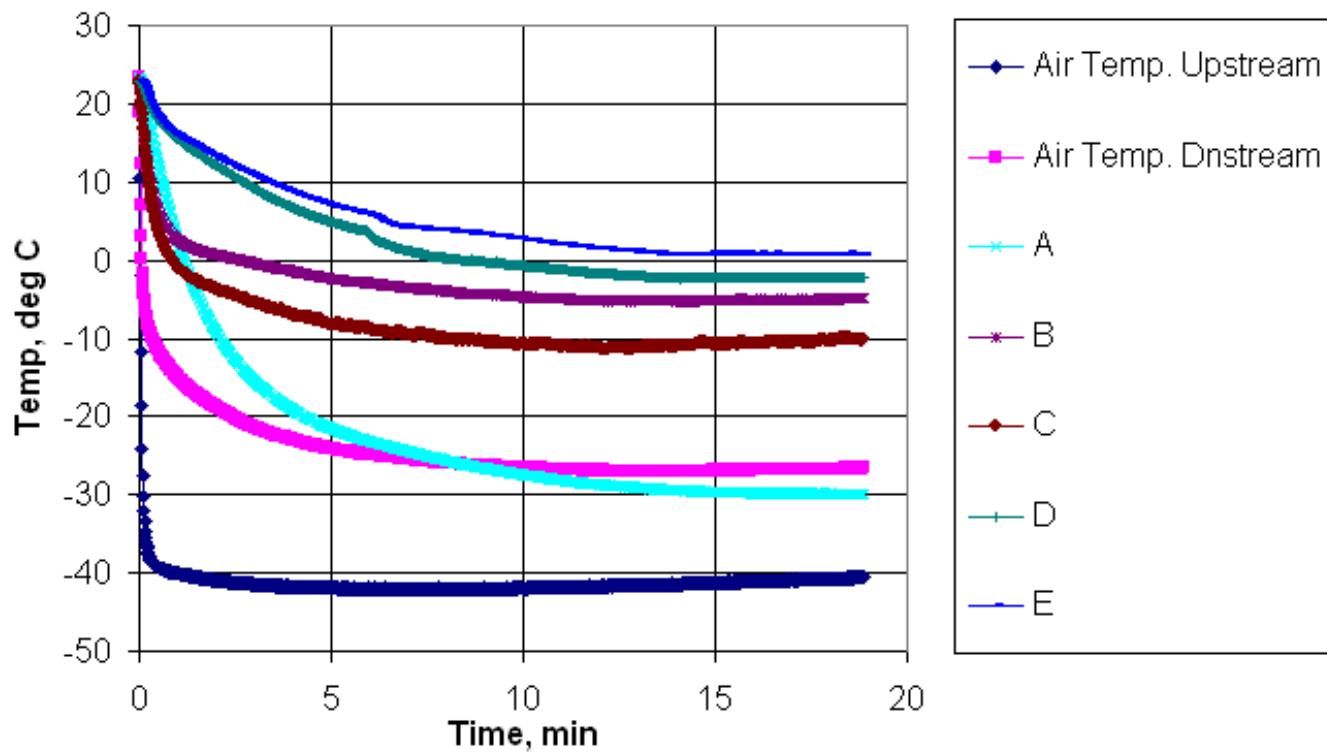


Figure 4.9. Temperature profiles with the preliminary heating system. Incoming air temperature: -40°C . Heaters and blowers were turned on simultaneously.

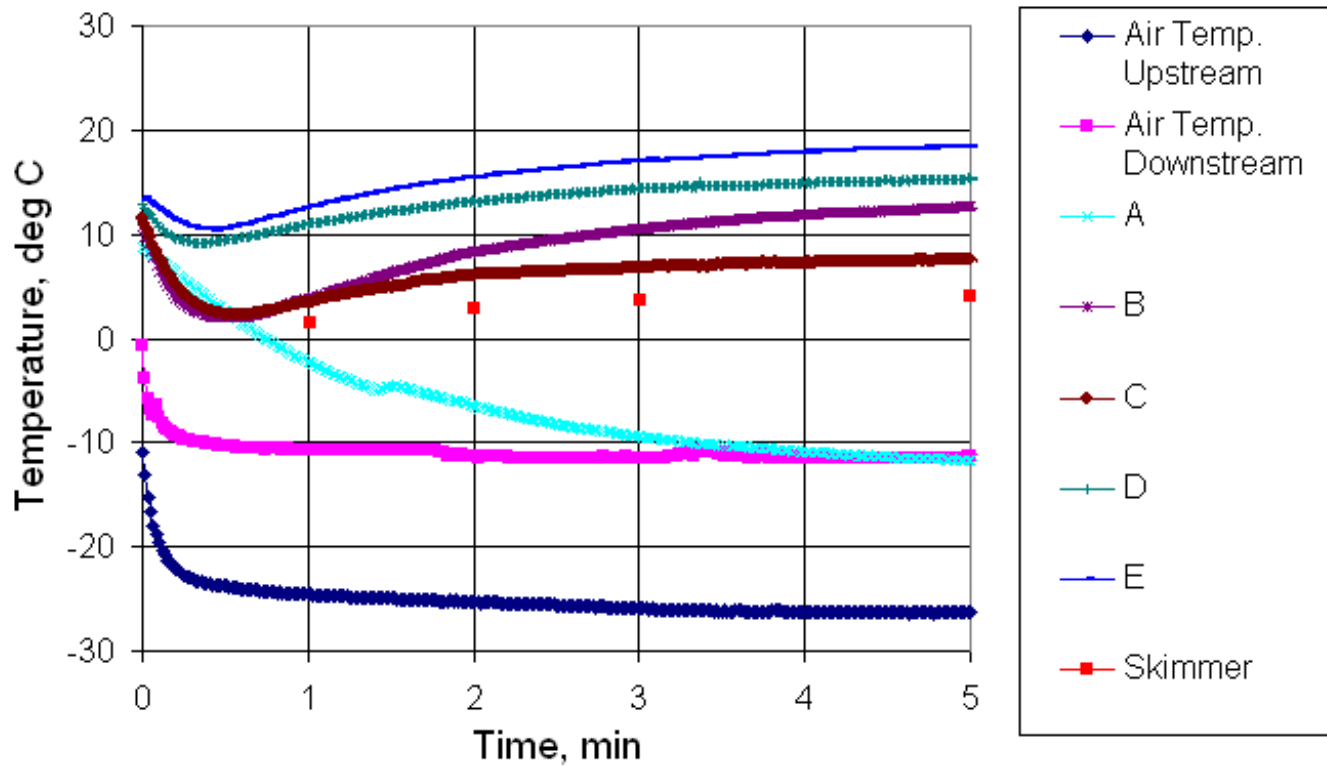


Figure 4.10. Temperature profiles with the preliminary heating system. Incoming air temperature: -26°C . Heaters and blowers were turned on simultaneously.

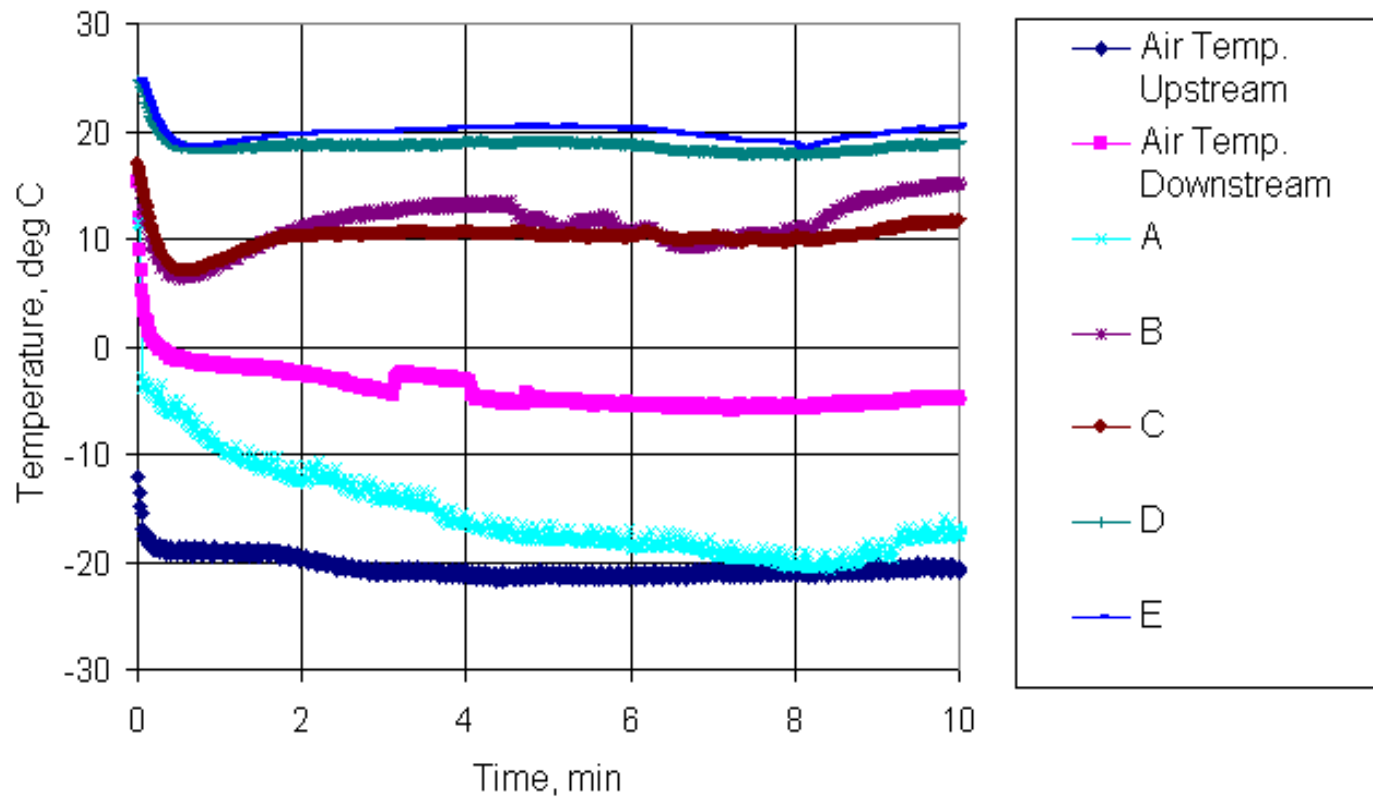


Figure 4.11. Temperature profiles with the preliminary heating system. Incoming air temperature: -20°C . Heaters and blowers were turned on simultaneously.

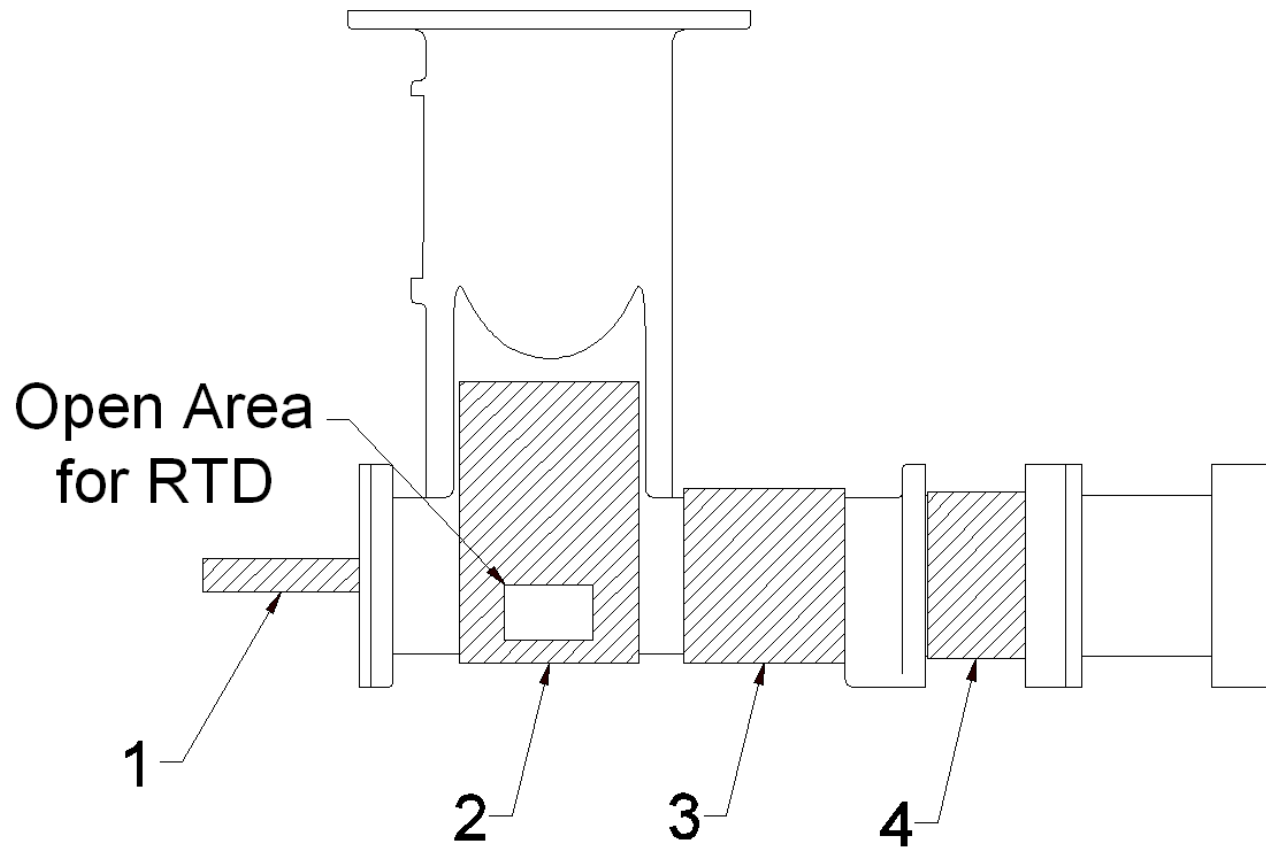
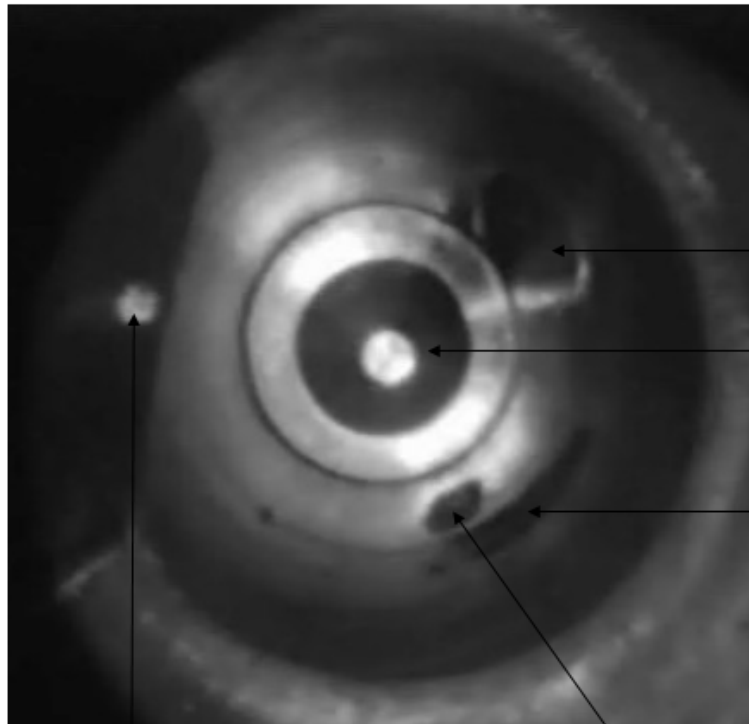


Figure 4.12. Open area location in the heater #2.



Slot

Vortex Finder

On the narrow band
between heater #2 and #3

Thin Film RTD, pasted the tip of the skimmer

On the open area (0.7"×0.7") for a RTD

Figure 4.13. Liquid freezing inside the 1250 L/min cyclone. Incoming air temperature: -26°C.

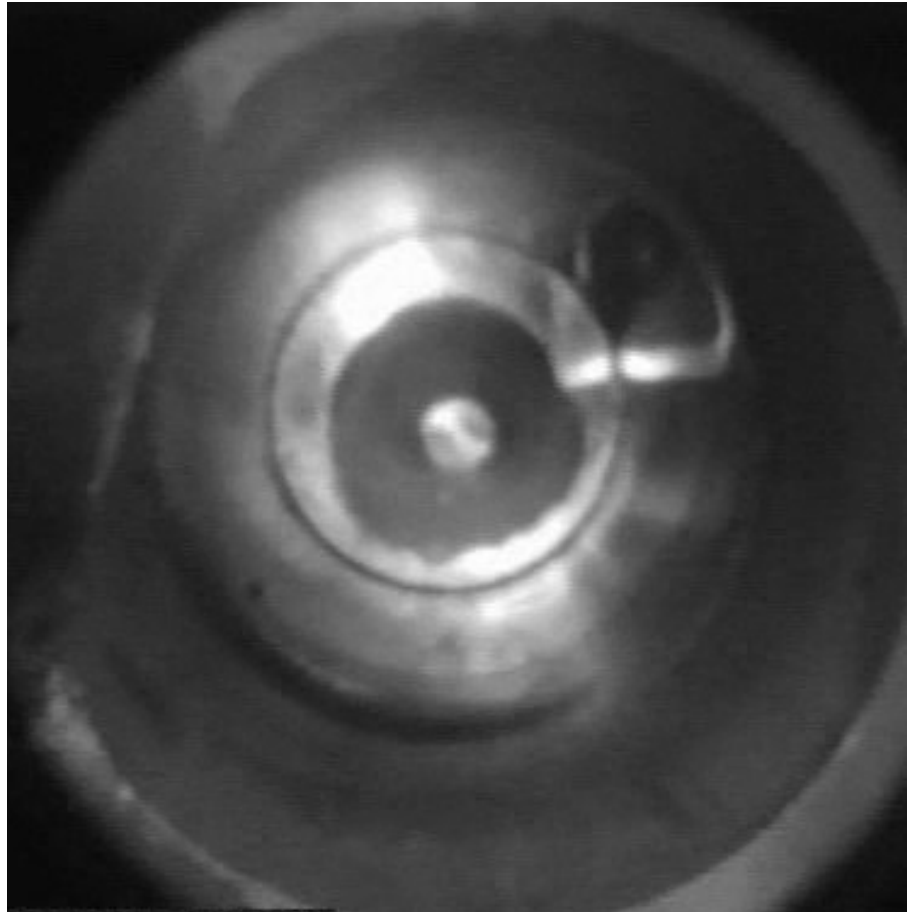
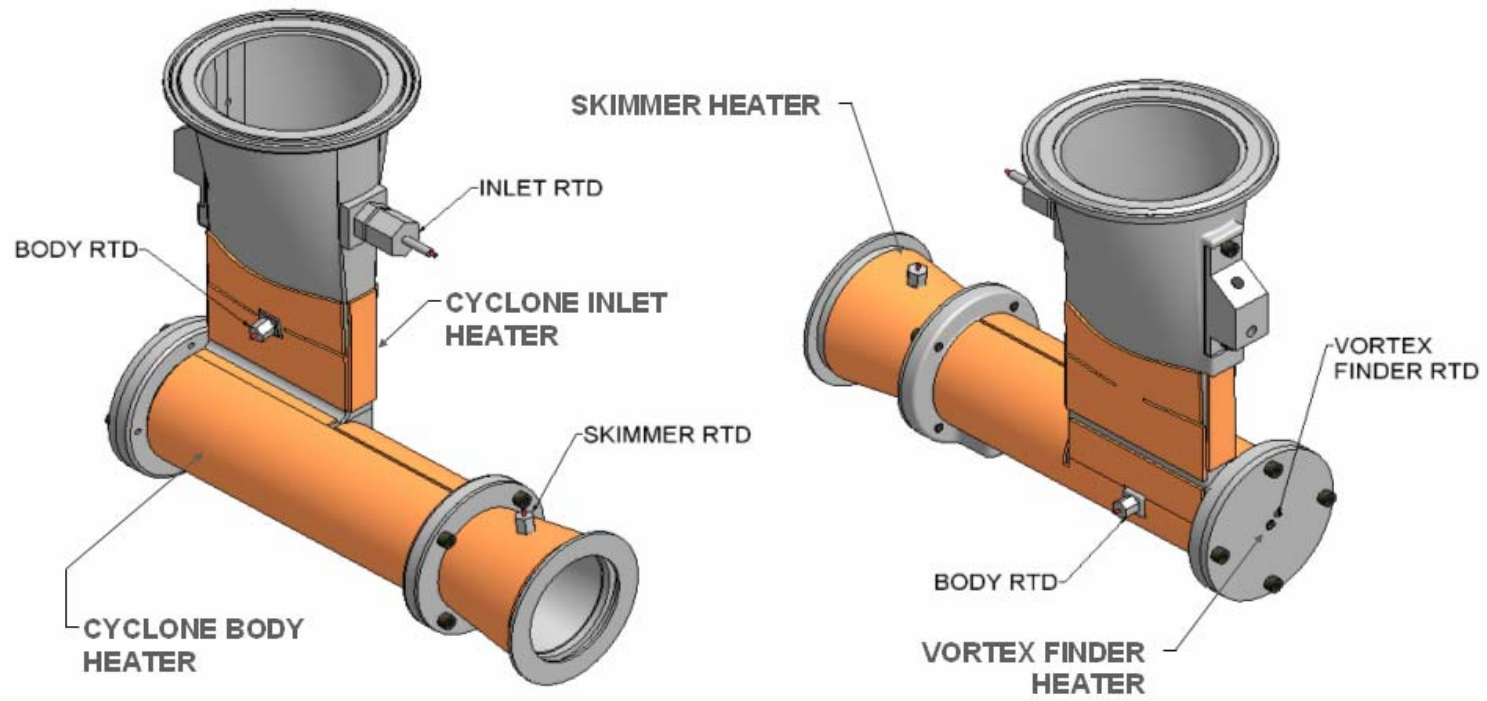
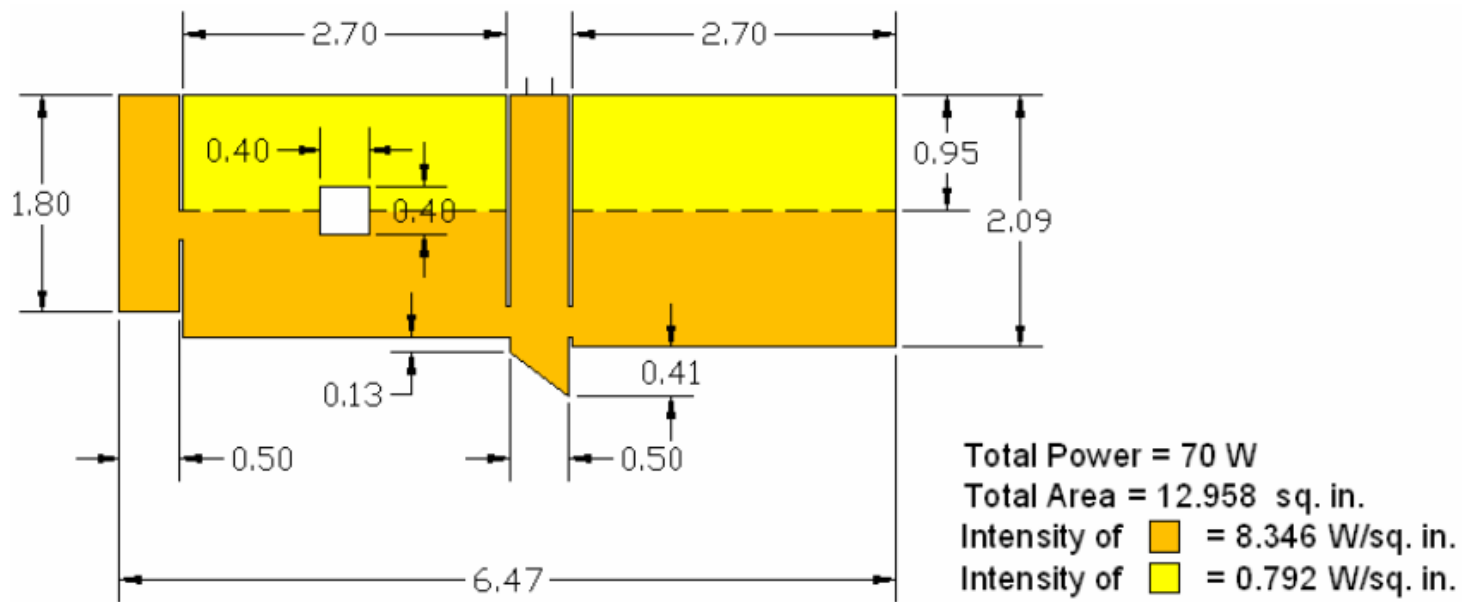


Figure 4.14. Liquid freezing on the vortex finder. Incoming air temperature: -26°C .



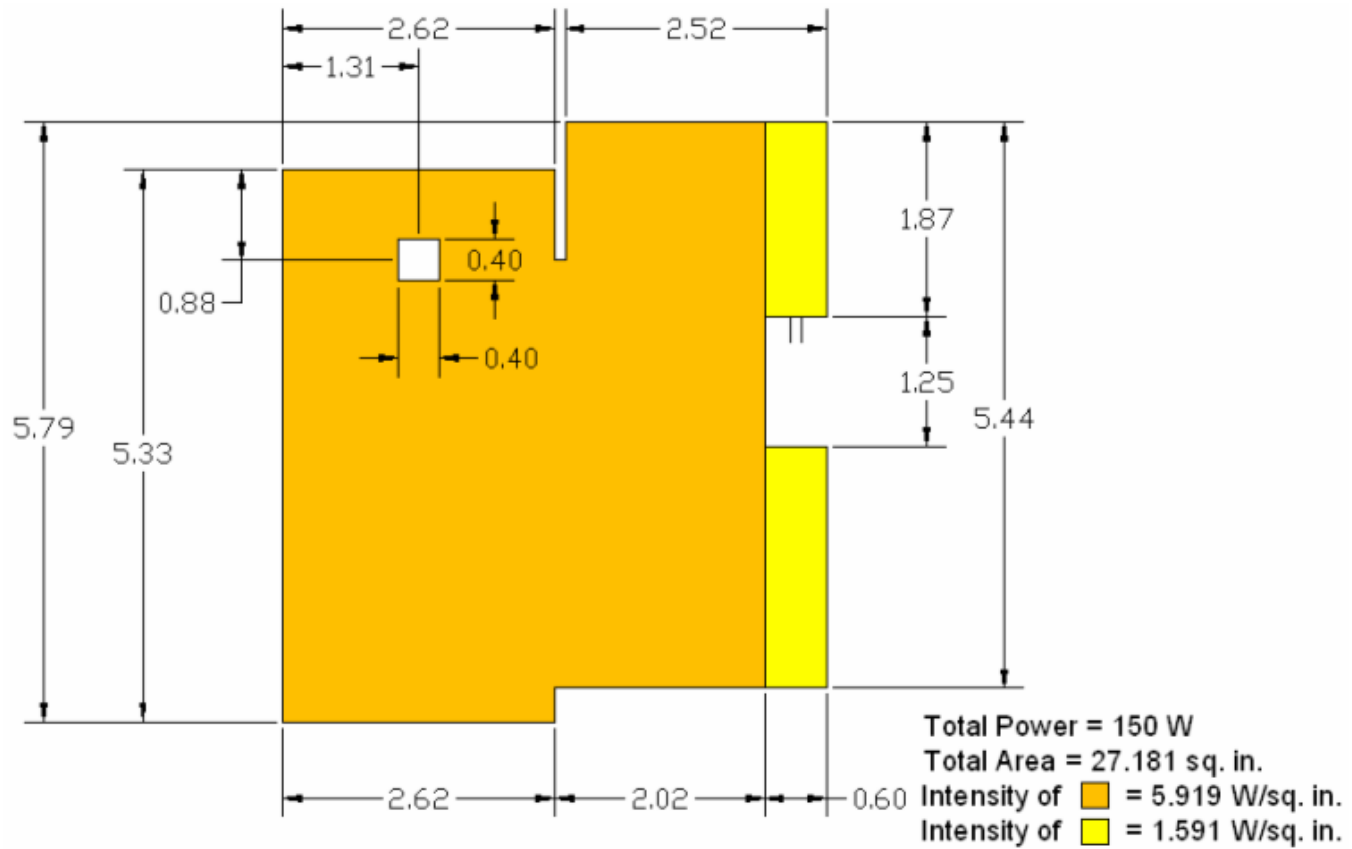
a) Heaters wrapped the cyclones

Figure 4.15. Final heating system for the 1250 L/min cyclone.



b) Top heater

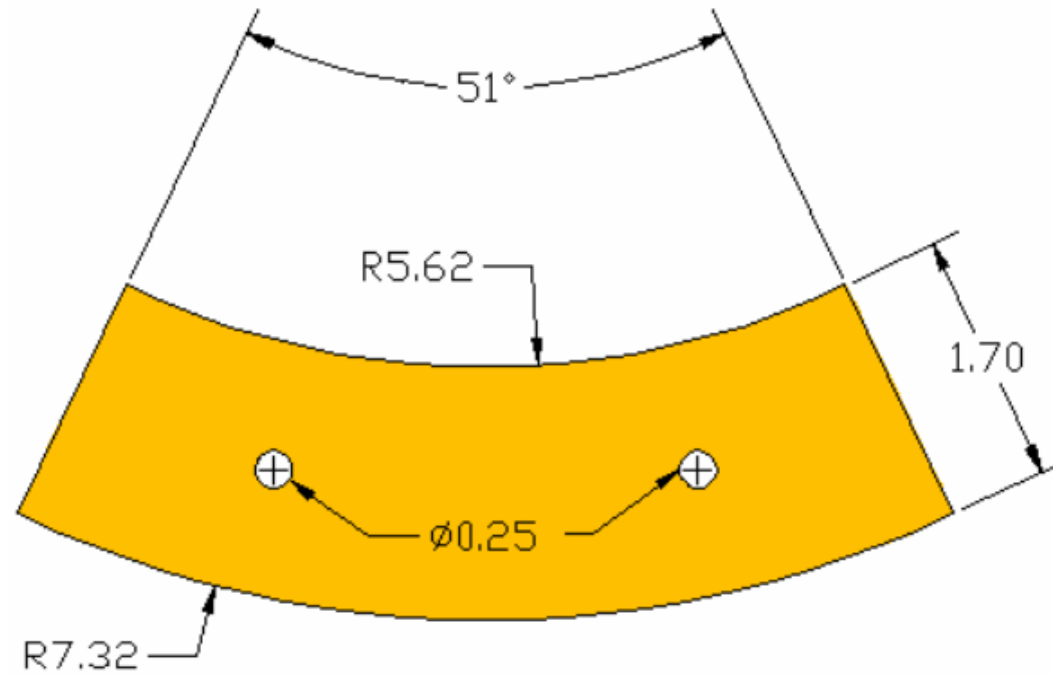
Figure 4.15 continued.



c) Bottom heater

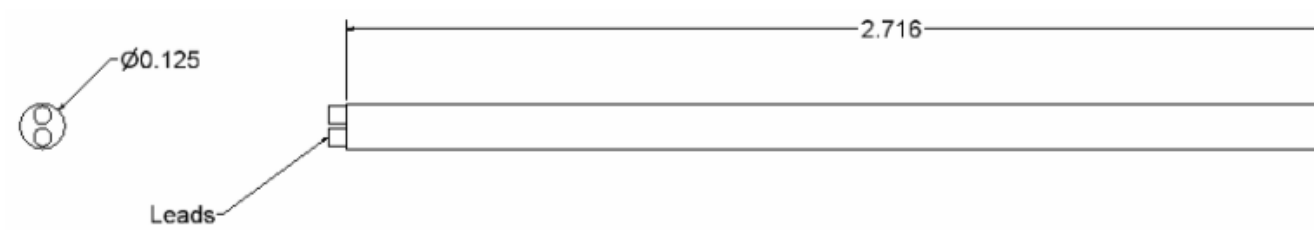
Figure 4.15 continued.

Skimmer Heater - Wraps
around the skimmer.

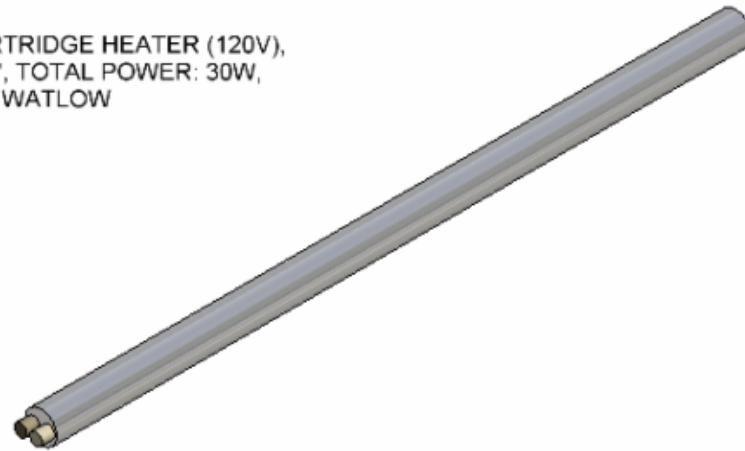


d) Skimmer heater

Figure 4.15 continued.



CUSTOMIZED CARTRIDGE HEATER (120V),
LEAD LENGTH: 12", TOTAL POWER: 30W,
MANUFACTURER: WATLOW



d) Vortex Finder cartridge heater

Figure 4.15 continued.

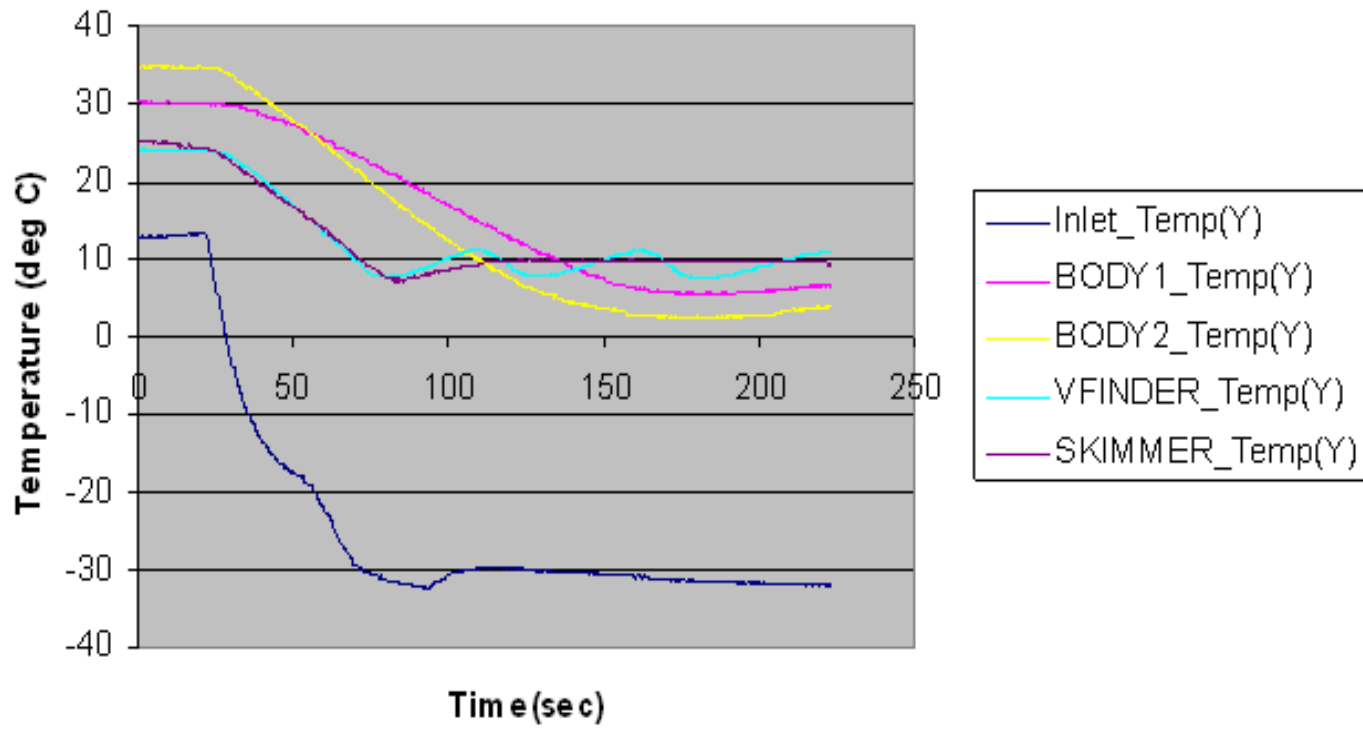


Figure 4.16. Temperature profiles with the final heating system. Incoming air temperature: -30° C. Heaters and blowers were turned on simultaneously.

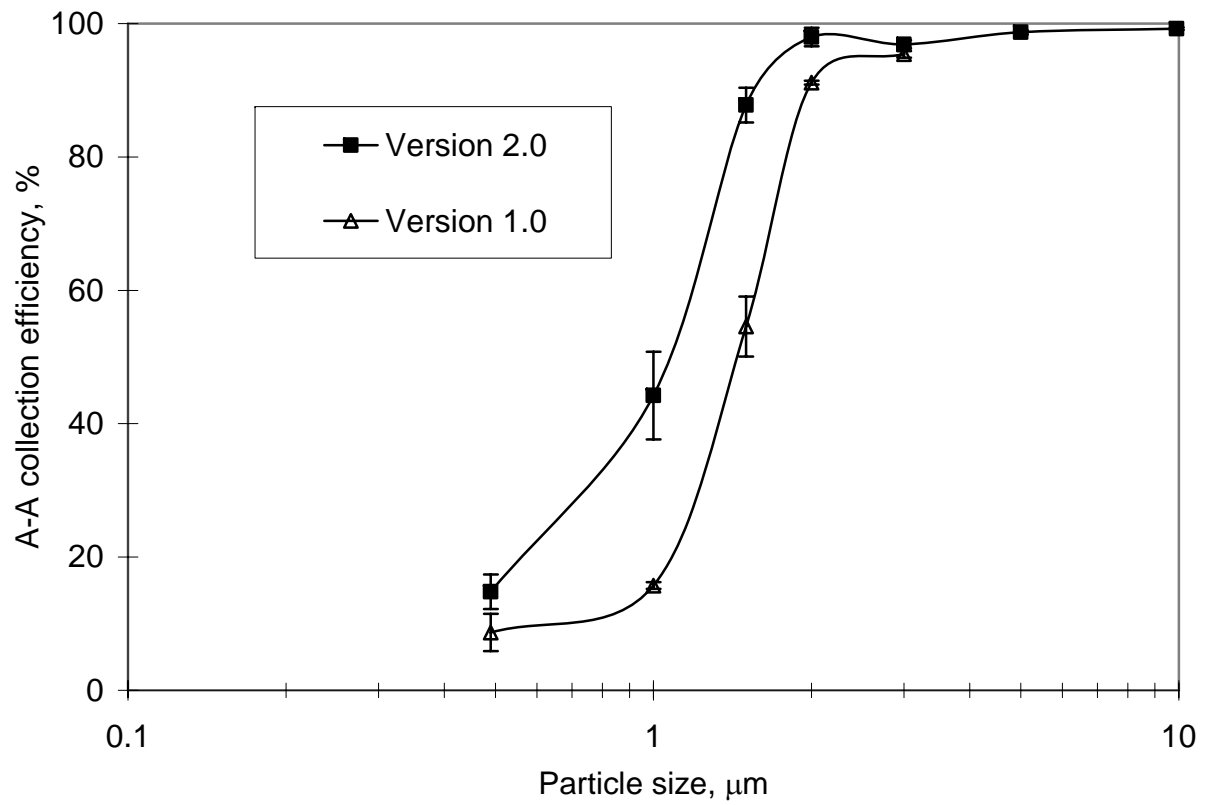


Figure 4.17. Aerosol-to-aerosol collection efficiency as a function of particle size.

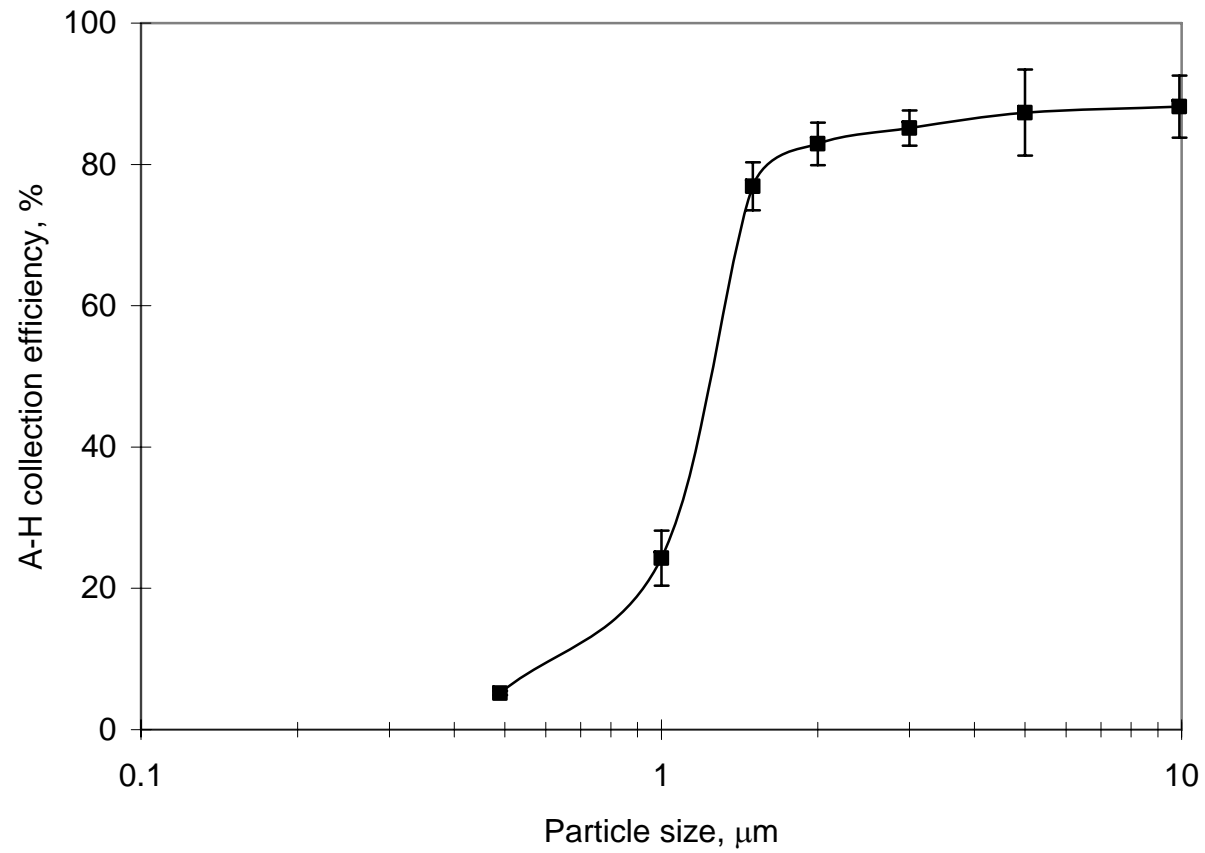


Figure 4.18. Aerosol-to-hydrosol collection efficiency as a function of particle size for the 100 L/min cyclone.
Liquid effluent flow rate: 0.1 mL/min.

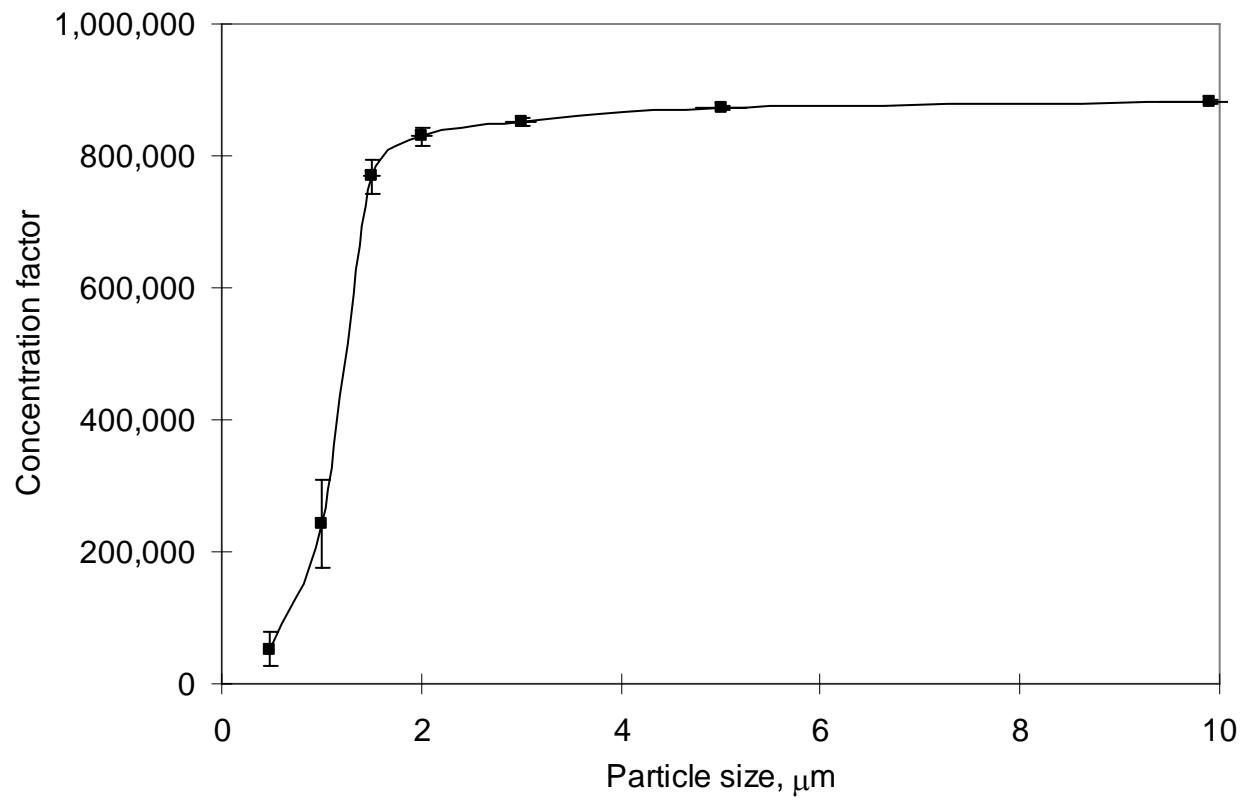


Figure 4.19. Concentration factor as a function of particle size for the 100 L/min cyclone.
Liquid effluent flow rate: 0.1 mL/min.

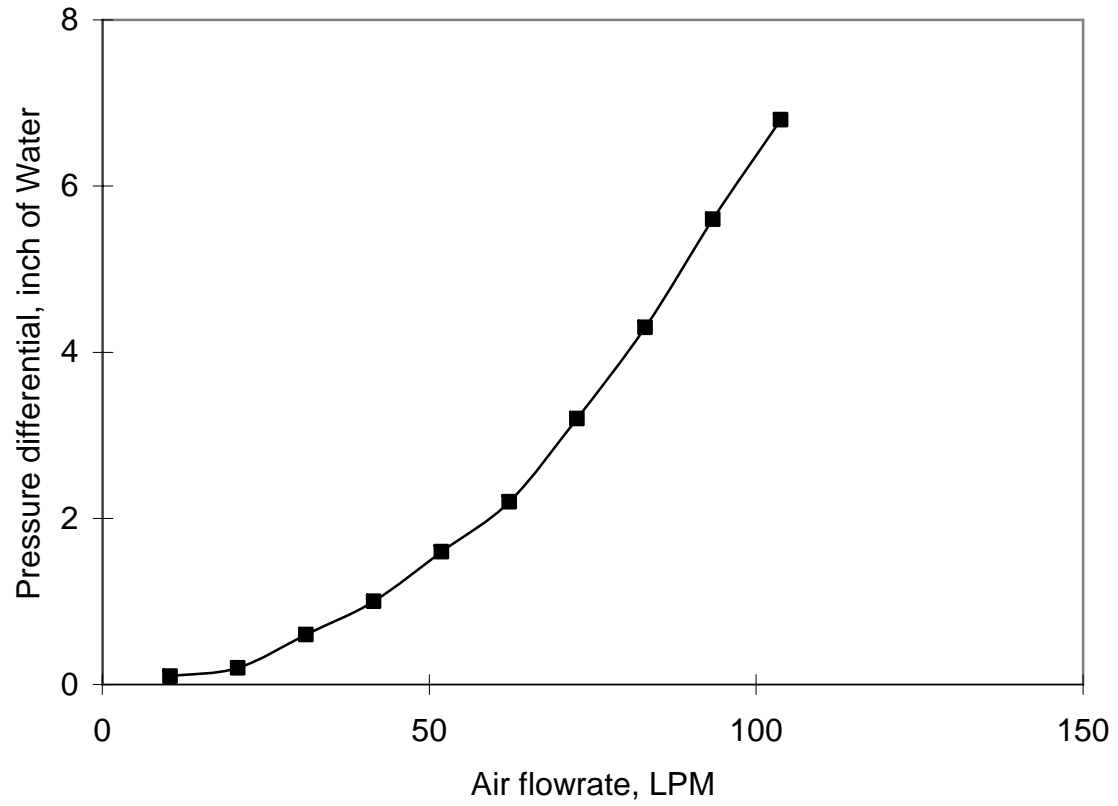


Figure 4.20. Pressure differential across the 100 L/min cyclone as a function of air flow rate.

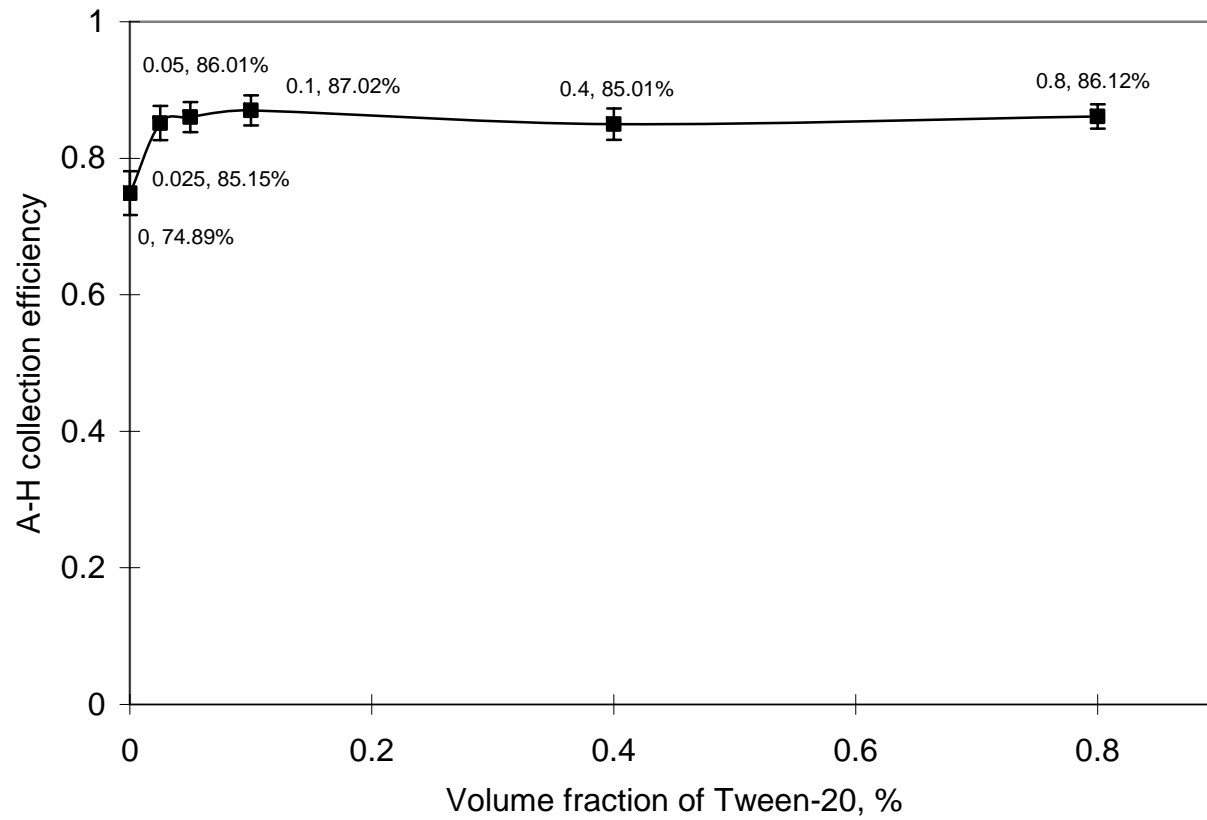


Figure 4.21. Aerosol-to-hydrosol efficiency for the 100 L/min cyclone as a function of volume fraction of Tween-20. Tested particle: 3 μm PSL. Liquid effluent flow rate: 0.1 mL/min.

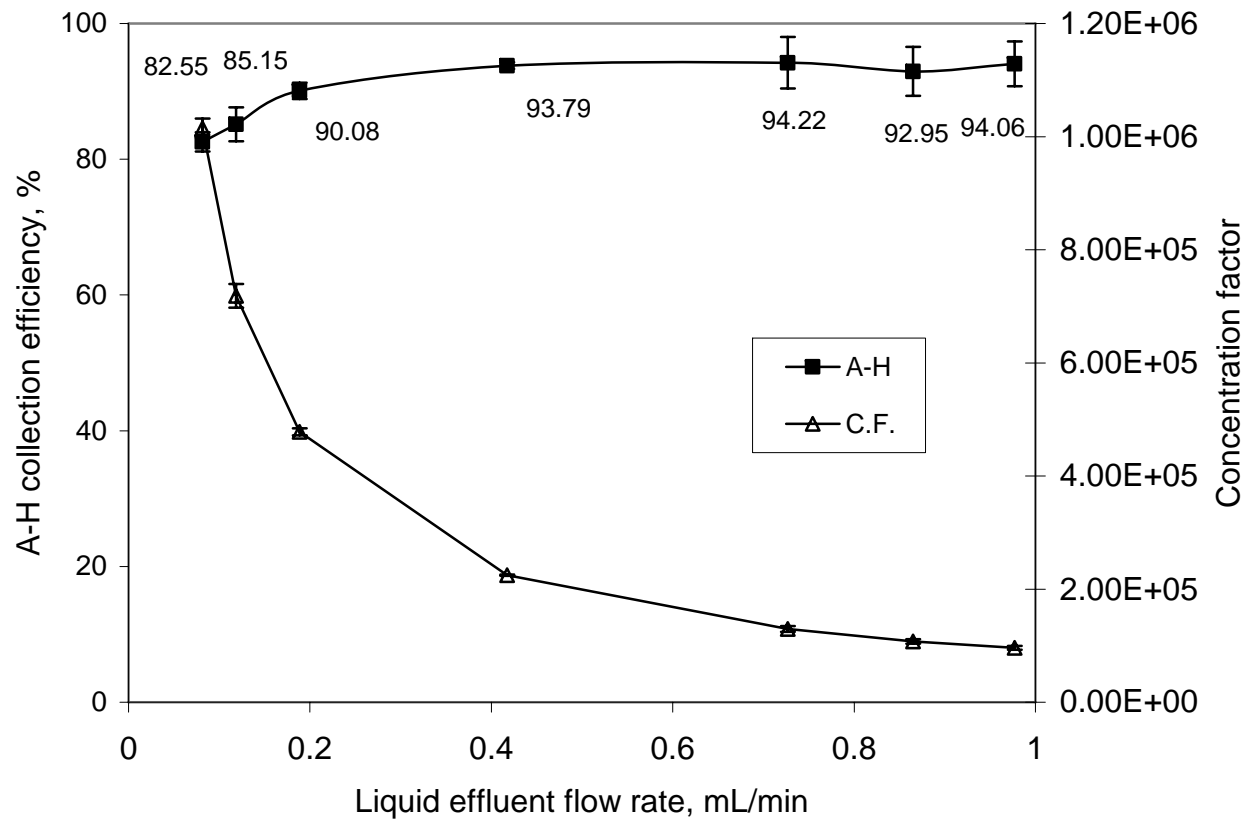


Figure 4.22. Aerosol-to-hydrosol collection efficiency & concentration factor for the 100 L/min cyclone as a function of the liquid effluent flow rate. Tested particle: 3 μm PSL.

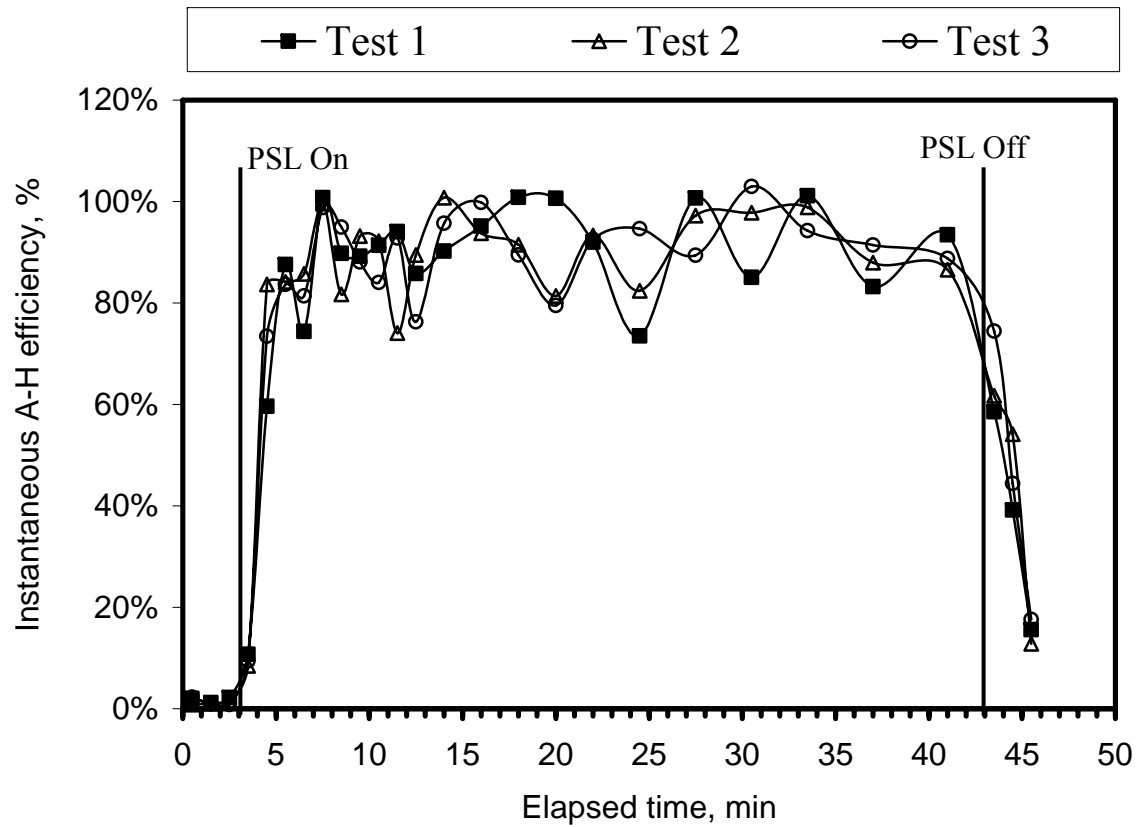


Figure 4.23. Instantaneous hydrosol collection efficiency with “wet start” for the 100 L/min cyclone as a function of time. Tested particle: 3 μ m PSL.

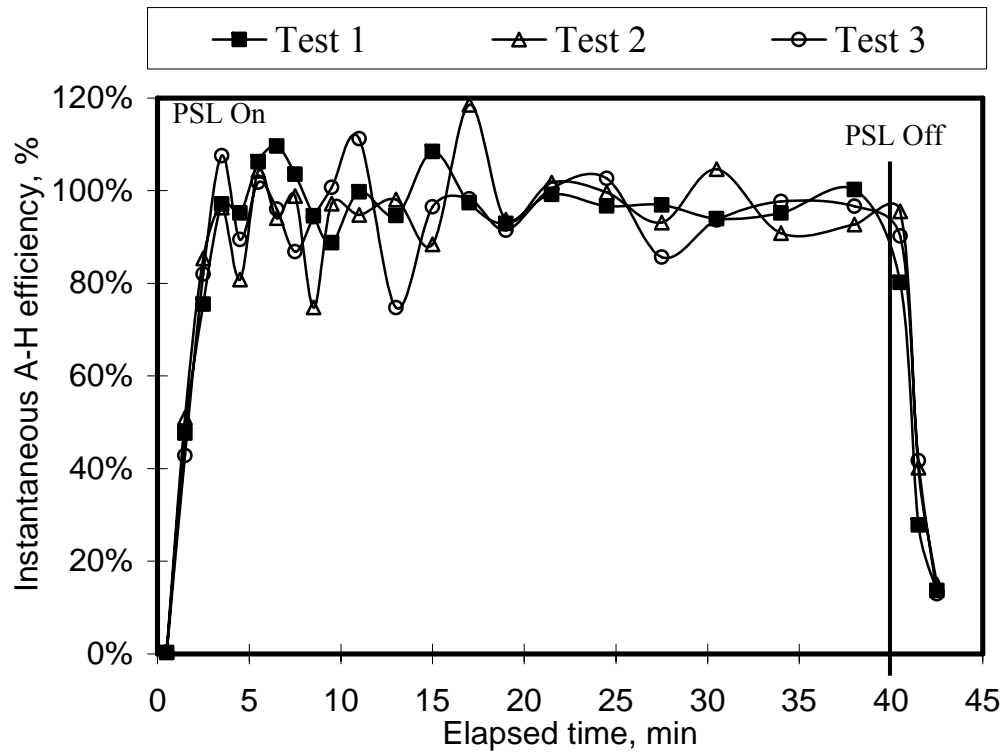


Figure 4.24. Instantaneous hydrosol collection efficiency with “dry start” for the 100 L/min cyclone as a function of time. Tested particle: 3 μ m PSL.

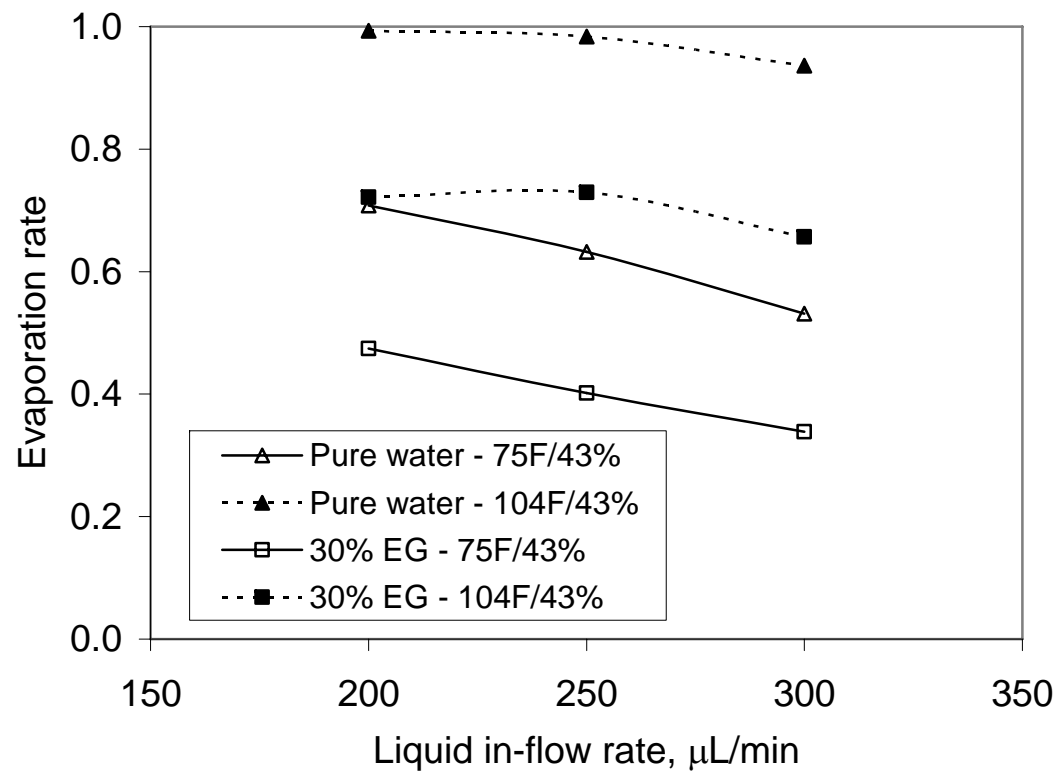


Figure 4.25. Evaporation rates with pure water and 30% EG at two different testing conditions.

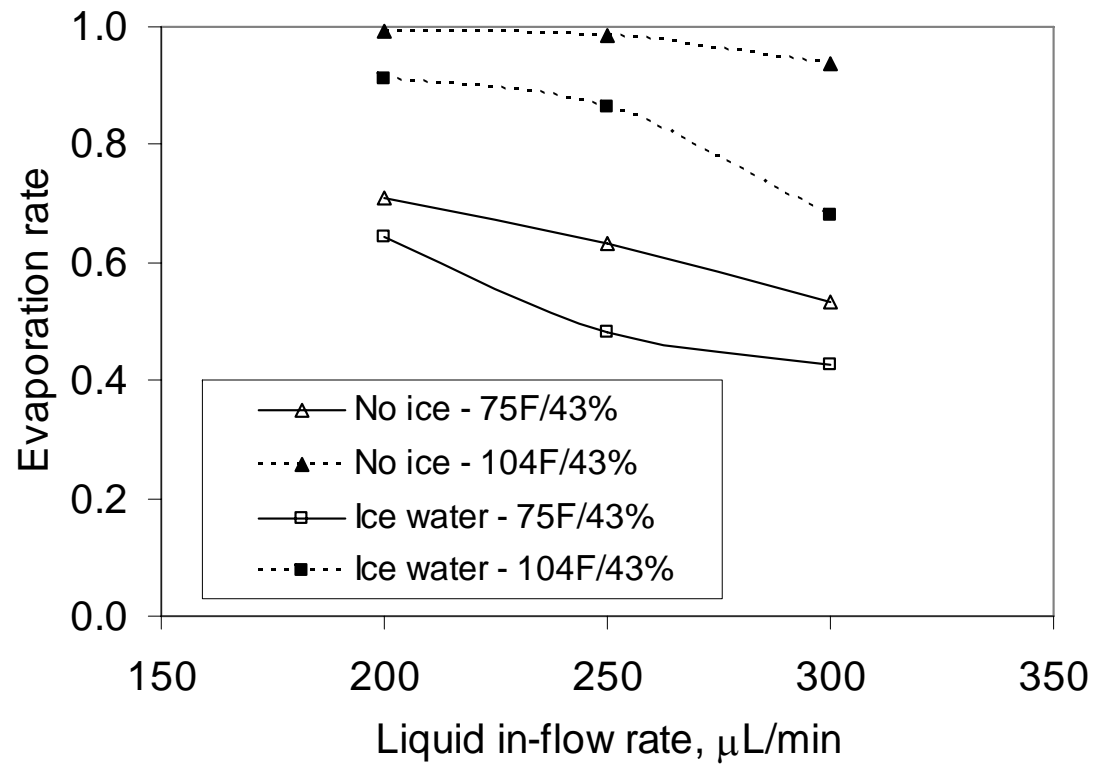


Figure 4.26. Evaporation rate with pure water in a cooled cyclone.

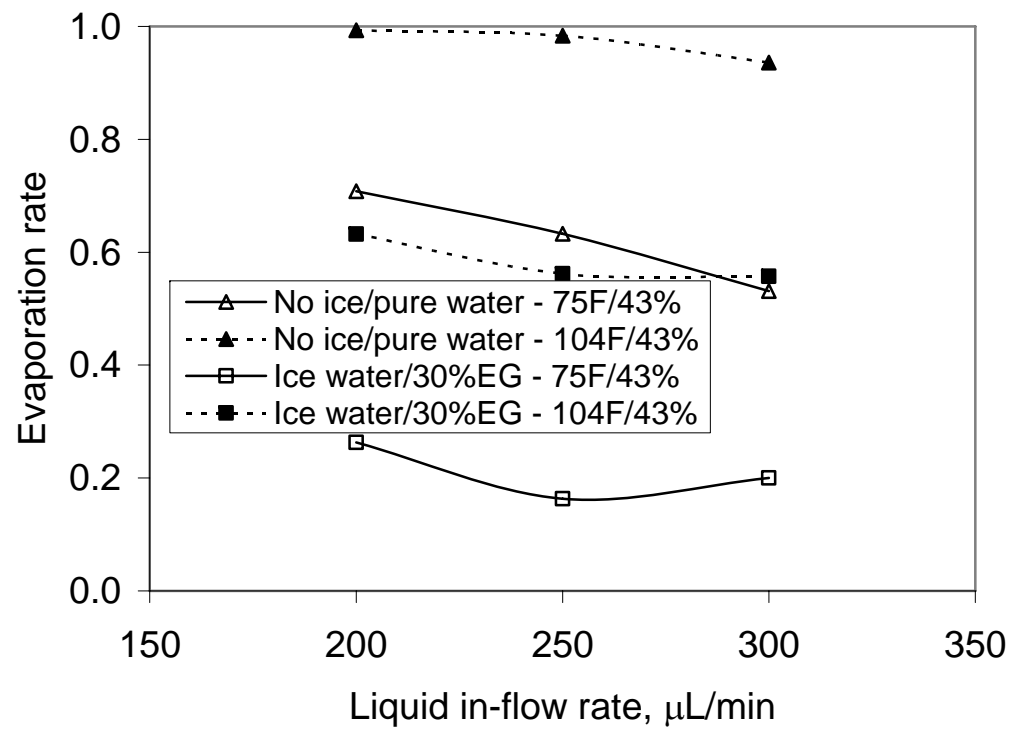


Figure 4.27. Evaporation rate with 30% EG in a cooled cyclone.

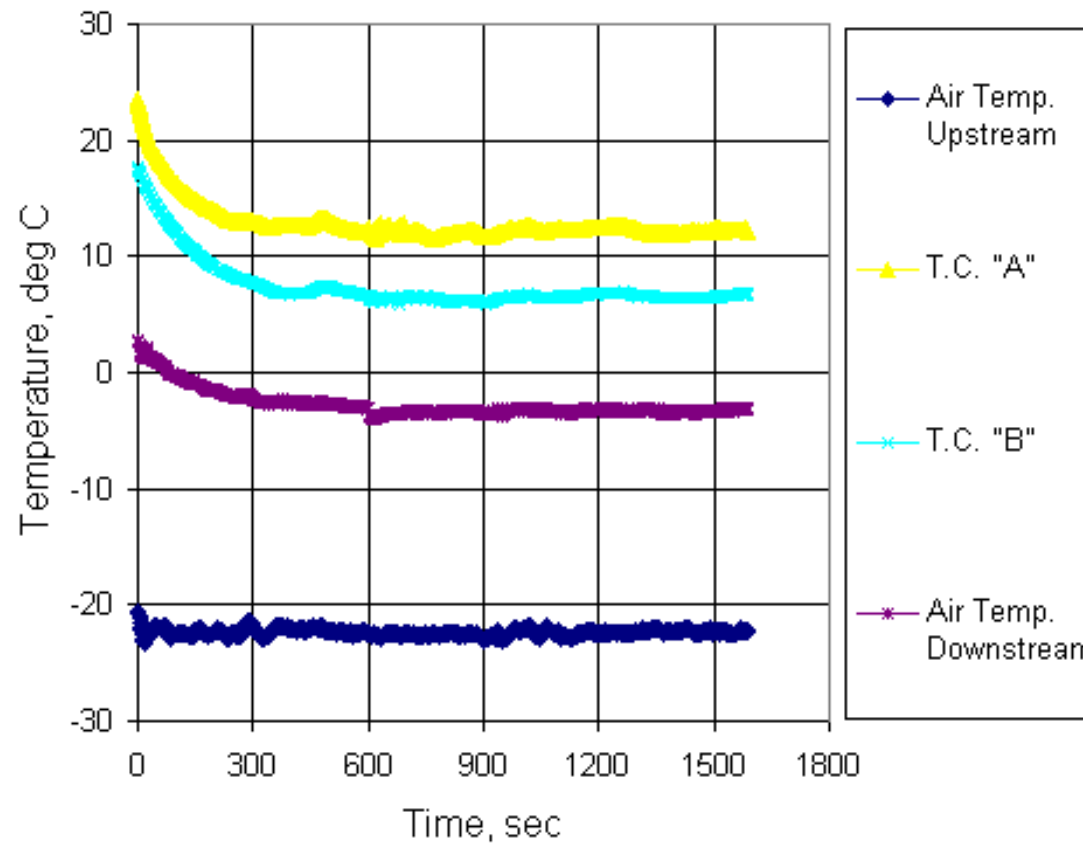


Figure 4.28. Temperature profiles when heat fluxes of 4.2 W/in^2 and 2.96 W/in^2 were applied to heater #2 and #3, respectively. No liquid Injection. Heating system and thermo-couple locations are shown in Figure 3.6.

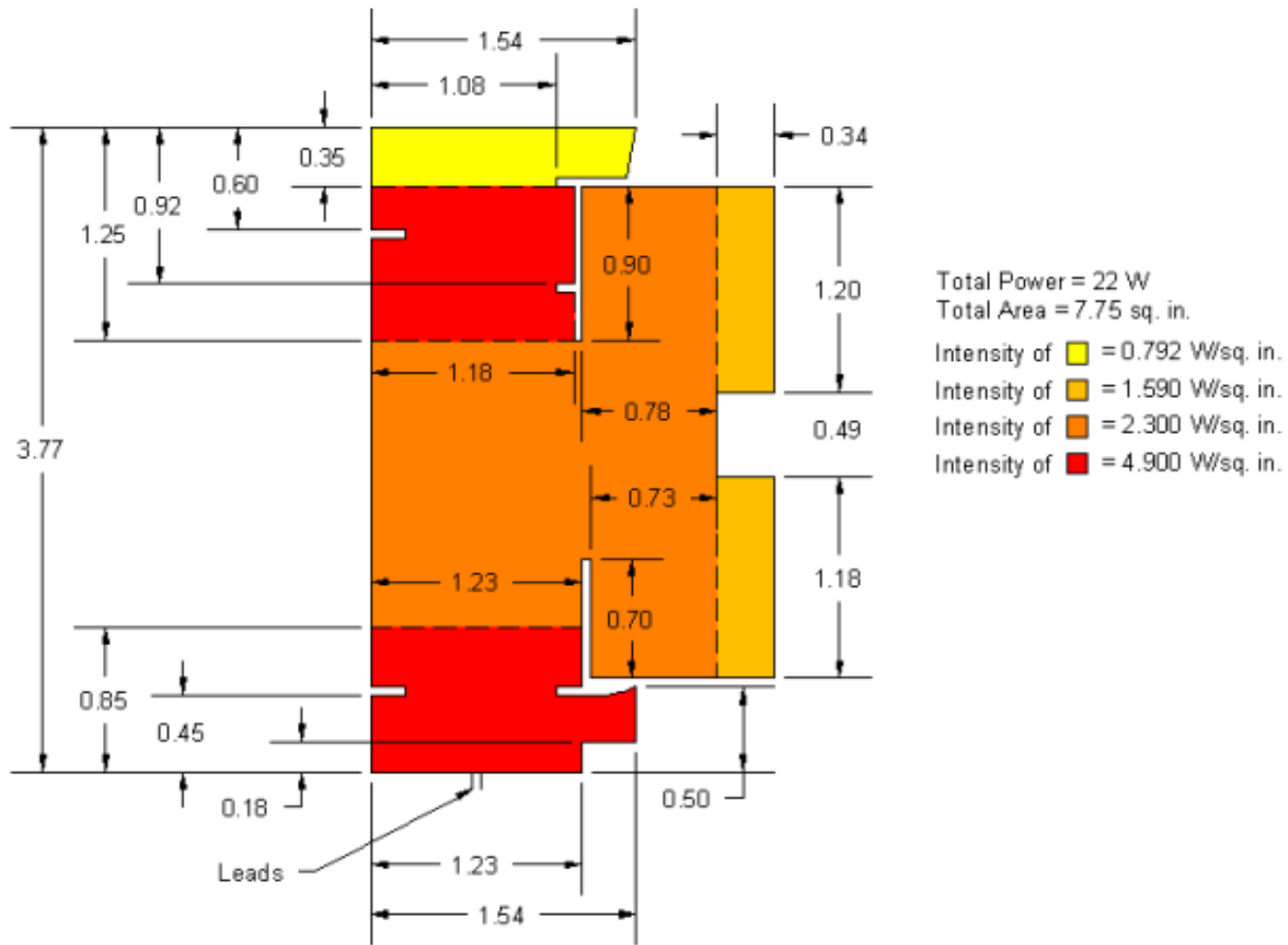
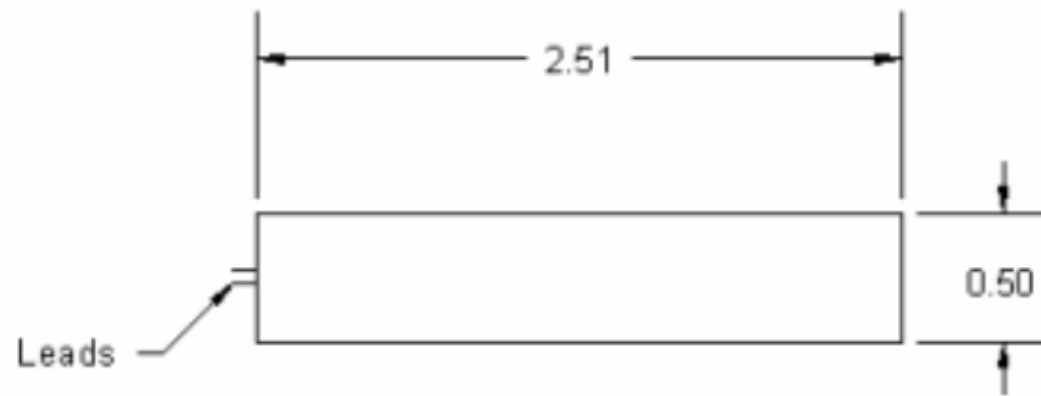
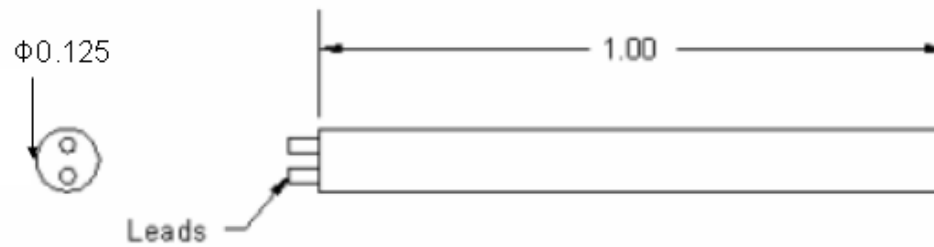


Figure 4.29. Final heating system for the 100 L/min cyclone.



Total Power = 4 W
 Total Area = 1.255 sq. in.
 Intensity = 3.19 W/sq. in.



Total Power = 1 W
 Total Area = 0.39 sq. in.
 Intensity = 2.55 W/sq. in.

Figure 4.29 continued.

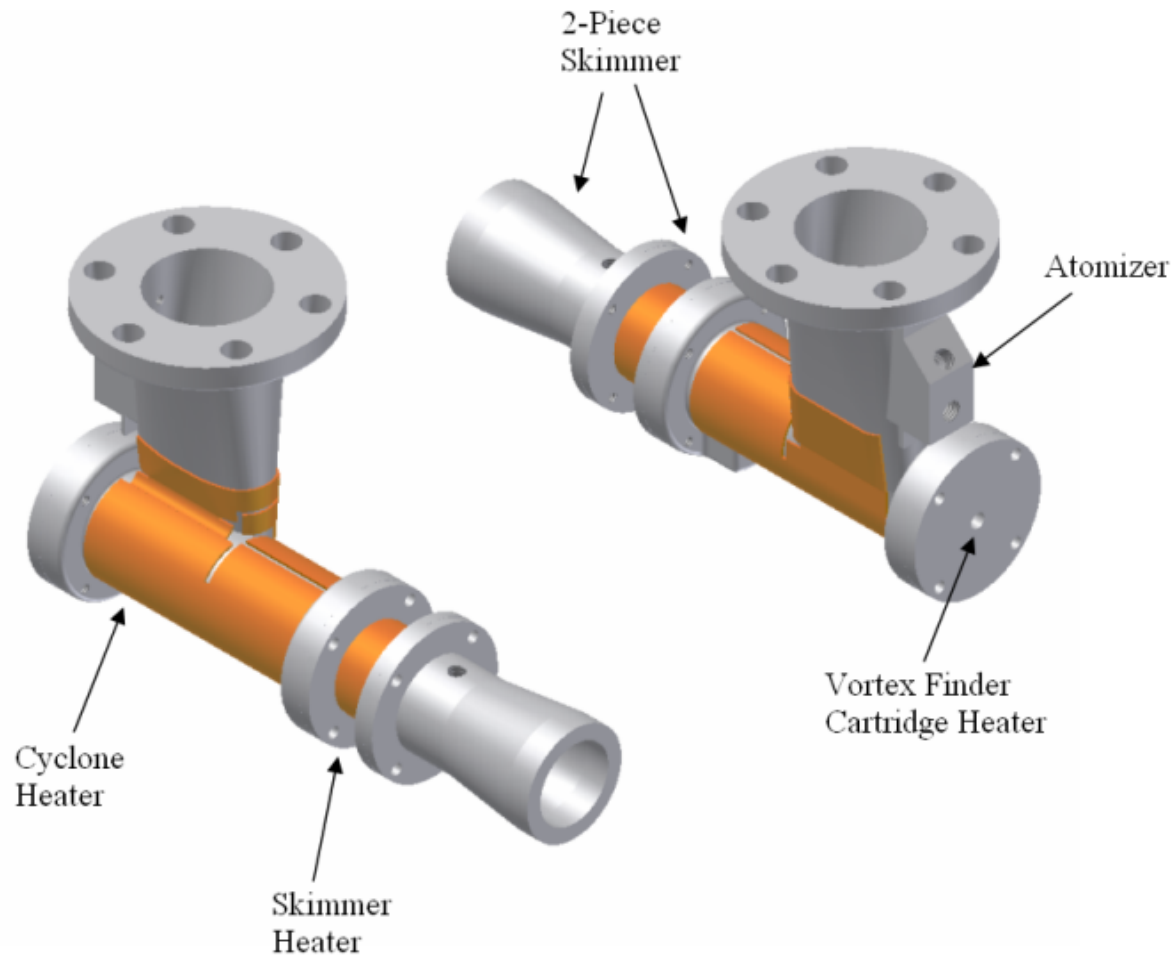


Figure 4.30. 100 L/min cyclone with the final heating system.

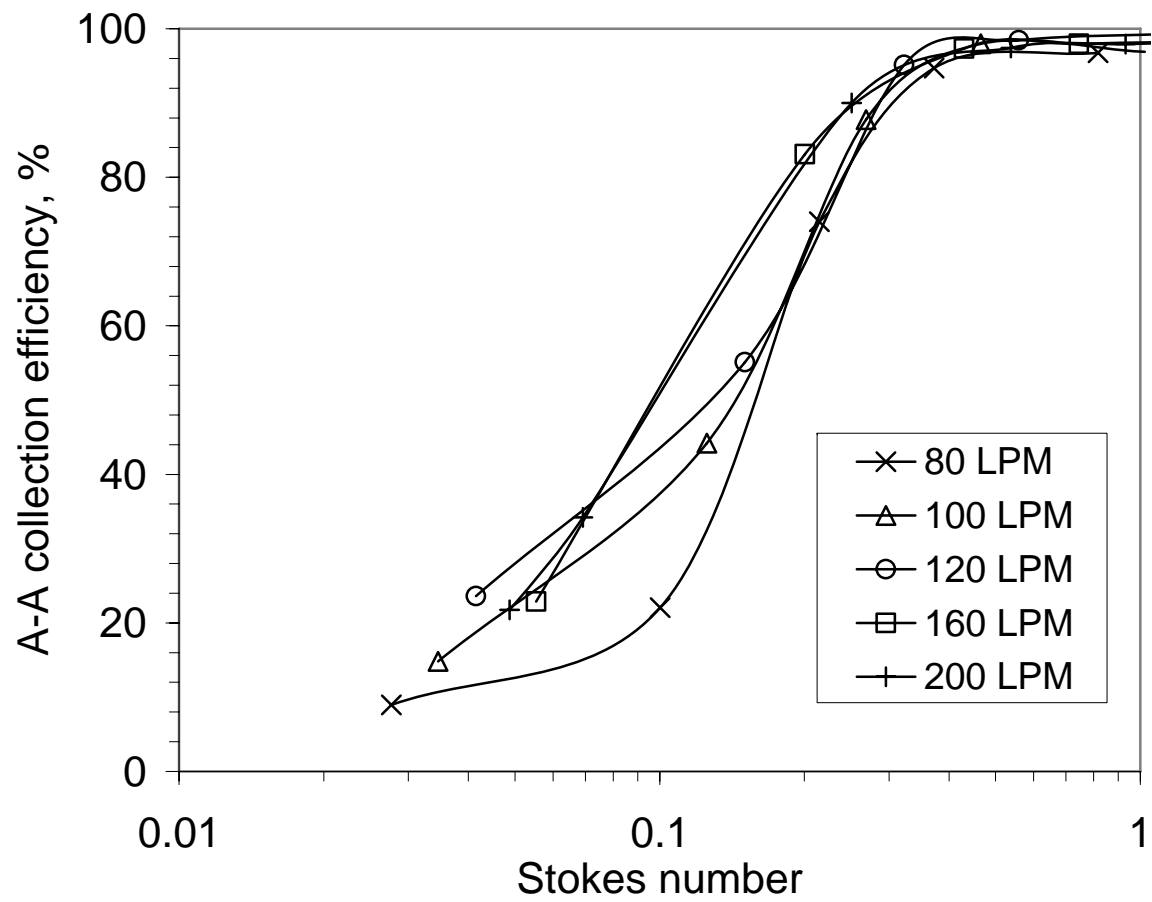


Figure 5.1. Aerosol-to-aerosol collection efficiency for the 100 L/min cyclone as a function of the Stokes number.

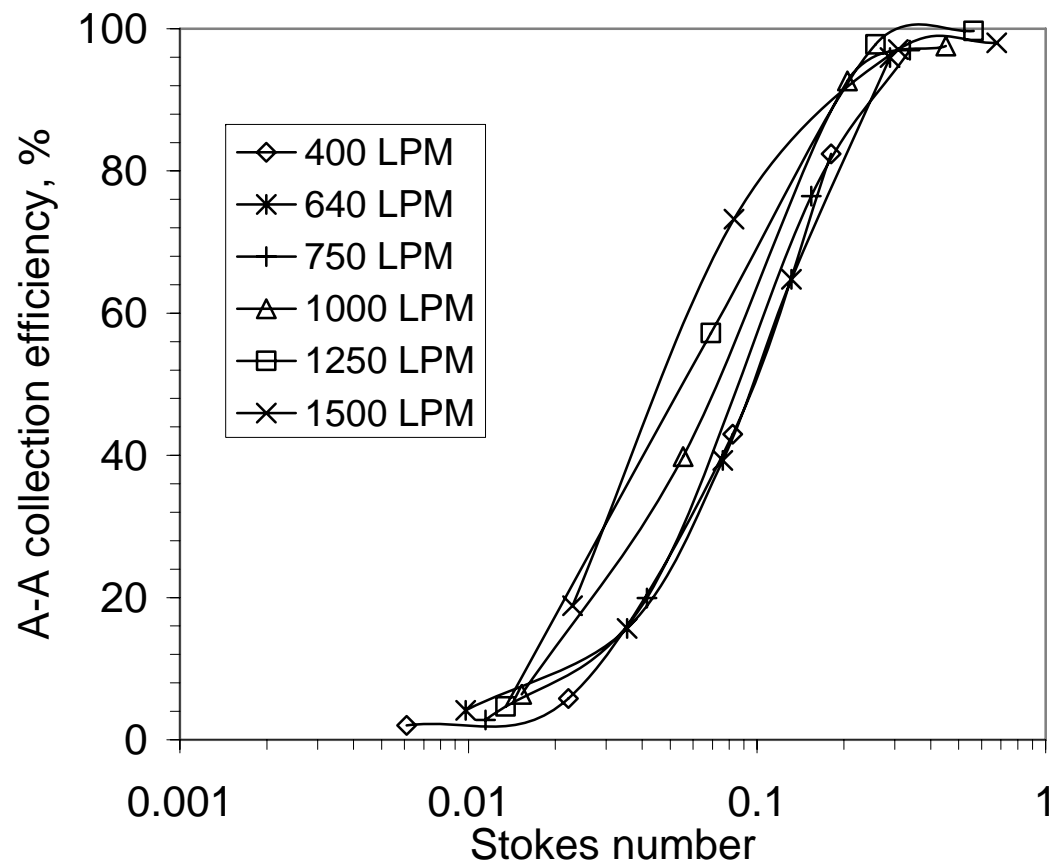


Figure 5.2. Aerosol-to-aerosol collection efficiency for the 1250 L/min cyclone as a function of the Stokes number.

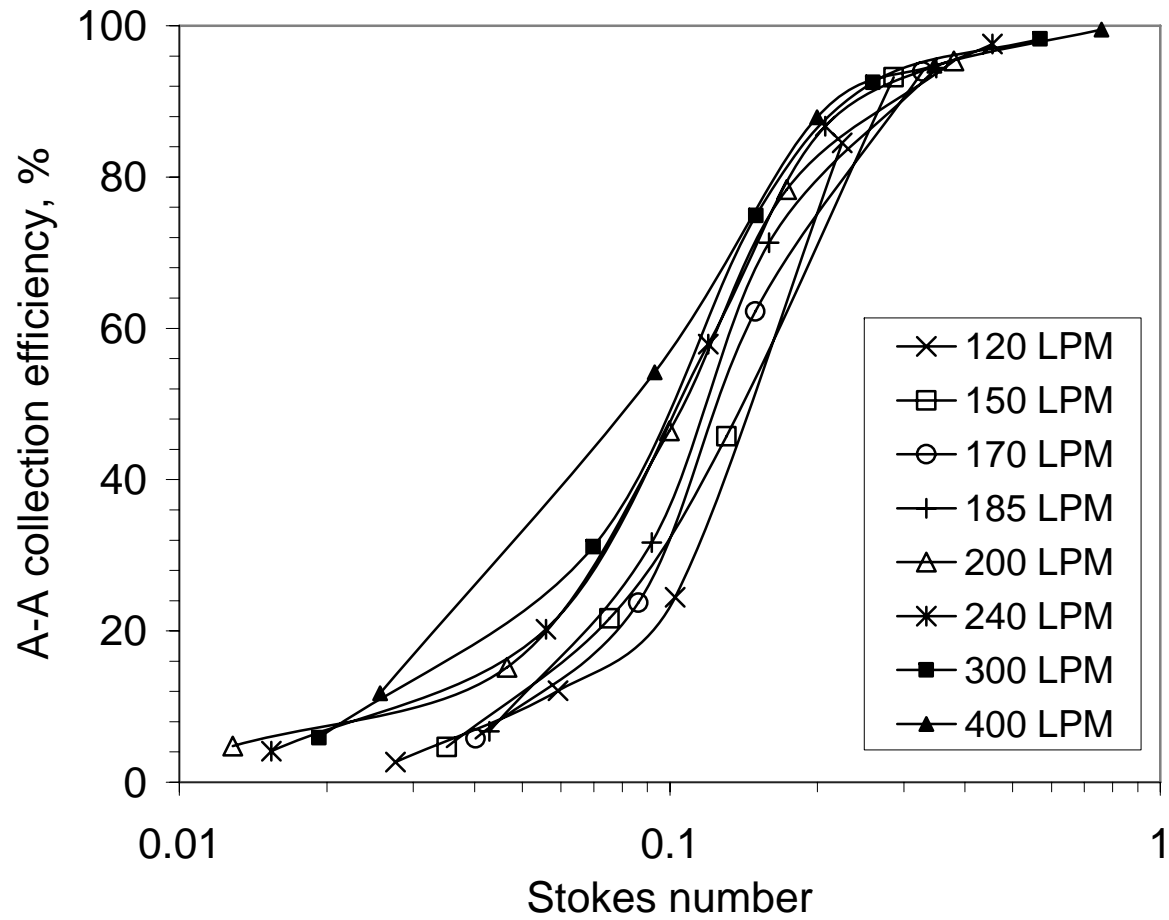


Figure 5.3. Aerosol-to-aerosol collection efficiency for the 300 L/min cyclone as a function of the Stokes number.

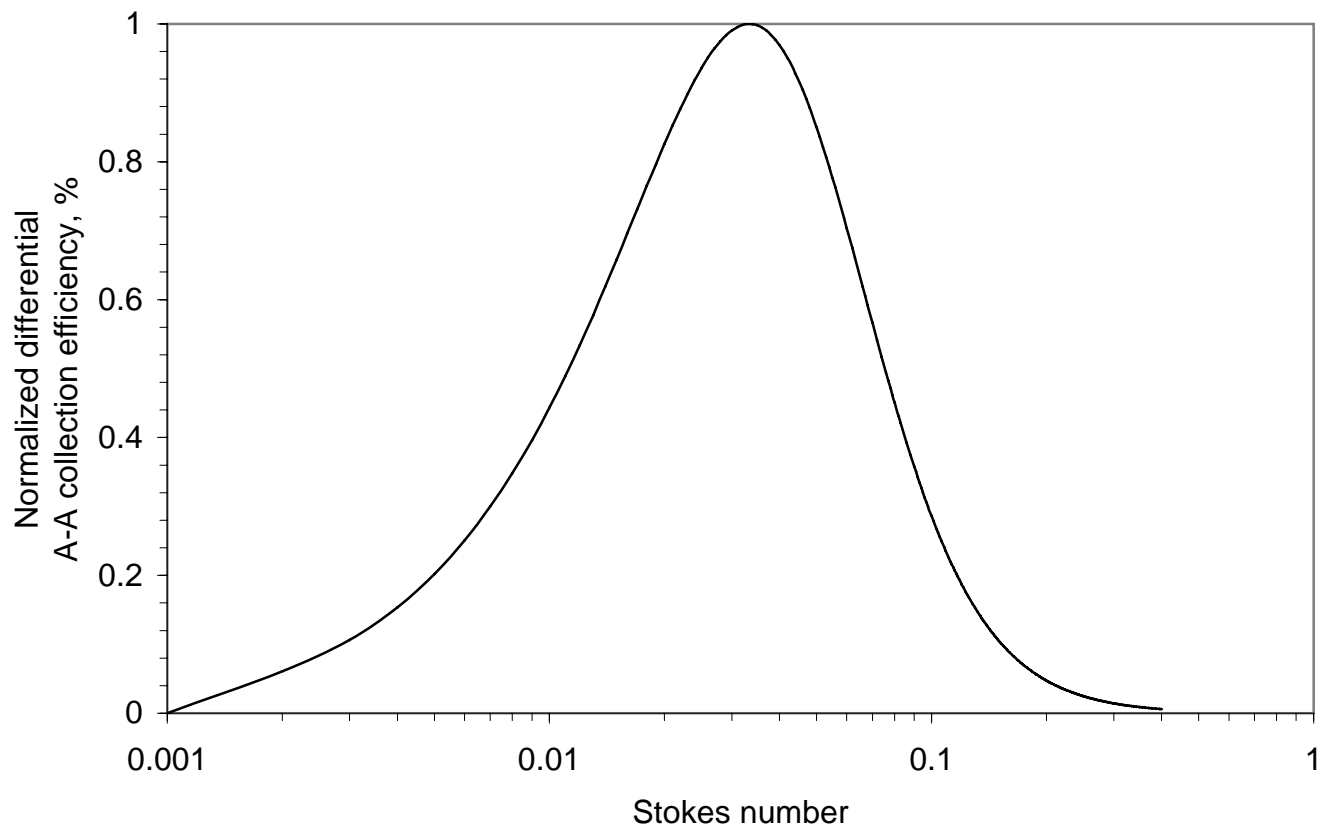


Figure 5.4. Normalized differential A-A collection efficiency for the 1250 L/min cyclone at 1250 L/min as a function of the Stokes number.

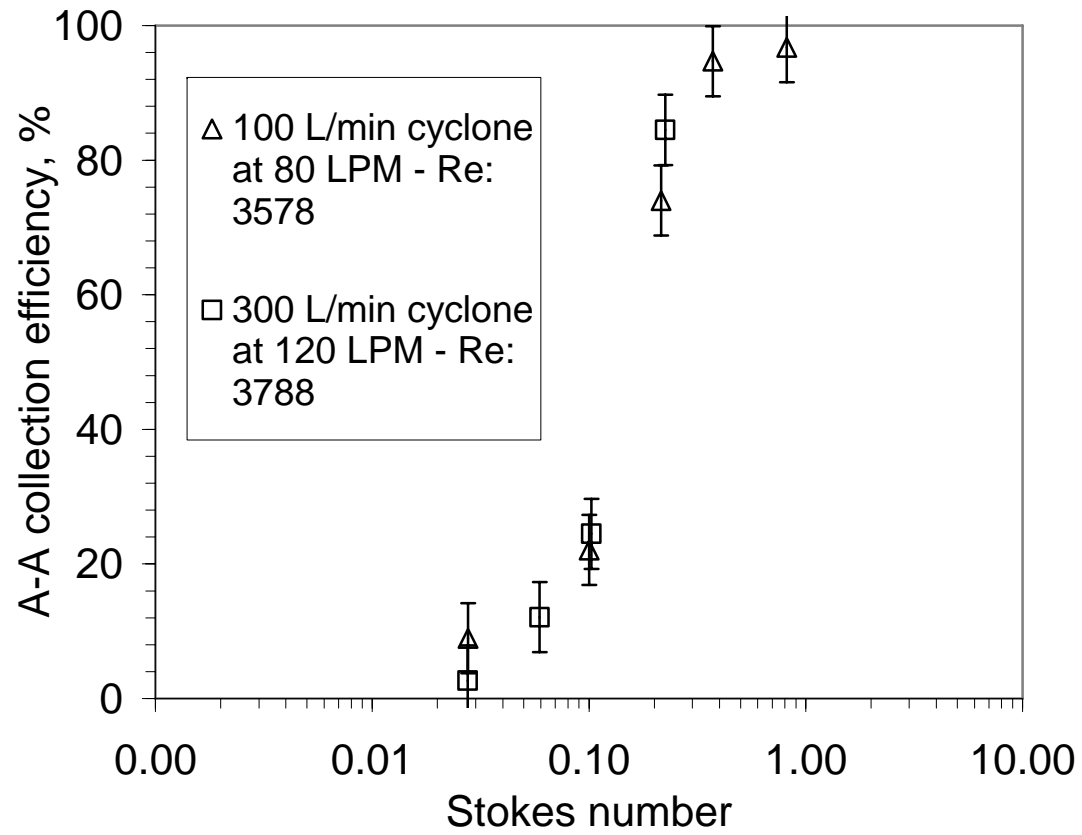


Figure 5.5. Comparison of the aerosol-to-aerosol collection efficiency of the 100 and 300 L/min cyclones operating at different flow rates, corresponding to the Reynolds number of 3600.

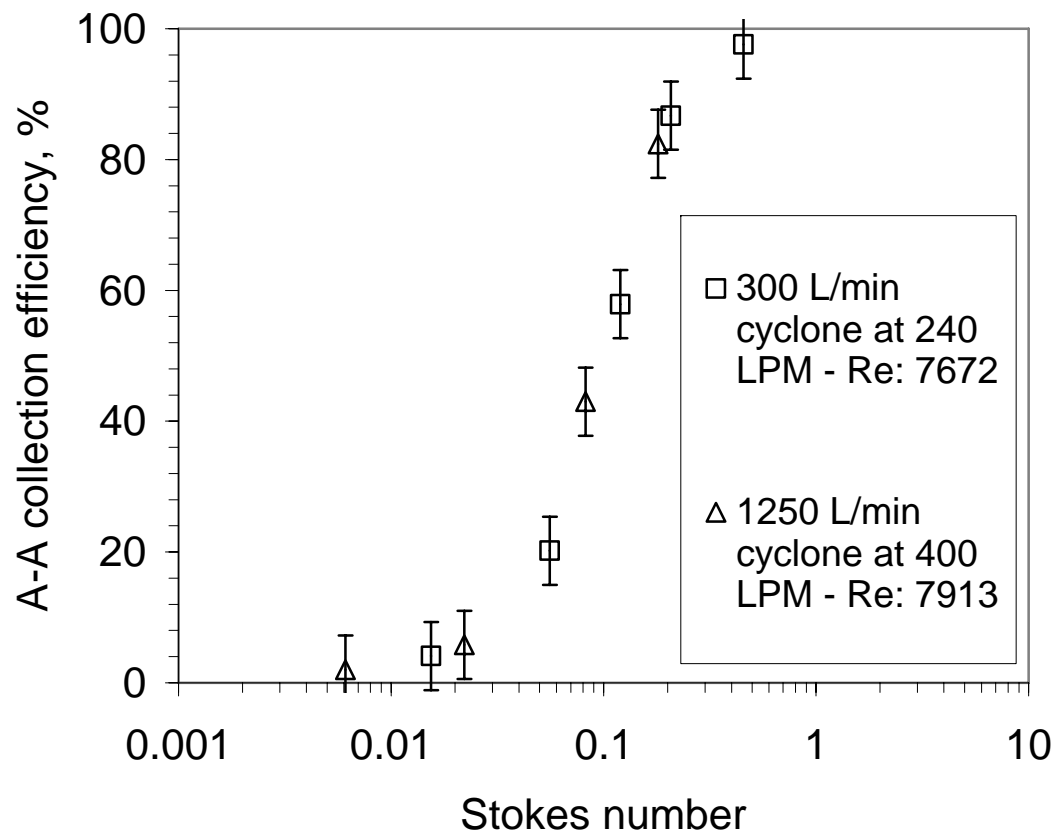


Figure 5.6. Comparison of the aerosol-to-aerosol collection efficiency of the 300 and 1250 L/min cyclones operating at different flow rates, but close to the Reynolds number value of 7800.

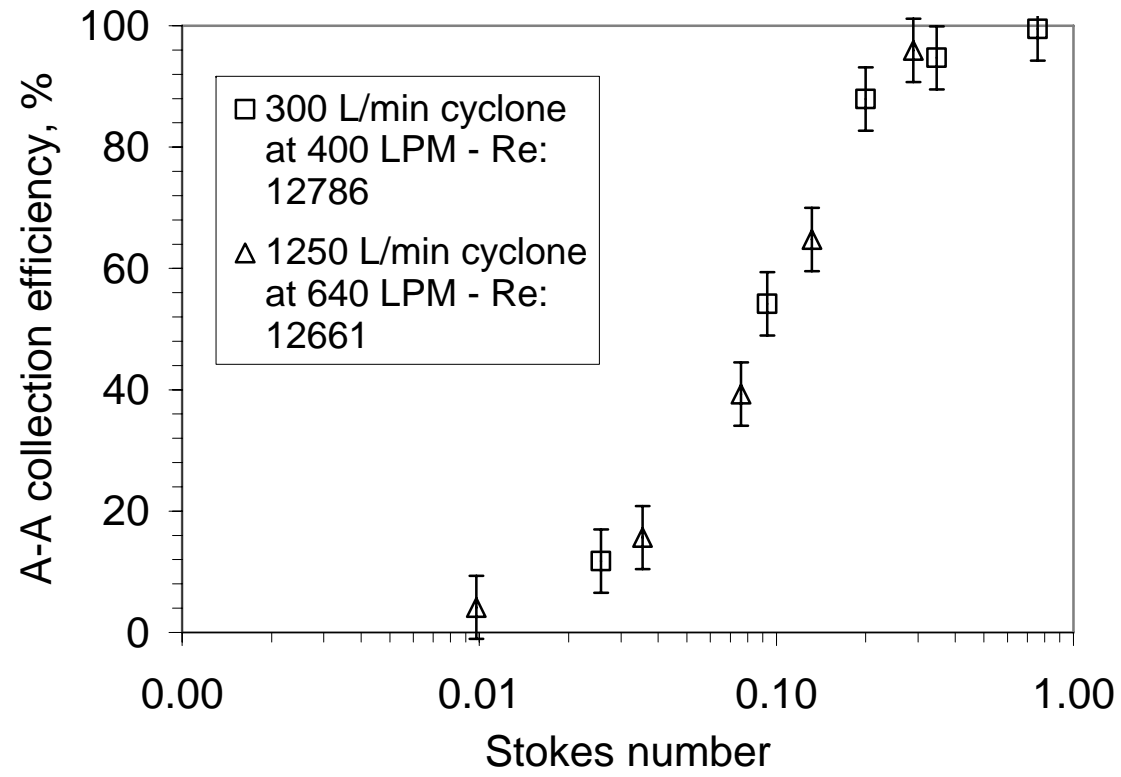
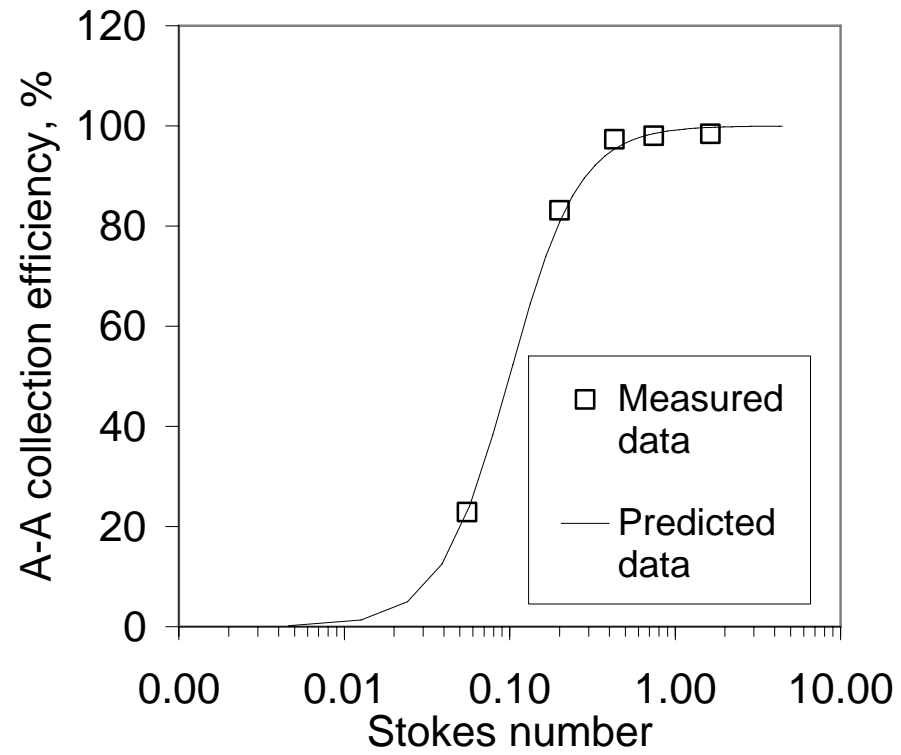
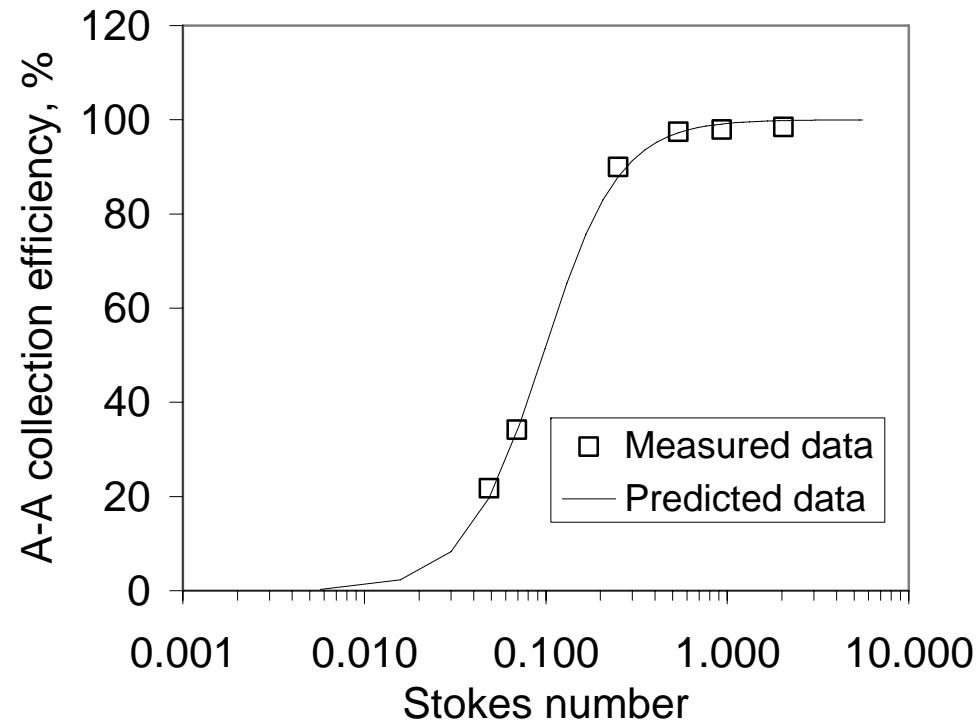


Figure 5.7. Comparison of the aerosol-to-aerosol collection efficiency for the 300 and 1250 L/min cyclones operating at different flow rates, but close to the Reynolds number of 12700.



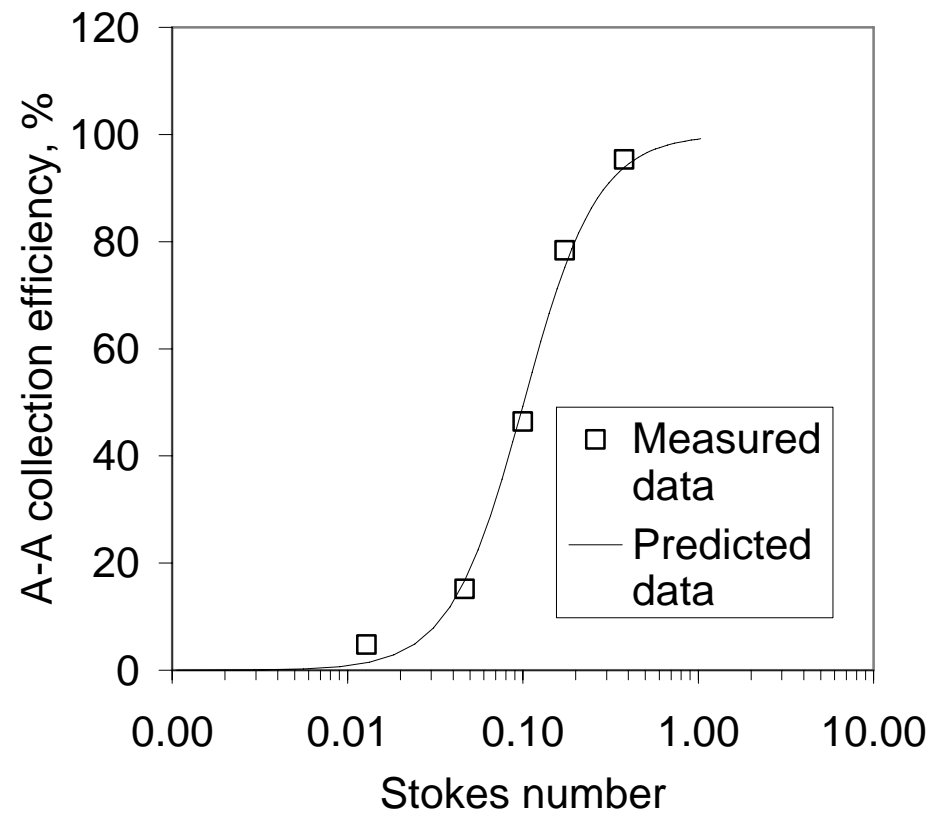
a) 100 L/min cyclone at 160 L/min, $Re=7155$, R-Square value: 0.997

Figure 5.8. Measured and predicted aerosol-to-aerosol collection efficiency as a function of the Stokes number for high Reynolds number region.



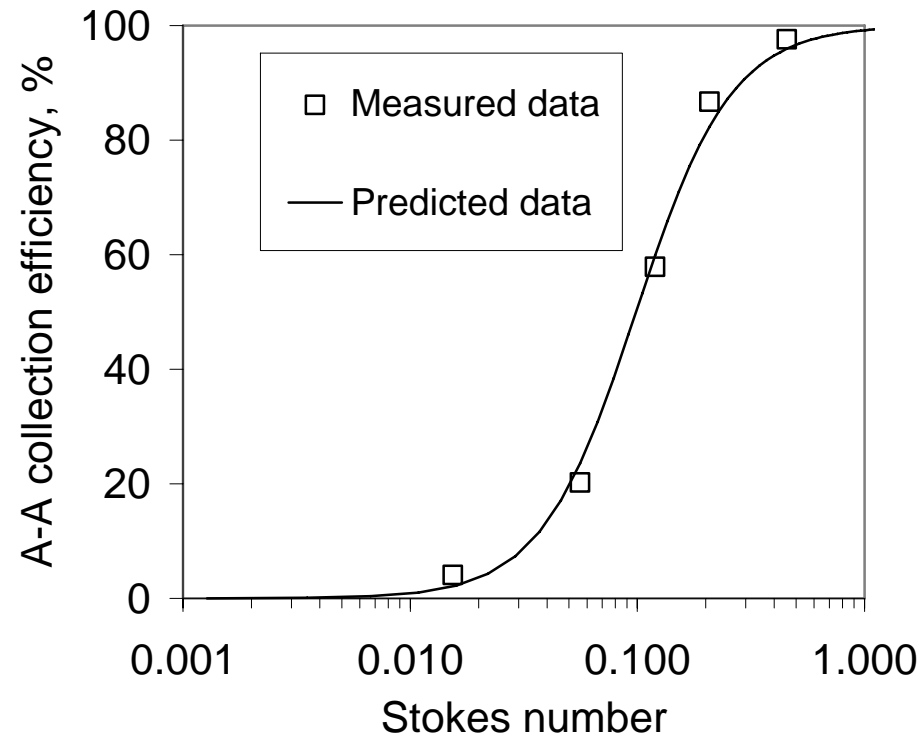
b) 100 L/min cyclone at 200 L/min, $Re=8944$, R-Square value: 0.998

Figure 5.8 continued.



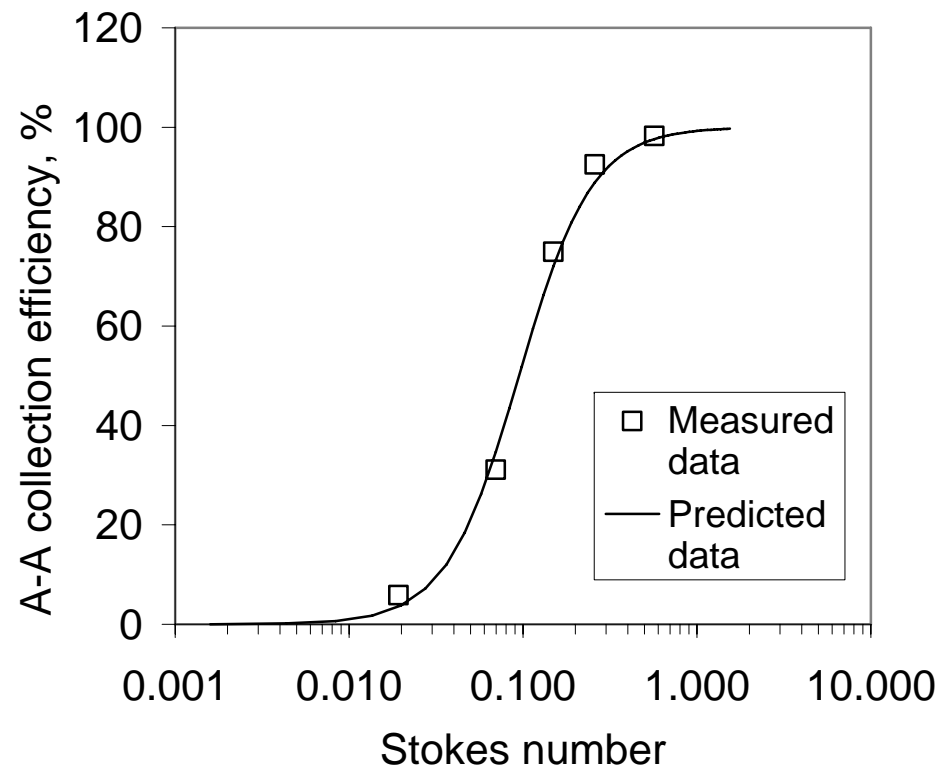
c) 300 L/min cyclone at 200 L/min, $Re=6393$, R-Square value: 0.995

Figure 5.8 continued.



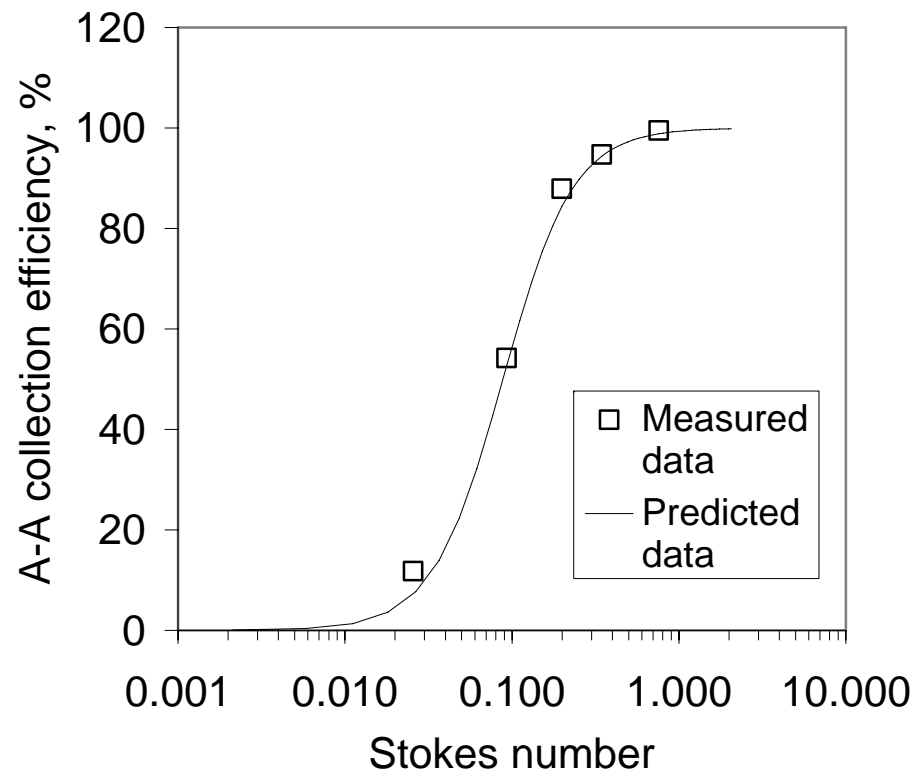
d) 300 L/min cyclone at 240 L/min, $Re=7672$, R-Square value: 0.994

Figure 5.8 continued.



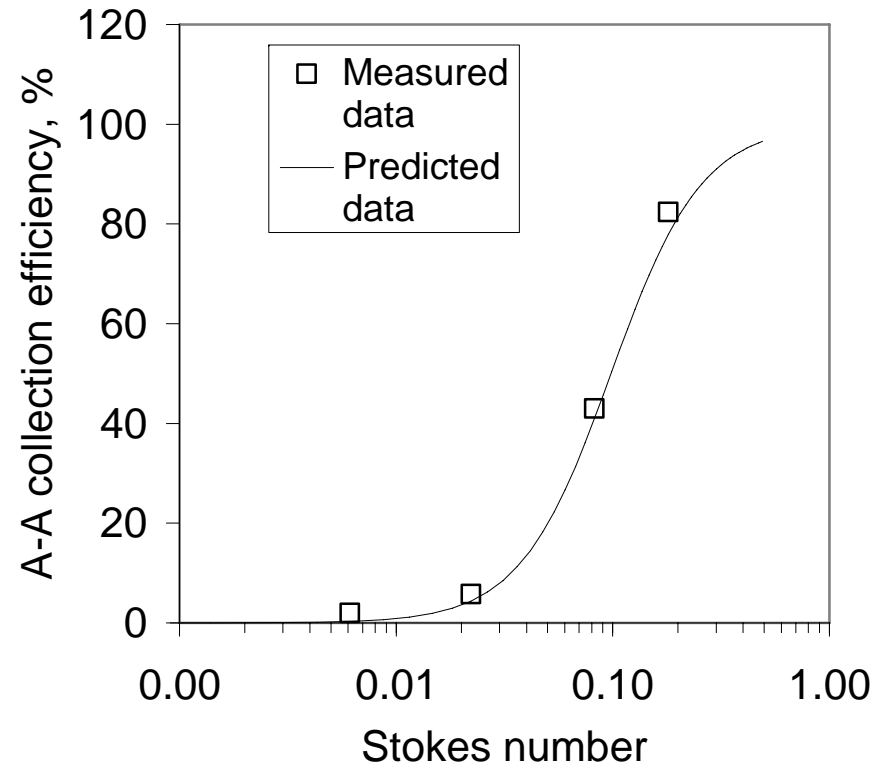
e) 300 L/min cyclone at 300 L/min, $Re=9590$, R-Square value: 0.994

Figure 5.8 continued.



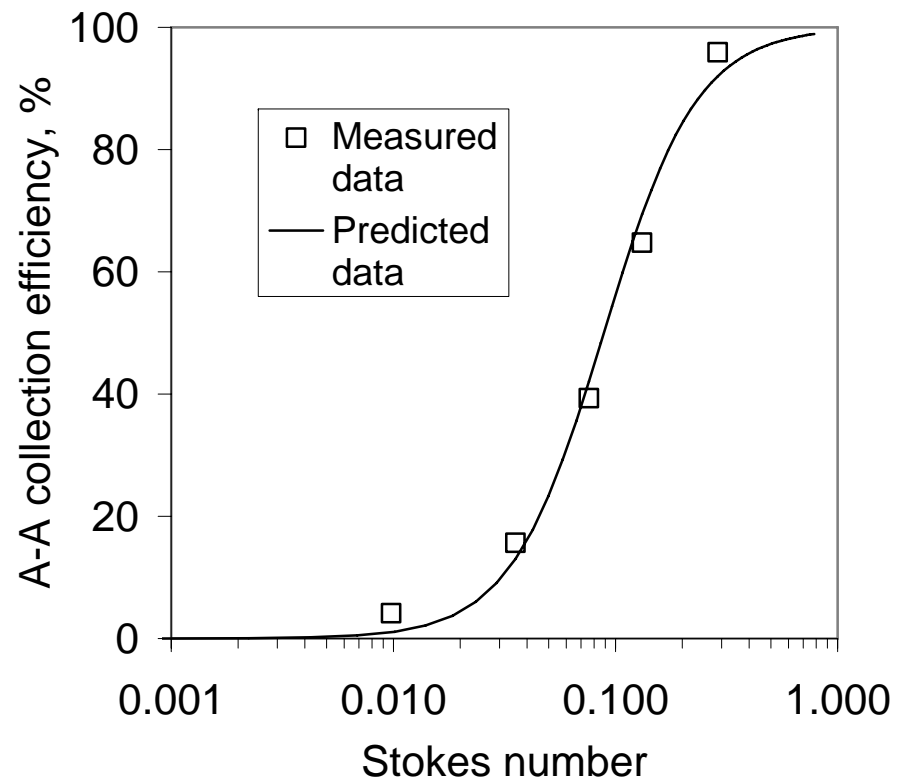
f) 300 L/min cyclone at 400 L/min, $Re=12786$, R-Square value: 0.994

Figure 5.8 continued.



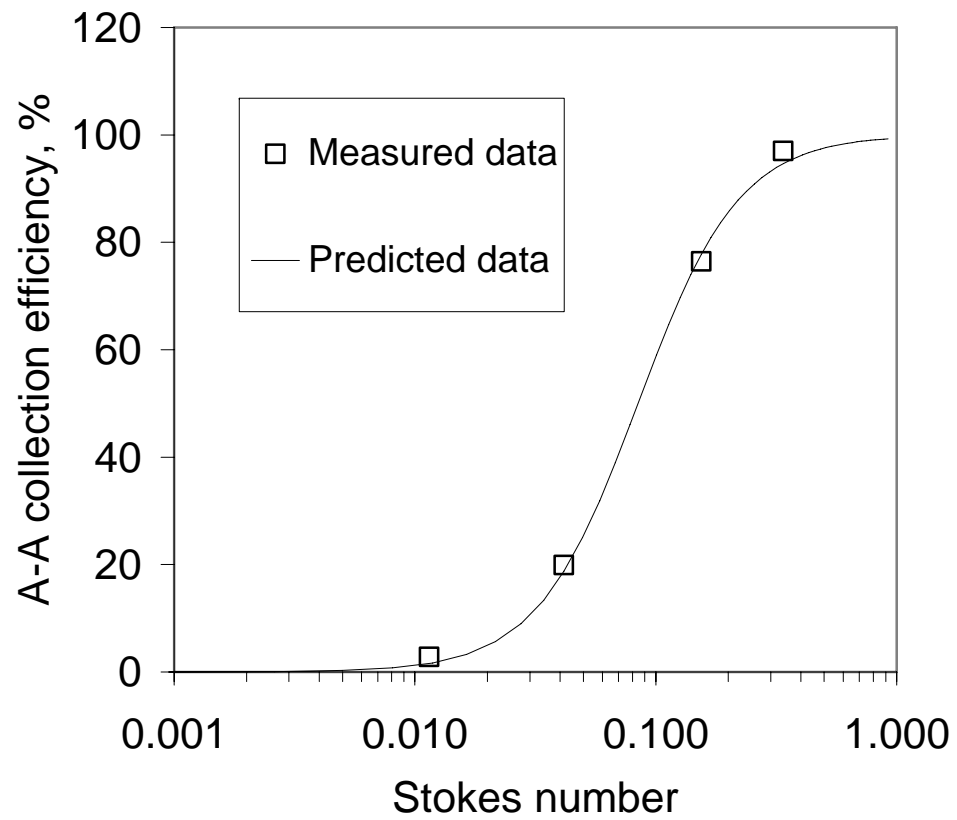
g) 1250 L/min cyclone at 400 L/min, $Re=7913$, R-Square value: 0.993

Figure 5.8 continued.



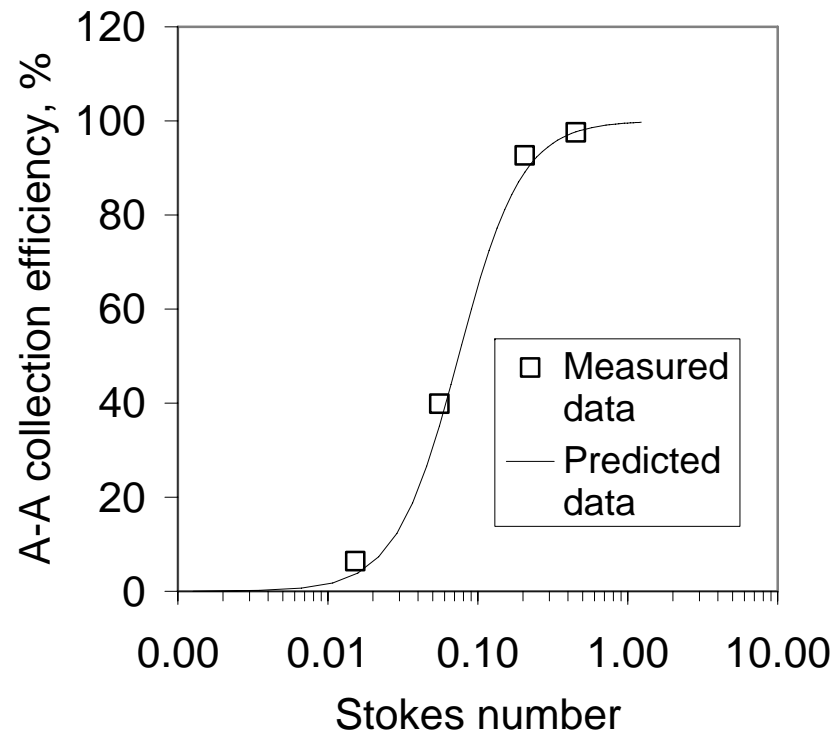
h) 1250 L/min cyclone at 640 L/min, $Re=12661$, R-Square value: 0.989

Figure 5.8 continued.



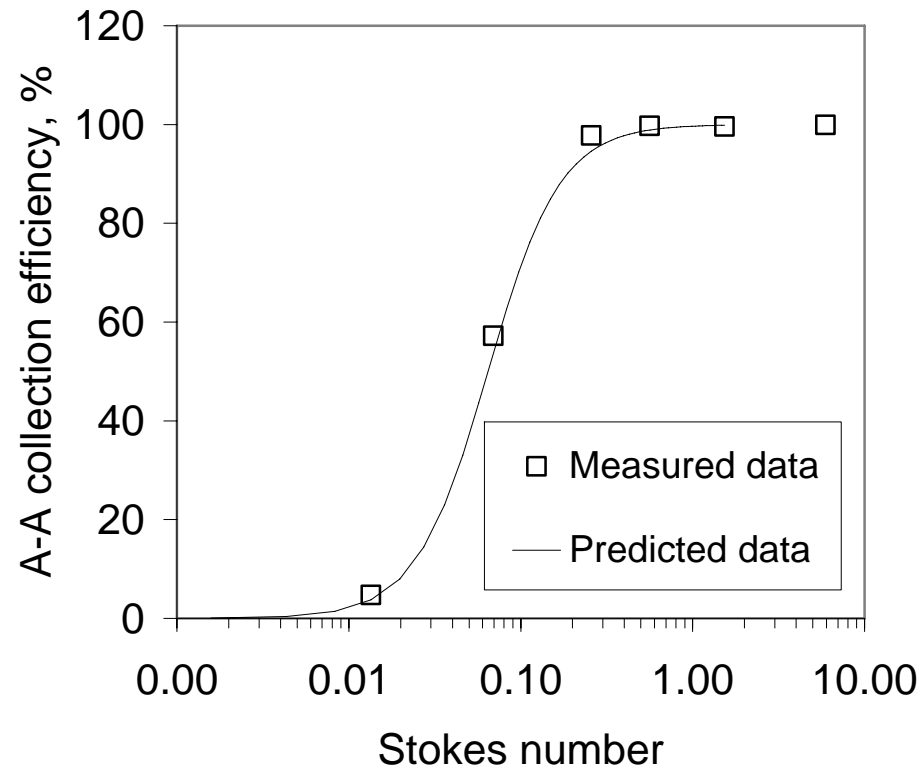
i) 1250 L/min cyclone at 750 L/min, $Re=14838$, R-Square value: 0.998

Figure 5.8 continued.



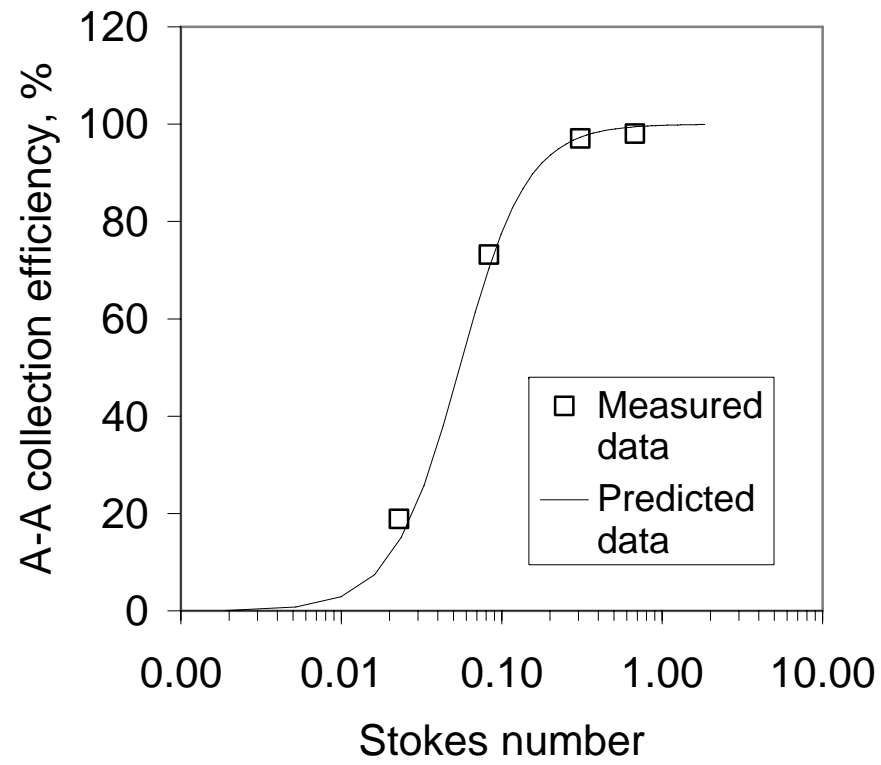
j) 1250 L/min cyclone at 1000 L/min, $Re=19784$, R-Square value: 0.993

Figure 5.8 continued.



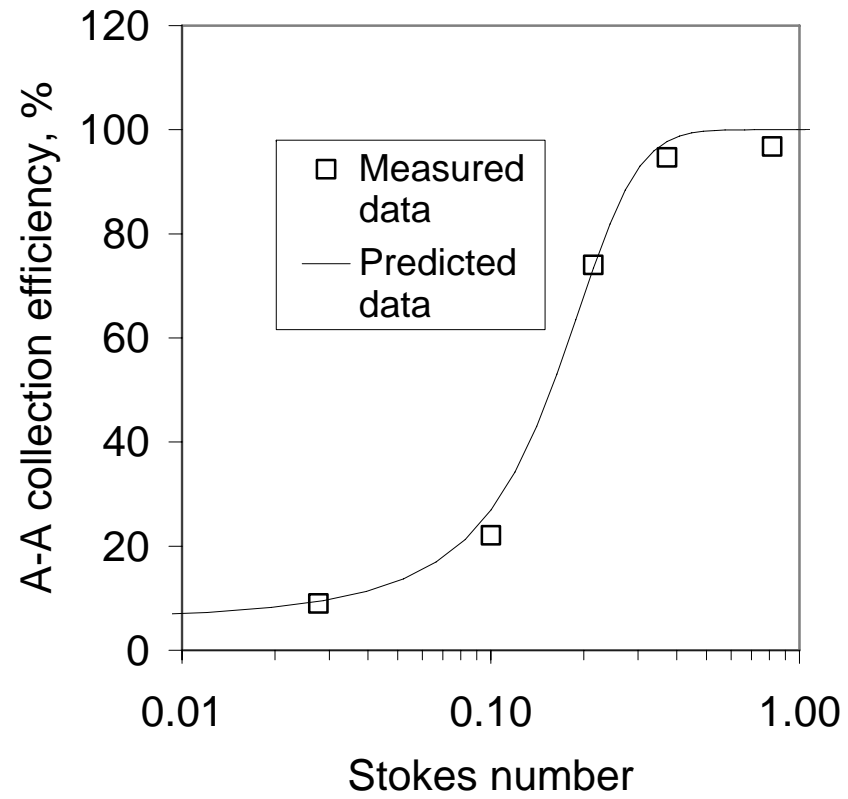
k) 1250 L/min cyclone at 1250 L/min, $Re=24729$, R-Square value: 0.996

Figure 5.8 continued.



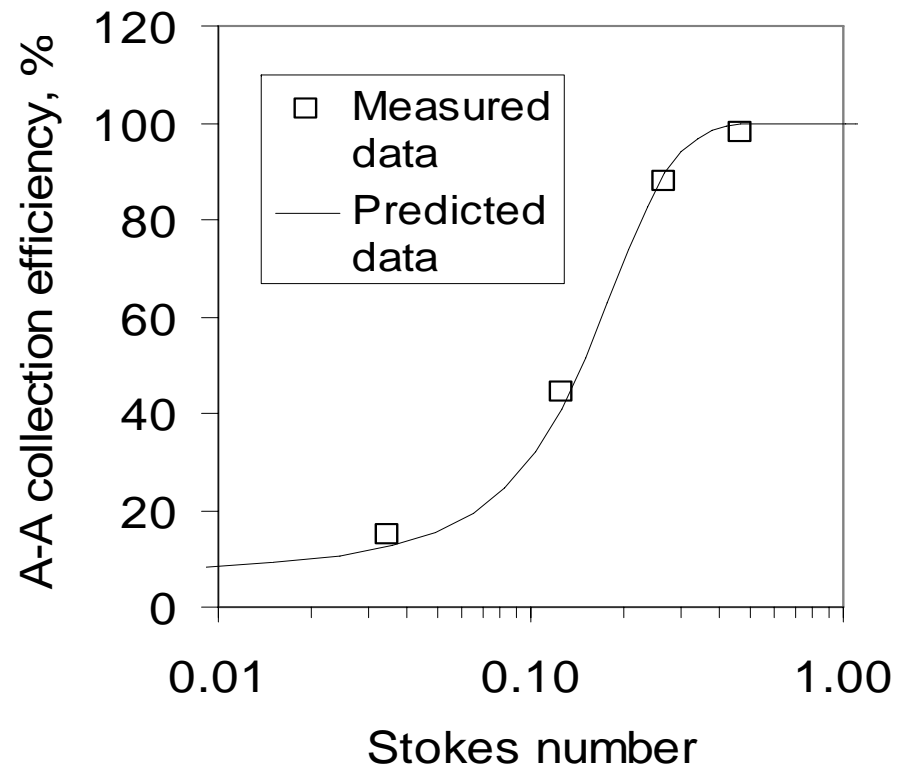
l) 1250 L/min cyclone at 1500 L/min, $Re=29675$, R-Square value: 0.994

Figure 5.8 continued.



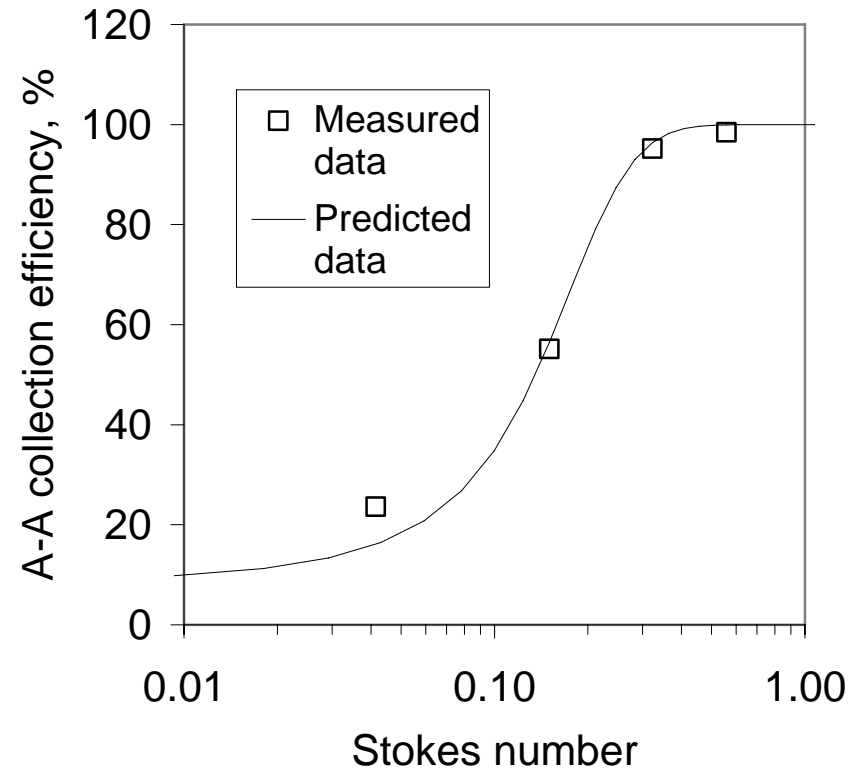
a) 100 L/min cyclone at 80 L/min, $Re=3578$, R-Square value: 0.993

Figure 5.9. Measured and predicted aerosol-to-aerosol collection efficiency as a function of the Stokes number for low Reynolds number region.



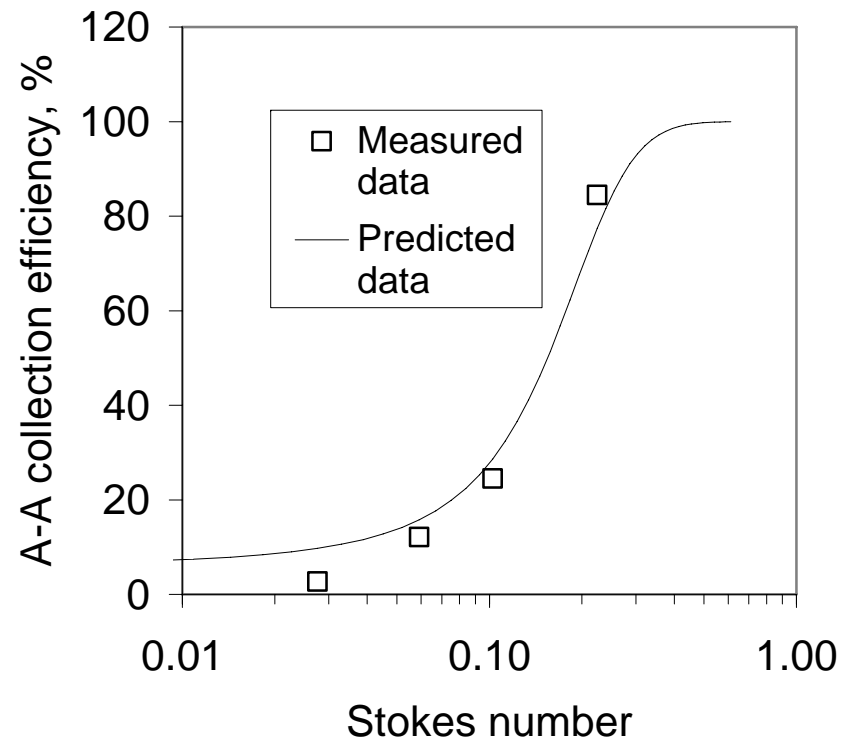
b) 100 L/min cyclone at 100 L/min, $Re=4472$, R-Square value: 0.994

Figure 5.9 continued.



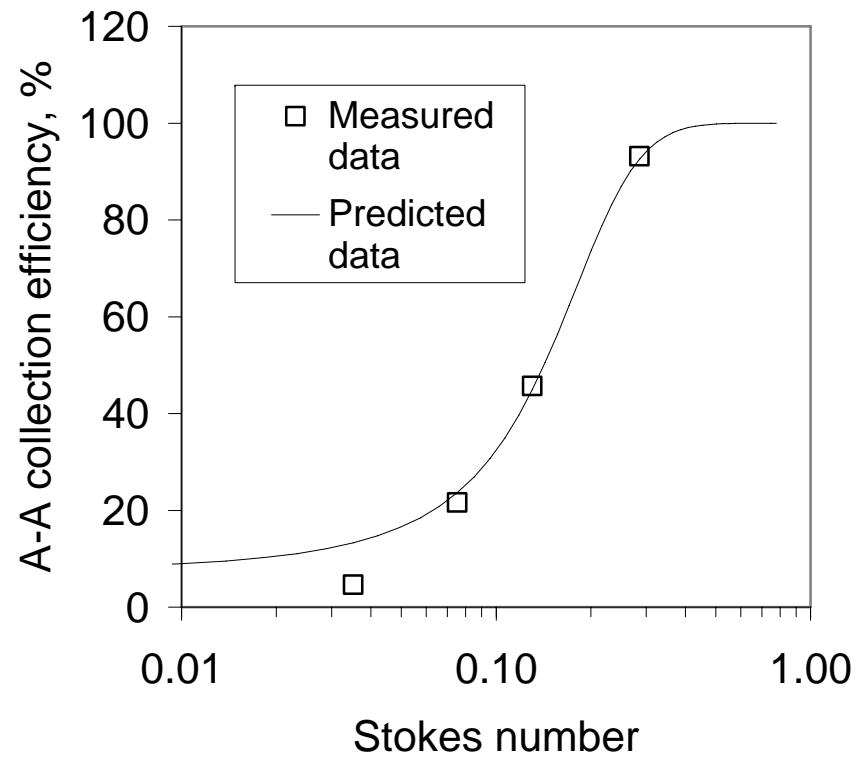
c) 100 L/min cyclone at 120 L/min, $Re=5366$, R-Square value: 0.988

Figure 5.9 continued.



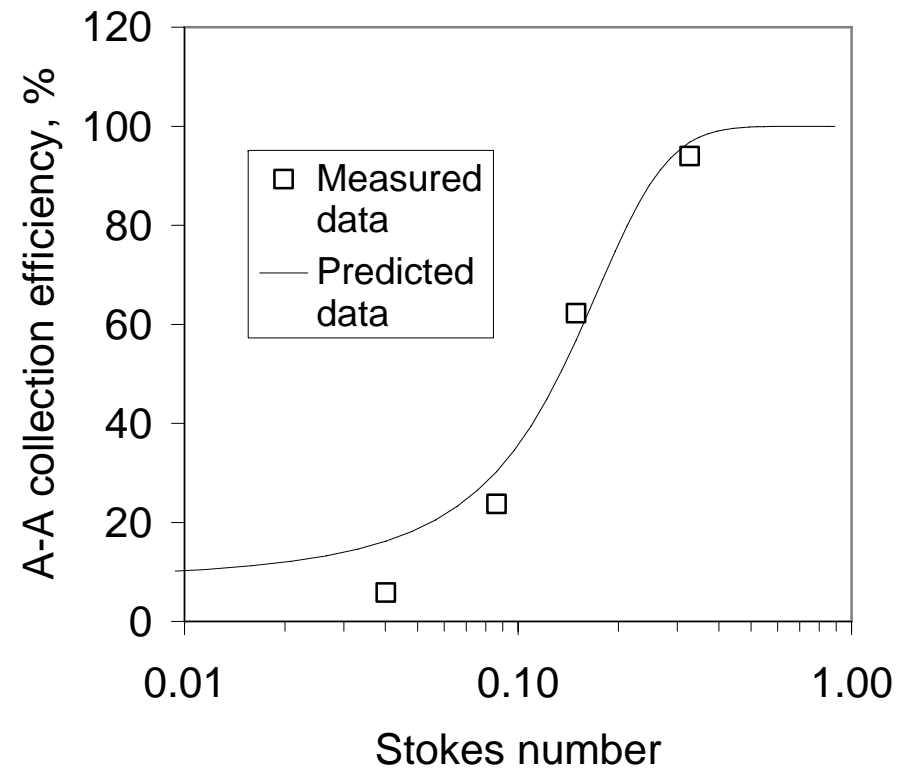
d) 300 L/min cyclone at 120 L/min, $Re=3788$, R-Square value: 0.968

Figure 5.9 continued.



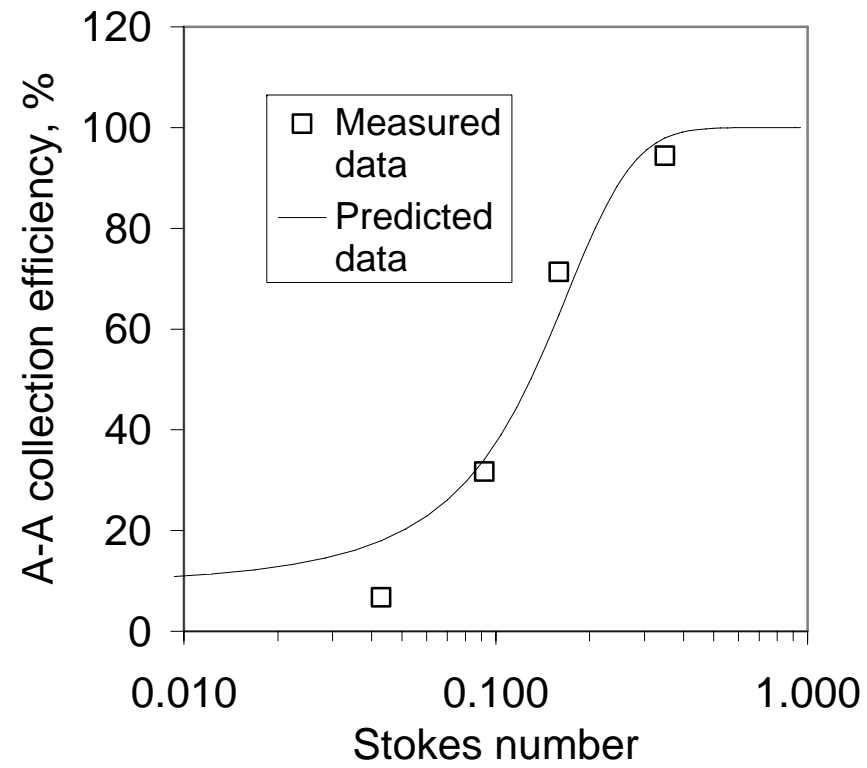
e) 300 L/min cyclone at 150 L/min, $Re=4824$, R-Square value: 0.982

Figure 5.9 continued.



f) 300 L/min cyclone at 170 L/min, $Re=5521$, R-Square value: 0.960

Figure 5.9 continued.



g) 300 L/min cyclone at 185 L/min, $Re=5885$, R-Square value: 0.953

Figure 5.9 continued.

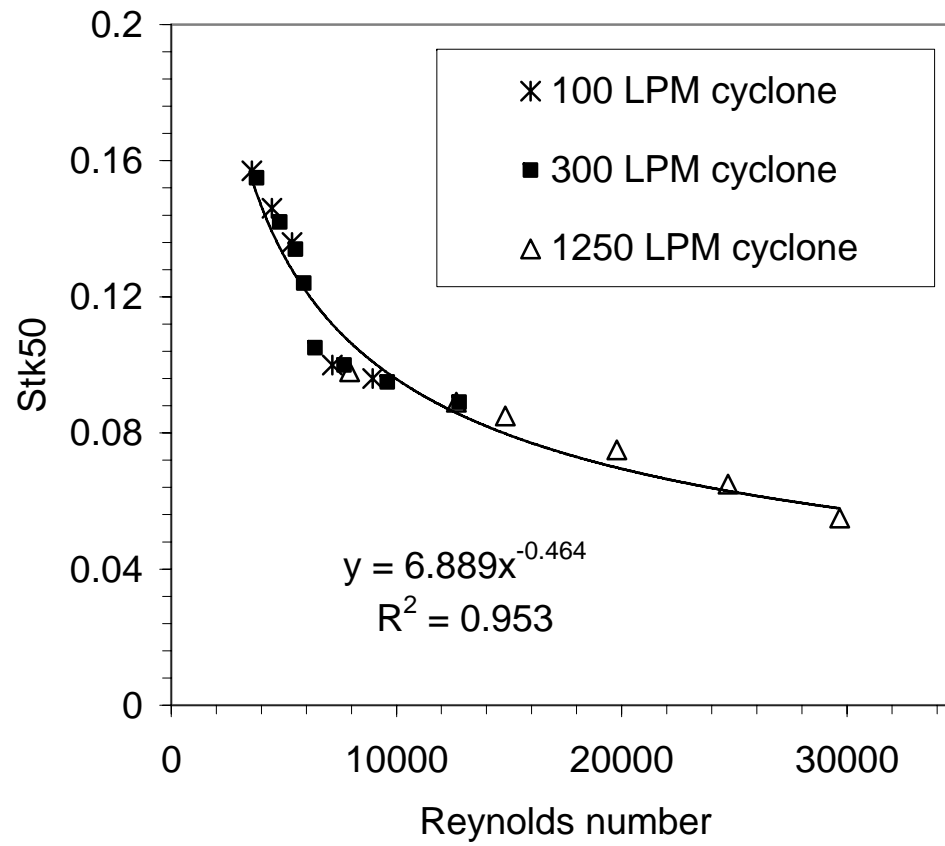


Figure 5.10. Stk_{50} values as a function of the Reynolds number.

Table 2.1. Comparison of the Black and Shaw cyclone with the 1250 L/min cyclone.

	Black and Shaw cyclone	1250 L/min cyclone
Flow Rate	900 L/min	1250 L/min
Inlet Length	1.8 in	2.5 in
Inlet Width	0.25 in	0.25 in
Body Diameter	1.125 in	1.5 in
Liquid Ring Volume	0.15 mL	None
Liquid By-Pass	Intermittent	None

Table 2.2. Representative dimensions for three cyclones.

	100 L/min Cyclone	300 L/min Cyclone	1250 L/min Cyclone
slot width	0.1077''	0.155''	0.25''
body length / slot length	2.33	2.33	2.37
body length / body diameter	3.88	3.88	3.95

Table 3.1. Uncertainty values in the Stokes number.

Particle size, μm	Uncertainty in the Stokes number, %
0.5	8.8
1	9.0
1.5	9.1
2	9.1
3	9.1
5	9.2
10	9.2

Table 3.2. Optical filters and tracer dye used in fluorometric analysis.

Particle Type	Tracer	Excitation	Emission
Polystyrene Latex	Duke Scientific, Blue	NB360	NB440
Polystyrene Latex	Duke Scientific, Green	NB460	NB490
Polystyrene Latex	Duke Scientific, Red	NB 540	NB590
Polystyrene Latex	Twilight Blue	NB 420	NB 490

Table 3.3. Power input to each heater element of the preliminary heating system for the 1250 L/min cyclone.

Heater No.	Power (W)
1	32
2	132
3	71
4	82
Total:	317

Table 3.4. Heater specifications of the preliminary heating system for the 100 L/min cyclone.

Heater	Part #	Size (inch)	Resistance (Ω)
1 Cartridge	WATLOW 8W @120V	D:0.125,L:1	
2 Inlet and Impacting	MINCO HK 5352	1.04x4.35	43.8
3 Middle	MINCO HK 5292	0.78x2.76	41.9
4 Liquid Port	MINCO HK 5208	0.3x3.11	44.1
5 Skimmer	MINCO HK 5242	0.5x2.5	35.1

Table 4.1. Comparison of heat flux between two heating systems for the 1250 L/min cyclone.

	Preliminary heating system	Final heating system
	W/sq-in	W/sq-in
Inlet	8.15	0.619~10.438
Front Body	8.15	5.919
Back Body	7.6	5.919
Hydrosol Outlet Area	None	1.591

Table 4.2. Series of procedures and time sequence followed in the time constant tests.

"Wet start" test	"Dry start" test
<ol style="list-style-type: none"> 1. Whole system on simultaneously excluding a nebulizer 2. Three 1 minute samples 3. Nebulizer ON 4. Ten 1 minute samples 5. Five 2 minute samples 6. Four 3 minute samples 7. Two 4 minute samples 8. Nebulizer OFF 9. Three 1 minute samples 	<ol style="list-style-type: none"> 1. Whole system on simultaneously including a nebulizer 2. Ten 1 minute samples 3. Five 2 minute samples 4. Four 3 minute samples 5. Two 4 minute samples 6. Nebulizer OFF 7. Three 1 minute samples

Table 4.3. Effect of EG concentration on the A-H collection efficiency. Liquid effluent flow rate: 0.1 mL/min.

EG concentration, %	A-H efficiency, %	STD, %
30	63.06	4.4
40	63.79	4.8
50	62.6	3.4

Table 4.4. Effect of EG concentration on the A-H collection efficiency. Liquid effluent flow rate: 0.16 ~ 0.19 mL/min.

EG concentration, % - Liquid effluent flow rate, mL/min	A-H efficiency, %	STD,%
30 - 0.16	92.39	1.2
40 - 0.173	93.45	0.5
50 - 0.188	93.98	1.9

Table 4.5. Effect of liquid effluent flow rate in the A-H collection efficiency.

EG concentration, % - Liquid effluent flow rate, mL/min	A-H collection efficiency, %	STD,%
30 - 0.04	41.01	4.4
30 - 0.1	63.06	4.4
30 - 0.16	92.39	1.2
30 - 0.22	91.69	1.4

Table 4.6. Effect of 30% EG in a cooled cyclone.

	Ice water surrounding the 100 L/min cyclone			
	0% EG (75F/55%)		30% EG (75F/55%)	
In flow rate, $\mu\text{L}/\text{min}$	Out flow rate, $\mu\text{L}/\text{min}$	A-H efficiency, %	Out flow rate, $\mu\text{L}/\text{min}$	A-H efficiency, %
100	56	58.5	86	61.9
150	119	72.9	150	76.9
200	141	79.9	200	81.3
250	185	88.3	233	89.1

Table 4.7. Initial heat flux value for -22°C .

Heater element	Power input, W	Heat flux, W/in^2
1 Cartridge	2	5
2 Inlet and Impacting	20	5
3 Middle	9	5
4 Liquid Port	3.5	5
5 Skimmer	4.2	5

Table 4.8. Optimized heat flux value for the cartridge heater.

Heater element	Power input, W	Heat flux, W/in ²
1 Cartridge	1	2.55
2 Inlet and Impacting	20	5
3 Middle	9	5
4 Liquid Port	3.5	5
5 Skimmer	4.2	5

Table 4.9. Optimized heat flux value for the cartridge and skimmer heater.

Heater element	Power input, W	Heat flux, W/in ²
1 Cartridge	1	2.55
2 Inlet and Impacting	20	5
3 Middle	9	5
4 Liquid Port	3.5	5
5 Skimmer	4	4.7

Table 4.10. Optimized heat flux for the preliminary heating system for -22°C.

Heater element	Power input, W	Heat flux, W/in ²
1 Cartridge	1	2.55
2 Inlet and Impacting	20	4.9
3 Middle	4.1	2.3
4 Liquid Port	1.1	1.59
5 Skimmer	4	4.7

Table 4.11. Initial heat flux value for -32°C.

Heater element	Power input, W	Heat flux, W/in ²
1 Cartridge	2	5
2 Inlet and Impacting	40	9.8
3 Middle	8.3	4.6
4 Liquid Port	2.1	3
5 Skimmer	7.8	9.4

Table 4.12. Optimized heat flux for the preliminary heating system for -32°C.

Heater element	Power input, W	Heat flux, W/in ²
1 Cartridge	1.5	3.82
2 Inlet and Impacting	35	8.64
3 Middle	5.5	3.08
4 Liquid Port	2.1	3
5 Skimmer	6	7.13

Table 5.1. Cyclone flow rate and corresponding Reynolds number based on the slot width.

<u>100 L/min Cyclone</u>		<u>300 L/min Cyclone</u>		<u>1250 L/min Cyclone</u>	
<u>Flow rate,</u>	<u>Reynolds</u>	<u>Flow rate,</u>	<u>Reynolds</u>	<u>Flow rate,</u>	<u>Reynolds</u>
<u>L/min</u>	<u>Number</u>	<u>L/min</u>	<u>Number</u>	<u>L/min</u>	<u>Number</u>
80	3578	120	3788	400	7913
100	4472	150	4824	640	12661
120	5366	170	5521	750	14838
160	7155	185	5885	1000	19784
200	8944	200	6393	1250	24729
		240	7672	1500	29675
		300	9590		
		400	12786		

Table 5.2. Coefficients of two sigmoid functions for two groups.

	High Reynolds number Region	Low Reynolds number Region
a	100	100
b	$0.114 - 2 \times 10^{-6} \times \text{Re}_{\text{SlotWidth}}$	$0.2 - 1.2 \times 10^{-5} \times \text{Re}_{\text{SlotWidth}}$
c	-2.07	0.057

VITA

Name: **Youngjin Seo**

Place of Birth: Taegu, Korea

Permanent Address: 848-11 Manchon-3-dong, SusungGu,
Taegu, Korea 706-023

Email Address: youngjin.seo@gmail.com

Education: B.S. in Aeronautical and Mechanical Engineering, Korea
Aerospace University, Koyang, Korea, 2002

M.S. in Mechanical Engineering, Texas A&M University,
College Station, Texas, 2004

Ph.D. in Mechanical Engineering, Texas A&M University,
College Station, Texas, 2007